PATERNAL PRECONCEPTIONAL ALCOHOL EXPOSURE ALTERS THE SPERM EPIGENETIC LANDSCAPE AND ADVERSELY AFFECTS OFFSPRING DEVELOPMENT

A Dissertation

by

YUDHISHTAR SINGH BEDI

Submitted to the Graduate and Professional School of
Texas A&M University
in partial fulfillment of the requirements for the degree of

DOCTOR OF PHILOSOPHY

Chair of Committee,	Michael Golding
Committee Members,	Dana Gaddy
	Tracy Clement
	Rajesh Miranda
Head of Department,	Larry Suva

December 2021

Major Subject: Biomedical Sciences

ABSTRACT

This research examines the effect of paternal alcohol consumption on fetal growth and on the sperm epigenetic and noncoding RNA profile. Earlier studies have found links between paternal preconception alcohol consumption and fetal growth, offspring behavior and programming of metabolism in the adult offspring. These studies have historically focused on transmission of alcohol exposure mediated changes in sperm DNA methylation and small noncoding RNAs.

Building on this set of research, we conduct our own analysis using a mouse model of voluntary chronic alcohol consumption. We examine the ability of paternal alcohol exposures to cause late-term fetal growth deficits. By measuring fetal and placental parameters at gestational day 16.5, we identify significant growth restriction accompanied by reduced placental efficiency in a sex-independent manner and significant enlargement of placentae of the male offspring. Using transcriptomic analyses in combination with chromatin immunoprecipitation for the regulatory protein CCCTC-binding factor (CTCF), we show that paternal alcohol influences placental gene regulation by altering patterns of large-scale chromatin architecture. Next, using small RNA sequencing, we show that alcohol significantly alters the abundance of different small noncoding RNA subpopulations in sperm. Using mass spectrometry, western blotting and Chromatin immunoprecipitation followed by deep sequencing (ChIP-seq), we further show that alcohol alters the populations of specific histone modifications globally and this is accompanied by differential enrichment of these histones at genes that are involved in neurodevelopment, cell adhesion and embryo development. Finally,

using the same approach we characterize changes in sperm histone profiles during epididymal transit. We find that histones associated with enhancers and a subset of gene promoters are differentially enriched in the caput and cauda epididymides.

Findings from our studies illuminate the complex epigenetic basis of the paternally transmitted effects of environmental exposures. They contribute to the existing literature by studying the impact of alcohol on sperm-retained histones and noncoding RNAs as well as its effects on placental epigenetics. Future studies looking at the early embryo developmental program in response to paternal environmental exposures can use similar methods to assess contributions of the sperm epigenome.

DEDICATION

To my dear aunt, Bulu Maasi, I wish you were still here with me as I complete this chapter of my life, and hope you would be proud of me today. I dedicate this dissertation to your memory. I miss you every day.

ACKNOWLEDGEMENTS

I'd like to thank my committee chair, Prof. Michael Golding for his support and guidance throughout this entire dissertation. I would have not covered such a wide breadth of research areas had it not been for his supervision and nudges along the course of where my project began to where it ended. I am very grateful for the invaluable insight and encouragement of my committee members. Prof. Tracy Clement's office and lab have always been a second academic home for me to find a support network and develop ideas for my project. I received invaluable help from Prof. Clement with my studies understanding the basics of male reproduction which provided the foundation for all the work in my dissertation. I thank Prof. Dana Gaddy for her support including feedback on my work, teaching me how to better communicate my research and for always providing the push across every milestone of my Ph.D. I am grateful to Professor Miranda for always being an excellent sounding board for research ideas and his excellent guidance on grant writing as well.

I couldn't have completed any of this work without the support of my fantastic friends and colleagues at the CVM who have provided the best support network - an essential requisite to survive graduate school. From the crew I started my course with including Carlos Pinzon, Richard Chang, Haiqing Wang, Cassandra Skenandore, Hanah Georges, Will Skiles and other members of the Reproductive Sciences Complex to the one and only #DreamTeam with Kara Thomas, Alexis Roach and Nicole Mehta at the Golding Lab, I am truly thankful for all the people I have met and known here.

I’d like to thank my parents for their unconditional love and support during my studies and even after, as I transition to a new position. Their constant belief in me and my life decisions has been a source of stability and security throughout the lows and highs of a life away in another country, especially in academia.

I am eternally grateful to my life partner, Upasana Garnaik, for always being there for me, understanding me, checking in on my mental health and for providing the necessary impetus to keep me going in times when I felt my own will lacking.

I would also like to acknowledge the Counselling and Psychological Services (CAPS) Division of Student Affairs. I feel fortunate to have had this resource available to me during graduate school.

Lastly, I would like to thank the folks at Carport Coffee, College Station, for caffeinating me and providing the necessary fuel to keep me going during my dissertation writing phase.

CONTRIBUTORS AND FUNDING SOURCES

Contributors

This work was supervised by a dissertation committee consisting of Professor Michael Golding [advisor] and Professor Tracy Clement of the Department of Veterinary Pharmacology and Physiology, Professor Dana Gaddy of the Department of Veterinary Integrative Biosciences and Professor Rajesh Miranda of the Department of Neuroscience and Experimental Therapeutics.

Animals used in these studies were maintained and treated by Kara Thomas, Alexis Roach, Richard Chang, Sarah Chronister and the student himself, with assistance from Kelly Thomas and Kaci Herman. The tissue preparation methods depicted in Chapter 2 were carried out with assistance from members of Professor Tracy Clement's lab. The sample preparation for immunohistochemistry was carried out by Chaitali Mukherjee at the CVMBS Core Histology Lab. Sperm TUNEL and CMA3 staining assays were carried out by Srijana Upadhyay and Professor Tracy Clement. The RNA sequencing analysis described in Chapters 2 and 3 were carried out by Richard Chang. The analyses depicted in Chapter 2 were conducted in part by Professor Tracy Clement of the Department of Veterinary Pharmacology and Physiology and were published in 2019. The Chromatin Immunoprecipitation experiments in Chapter 3 were carried out by Haiqing Wang and DNA methylation analysis was conducted by Dr. William Skiles. Sperm Histone isolation and Western Blots described in Chapter 4 were optimized with assistance from Dr Nicole Mehta. Ram reproductive tract and sperm collection was

carried out by Alexis Roach. The animals were kindly provided by Professor Dana Gaddy. We thank the technical support for Sperm ChIP-sequencing projects from the Cancer Prevention and Research Institute of Texas (CPRIT RP180734).

All other work conducted for the dissertation was completed by the student independently.

Funding Sources

Graduate study was supported by Professor Michael Golding and the Department of Veterinary Pharmacology and Physiology at the College of Veterinary Medicine.

This work was supported by a Medical Research Grant from the W.M. Keck Foundation and NIH grant R01AA028219 from the NIAAA. Its contents are solely the responsibility of the authors and do not necessarily represent the official views of the W.M. Keck Foundation or the National Institute of Health.

NOMENCLATURE

ChIP	Chromatin Immunoprecipitation
CMA3	Chromomycin A3
CpG	5'-Cytosine-phosphate-Guanosine-3'
CTCF	CCCTC-binding factor
DNA	Deoxyribonucleic acid
FASDs	Fetal Alcohol Spectrum Disorders
FPKM	Fragments Per Kilobase or transcript per Million mapped reads
GD	Gestational Day
H3/H4	Histone H3/H4
miRNA	microRNA
MS	Mass Spectrometry
PFA	para-formaldehyde
PBS	phosphate buffered saline
PTM	Post-translational modification
qPCR	quantitative Polymerase Chain Reaction
RNA	Ribonucelic Acid
RRBS	Reduced Representation Bisulfite Sequencing
tRNA	transfer RNA
tRF	tRNA fragments
TUNEL	terminal deoxynucleotidyl transferase dUTP nick-end-labeling

TABLE OF CONTENTS

LIST OF FIGURES

LIST OF TABLES

1. INTRODUCTION

Alcohol is a notorious teratogen and periconceptional exposures have been linked to a spectrum of growth, structural and central nervous system deficits in the fetus, known as Fetal Alcohol Spectrum Disorders (FASDs), that perpetuate into childhood, adolescence and even adulthood (Moore and Riley, 2015). The prevalence of high rates of FASDs, alcohol-related birth defects and neurodevelopmental disorders across continents informs us that management of FASDs is a significant burden for every community (Roozen et al., 2016). Due to the link with gestational exposures, research into FASD has focused on the singular role of the mother (Carter et al., 2013)(Figure 1.1). However, a growing body of research has linked paternal preconception alcohol with deficits in fetal growth, offspring behavior, long-term metabolic outcomes (Abel, 2004; Chang et al., 2017; Finegersh et al., 2015; Rompala et al., 2019; Zhang et al., 2019).

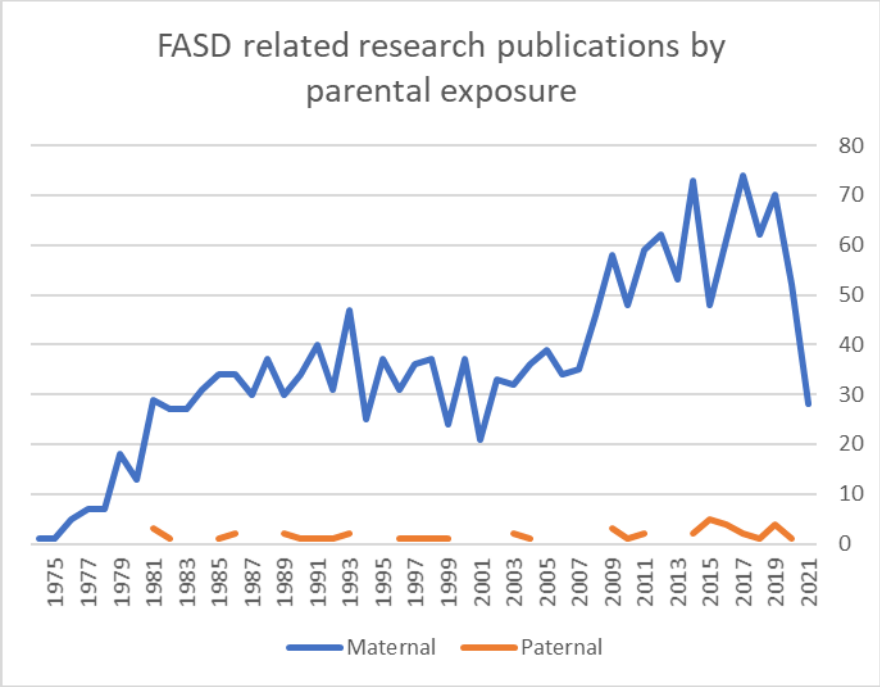

Figure 1.1 Line plot of research outputs in PubMed studying Fetal alcohol spectrum Disorders by parent of exposure

In this dissertation, I outline research from our lab examining the effects of paternal alcohol consumption on fetal growth deficits. In doing so, we study the underlying epigenetics that associate with altered transcriptional networks in the placenta of alcohol-sired fetuses. Furthermore, our research also determines epigenetic mechanisms that transmit the memory of environmental exposures to the offspring via sperm chromatin and small noncoding RNAs. Lastly, we examine histone modifications in post-testicular sperm and uncover a highly dynamic process of chromatin reorganization during the period of epididymal maturation.

In Chapter 2, we evaluate the impact of chronic paternal alcohol consumption on fetal and placental growth. Previously, our lab has shown that chronic alcohol exposure in male C57BL/6J mice led to fetal growth restriction in only the female offspring,

which was measured at gestational day 14.5 (GD 14.5) (Chang et al., 2017). Here, we found that during the exponential growth phase of the fetus, which occurs after GD 14.5 (Mu et al., 2008), larger and more significant growth deficits were apparent in a sex-independent manner (Bedi et al., 2019). Pregnancies from alcohol-exposed and control sires were terminated at GD 16.5 and fetal and placental mass and morphometrics informed us of fetal growth restriction and reduced placental efficiencies, that were more severe in male offspring.

This chapter also determines the effects of chronic alcohol exposure on male reproductive physiology. While our previous study found no significant effect of alcohol on sperm motility, count or fertility (Chang et al., 2017), we did not assess all aspects of male reproductive health. Other studies done in rodent models using sexually mature males have reported a wide spectrum of effects from defects in sperm *in vitro* fertilization dynamics including nuclear decondensation (Sanchez et al., 2018) to hormonal imbalances and testicular damage (Anderson et al., 1980; Martinez et al., 2009) and, in some cases, no deleterious effects were observed at all (Cicero et al., 1990). Here, we thoroughly assess markers of reproductive physiology including gross testicular, epididymal and seminal vesicle weights, serum testosterone levels and seminiferous tubule morphology. We also analyze changes in sperm viability, DNA damage and chromatin damage in response to alcohol. We found no difference in any of the abovementioned markers and conclude that the chronic preconception alcohol model we use does not associate with adverse effects on male reproductive physiology or sperm viability.

Sperm carry a vast payload of small noncoding RNAs including microRNAs, piRNAs, tRNAs and tRFs (Amanai et al., 2006; Hutcheon et al., 2017; Peng et al., 2012). While their roles

during early development are still poorly understood, several studies have implicated alterations in the abundance of specific sets of these RNAs in the transmission of adverse health outcomes. As examples, small ncRNAs altered in response to paternal environmental exposures such as high fat diet (Chen et al., 2016a) and stress (Rodgers et al., 2015) can, in isolation, induce similar defects when injected into naïve one-cell stage embryos. We isolate sperm RNA from alcohol-exposed sires, and use deep sequencing for RNAs smaller than 100nts. By mapping the resulting reads to known databases of microRNAs, piRNAs, tRNAs and tRFs, we determine the small noncoding RNA profile of sperm in response to alcohol. We report that alcohol alters the abundance of small RNA populations, particularly the ratio of tRFs to piRNAs is lower than in control sperm. Also, we identify three microRNAs, mir-142, mir-21 and mir-30a, that are significantly altered in alcohol exposed sperm.

In Chapter 3, we follow up on data from our previous study where we discovered altered transcriptional clusters of genes in the placenta of alcohol-sired fetuses (Chang et al., 2017). Here, we show that alcohol exposure induces altered localization of the insulator binding protein, CCCTC-binding factor (CTCF), at multiple loci, including several gene clusters that are dysregulated in the placental transcriptome. In order to do so, we use chromatin immunoprecipitation followed by sequencing (ChIP-seq) to determine regions of enrichment for CTCF in the placental genome. Our research shows that paternal exposures can have an impact on long-range chromatin dynamics of the placenta by influencing the binding of regulatory proteins to their DNA elements.

In Chapter 4, we examine post-testicular sperm maturation in the context of histone posttranslational modifications (PTMs) and the enrichment of different histone PTMs in sperm isolated from the caput and cauda epididymis. Here, we present novel evidence highlighting the active remodeling of sperm chromatin that occurs in the epididymal transit of sperm. We use a

mass spectrometry (MS)-based analysis to first identify differentially enriched histone PTMs across the two sperm populations. We then proceed to verify the candidate PTMs with high degree of change and abundance by western blotting. Based on our findings, we select H3K27ac and H3K9me2, both of which are associated with enhancers, as well as in the case of H3K27ac, gene promoters, and use ChIP-seq to identify differential genomic regions of enrichment. Our work uncovers a highly dynamic sperm epigenome in the period of epididymal maturation suggesting that this is an important window wherein paternal exposures can influence the epigenetic landscape and have undesirable effects on the offspring.

In the final chapter, we examine the effects alcohol has on the sperm-retained histone PTMs. Using MS, western blotting and ChIP-seq we identify differential enrichment of histone modifications H3K4me3 and H3K9me2 in alcohol exposed sperm. Using pathway analysis, we identify an intersection of the affected gene networks in neurodevelopment, cell adhesion and embryo development. This is the first study that identifies these changes in the context of paternal alcohol exposure and will inform future studies that assess the role of the paternal exposures in the transmission of FASD phenotypes and other alcohol related deficits in offspring.

2. ALTERATIONS IN SPERM-INHERITED NONCODING RNAS ASSOCIATE WITH LATER-TERM FETAL GROWTH RESTRICTION INDUCED BY PRECONCEPTION PATERNAL ALCOHOL USE[*]

2.1. Introduction

Developmental plasticity refers to the dynamic ability of one genotype to produce multiple phenotypes in response to different environmental stimuli (Hochberg et al., 2011). This phenomenon enables the best chances of reproductive success but can also associate with the development of functional deficits and disease. Indeed, there are multiple instances where the predisposition of offspring to develop diseases later in life can be traced to a fetal compensation to an early life stressor (Feil and Fraga, 2012). For example, small-for-gestational-age babies have an increased risk of developing metabolic diseases, such as type two diabetes, and both cardiovascular morbidity and mortality as adults (Gluckman et al., 2009; Padmanabhan et al., 2016). These observations helped found the Developmental Origins of Health and Disease hypothesis, and established the current recognition of the importance intrauterine development has in lifelong health.

Less well defined are the abilities of parental life history to influence organism phenotype. Although not as well characterized as intrauterine encounters, parental exposures prior to conception also exert a significant impact on offspring health and

[*] Reprinted with permission from "Alterations in sperm-inherited noncoding RNAs associate with late-term fetal growth restriction induced by preconception paternal alcohol use" by Bedi et al. 2019. *Reproductive Toxicology*, 87, pp. 11-20, Copyright [2019] by Bedi et al.

development (Lane et al., 2014). Thus, in addition to uterine programming, the processes of germline programming that occur during gametogenesis also have the ability to impact offspring phenotype and influence the developmental plasticity of the next generation. Recently, preconception male exposures to a range of environmental factors have been linked to alterations in the developmental program of sperm and correlated with increased rates of structural and metabolic defects in the next generation (Anway et al., 2005; Carone et al., 2010; Chang et al., 2017; Chen et al., 2016a; Dias and Ressier, 2014; Donkin et al., 2016; Esakky et al., 2016; Fullston et al., 2013; Gapp et al., 2014a; Lambrot et al., 2013; Ng et al., 2010; Radford et al., 2012, 2014; Rompala et al., 2018; Sharma et al., 2016; Shea et al., 2015; Sun et al., 2018; Terashima et al., 2015; Wei et al., 2014; Zeybel et al., 2012). These studies challenge the singular importance of maternal in utero exposures and implicate paternal exposure history as an additional and important mediator of both developmental defects and environmentally-induced disease.

The molecular mechanisms by which preconception stressors heritably influence cellular phenotypes are still very poorly understood. Molecular processes that allow the stable propagation of either chromatin-states or epigenetic information from one generation of cells to the next are hypothesized to play a role in transmitting the cellular memories of past exposures through gametogenesis to the offspring (Rando and Simmons, 2015). Specifically, mature sperm carries epigenetic information in patterns of DNA methylation, the region-specific retention of histones and DNA binding factors (like CTCF), as well as populations of small noncoding RNAs (ncRNAs). However, studies examining paternally-inherited abnormalities in growth and metabolic function

have provided evidence to both support and refute the involvement of sperm-inherited changes in DNA methylation in the transmission of these phenotypes (Carone et al., 2010; Chang et al., 2017; Ng et al., 2010; Radford et al., 2012; Shea et al., 2015; Sun et al., 2018; Wei et al., 2014). Similarly, although select regions of the sperm genome retain histones, it is unclear if this epigenetic information persists through the remodeling of the paternal genome during syngamy, or have the ability to transmit through the cell cycle (Henikoff and Shilatifard, 2011; O'Doherty and McGettigan, 2015). The strongest candidate to date has been the transmission of paternally inherited ncRNAs. In these studies, the injection of either total sperm RNAs or a subset of sperm RNAs (for example, microRNAs or tRNA-derived small RNAs) into normal zygotes can recapitulate some paternal phenotypes induced by mental or metabolic stressors (Chen et al., 2016b). However, the mechanisms through which the effects of sperm-inherited ncRNAs persist into later life remain poorly defined (Conine et al., 2018).

In the United States, 70% of men drink and 40% drink heavily, with 8.3% reporting the routine consumption of more than two drinks per day (Naimi et al., 2003; White et al., 2006). Despite the nearly ubiquitous and constant exposure during reproductive ages, we currently have a very poor understanding of the effects chronic preconception alcohol use has on male reproductive physiology and the sperm-inherited developmental program. Using a mouse model of voluntary consumption, our lab recently described an association between chronic preconception paternal alcohol use and deficits in both placental function and offspring growth (Chang et al., 2017, 2019a). Importantly, these phenotypes did not associate with any measurable alterations in

sperm-inherited patterns of DNA methylation (Chang et al., 2017). Therefore, the question of how the memory of chronic alcohol use transmits to the offspring remains unresolved.

Mechanistic studies in rodents have revealed that alcohol impairs the endocrine-reproductive axis, indicating male alcohol use may impact foundational aspects of reproductive function (Canteros et al., 1995; Young Lee et al., 2010). In addition, multiple studies in humans and rodents have indicated that chronic alcohol use negatively impacts the integrity of the sperm nucleus (Anifandis et al., 2014; Joo et al., 2012; Rahimipour et al., 2013; Sanchez et al., 2018; Talebi et al., 2011). Finally, using an inhalation model of exposure, Rompala and colleagues recently described alcohol-induced alterations in the profile of sperm derived ncRNAs (Rompala et al., 2018). However, whether facets of male reproductive function, sperm nuclear structure or the profile of sperm-inherited ncRNAs are altered in our model of voluntary alcohol consumption and associate with the development of the observed growth defects remains to be resolved.

2.2. Materials and Methods

2.2.1. Animal Work

All experiments were conducted under AUP 2017–0308 and approved by the Texas A&M University IACUC. Individually caged C57BL/6J (RRID: IMSR_JAX:000664) postnatal day 90 adult males were obtained and housed in the

Texas A&M Institute for Genomic Medicine, fed a standard diet (catalog# 2019, Teklad Diets, Madison, WI, USA) and maintained on a 12-hour light/dark cycle. In this study, we employed a voluntary model of alcohol exposure known as Drinking in the Dark. This model of exposure avoids the stress associated with forced feeding and mitigates the known impact of stress on the sperm-inherited epigenetic program (Gapp et al., 2014a). Using methods described previously (Chang et al., 2017), males were provided limited access to ethanol during a four-hour window, beginning one hour after the initiation of the dark cycle. During this four-hour window, experimental males were provided access to a solution of 10% (w⁄v) ethanol (catalog# E7023, Millipore-Sigma, St. Louis, MO, USA) and 0.066% (w⁄v) Sweet'N Low (Cumberland Packing Corp, Brooklyn NY, USA). Control males received a solution of 0.066% (w⁄v) Sweet'N Low alone. After each session, the amount of fluid consumed by each mouse was recorded.

Once consistent patterns of drinking were established, males were maintained on this protocol for a period of 70 days. Subsequently, two naturally cycling females were placed in a new cage along with each exposed male. During these matings, males were not provided access to the alcohol/control preconception treatments. The next morning, matings were confirmed by the presence of a vaginal plug and both the male and female mice were returned to their original cages. Males were allowed a 24-hour rest period, during which the preconception exposure was resumed and then used in a subsequent mating. This procedure was repeated until each male had produced a minimum of two pregnancies. Subsequently, males were euthanized by CO_2 asphyxiation and cervical dislocation, blood collected post-mortem and the male reproductive tract excised.

Pregnant dams were maintained on a Breeder diet (catalog# 5058, LabDiet, St. Louis, MO, USA), subjected to minimal handling and euthanized by CO_2 asphyxiation and cervical dislocation on gestational day 16.5. The female reproductive tract was excised, the gestational sac removed and fetal tissues weighed.

2.2.2. Measurement of Physiological Parameters

Male plasma alcohol concentrations were measured using the Ethanol Assay Kit (catalog# ECET100, BioAssay Systems, Hayward, CA, USA) according to the manufacturer's protocol. Levels of serum testosterone were determined using an ELISA at the Ligand Assay and Analysis Core at the University of Virginia Center for Research in Reproduction. Serum levels of corticosterone were measured using the Corticosterone ELISA kit (catalog# EC3001–1, AssayPro, St. Charles, MO, USA) according to the recommended protocol.

2.2.3. Sperm and Tissue Collection & Histology

The male reproductive tract, liver, and spleen were excised, trimmed of fat and their weights recorded. To collect mature sperm, cauda epididymides and roughly 1 cm of vas deferens were placed in 500 µL of pre-warmed (37ºC) Human Tubal Fluid (HTF) medium (catalog# ZHTF-100, Zenith Biotech, Blue Bell, PA, USA) in 12 well plates. Four or five incisions were made to the cauda to allow sperm to swim out and the vas deferens were carefully squeezed using forceps to expel their contents. Plates were allowed to incubate at 37ºC for 10 minutes. Sperm counts were performed by diluting a

10µl aliquot 1:50 in diH_2O and counting on a Neubauer chamber slide. Post-incubation, HTF media containing mature sperm were carefully layered over a pre-warmed (37ºC) gradient consisting of 350 µL each of 40% and 80% PureSperm (catalog#s PS40 and PS80, Spectrum Technologies, Healdsburg, CA, USA) in 1.5 mL microcentrifuge tubes and spun at 650g for 25 min. The pellet was then washed in 1mL of 1% BSA in PBS, and either immediately fixed for microscopic analyses or spun down, snap frozen in liquid Nitrogen and stored at −80ºC. To determine cell counts, 10 µL of caudal sperm from the last wash was used. Using microscopy, the purity of all samples was judged to be greater than 99%. After removal of encapsulating tunica, one testis from each animal was snap frozen in liquid nitrogen. The other testis was punctured with a 21 G needle and then fixed overnight in Bouin's solution. Bouin's fixed testes were paraffin embedded and stained using standard procedures for Hematoxylin and Eosin (H&E). H&E-stained sections were imaged under bright field using the Leica DMi8 microscope (Leica microsystems, Germany). Cross-sectional areas of tubules were measured using the area line tool in the Leica Application Suite X (LAS X) analysis software package. All tubules exhibiting longitudinal sectioning were excluded, while all tubules cut transversely into cross-sections were included in the analysis. Two non-sequential stained sections per animal were analyzed and a total of three animals per treatment were used in the comparison of calculated areas.

2.2.4. CMA3 staining

An equal volume of 3:1 methanol:acetic acid was added to PBS suspended sperm and samples incubated at 4ºC for 5 min. Samples were spread on glass slides and allowed to air dry at room temperature. Slides were treated for 20 minutes with 100 µL CMA3 solution: 0.25 mg/mL CMA (catalog# C2659, Millipore-Sigma, St. Louis, MO, USA) and 10mM $MgCl_2$, McIlvain's buffer (17 mM citric acid, 164 mM Na_2HPO_4, pH 7.0). Slides were rinsed with PBS and mounted with Prolong Gold Antifade Mountant (catalog# P36930, Thermo-Fisher, Waltham, MA, USA) and then kept at 4ºC overnight. Evaluation of fluorescence was done for a minimum of 200 spermatozoa on each slide.

2.2.5. Sperm TUNEL Assay

The APO-DIRECT kit (catalog# 556381, BD Pharmingen, San Jose, CA, USA) was used for terminal deoxynucleotidyl transferase dUTP nick-end-labeling (TUNEL) to assess DNA damage. Approximately 3 million sperm per sample were resuspended in 4% PFA at room temperature for 1 hour. Samples were then spun down at 300xg for 5 minutes and washed twice with PBS. Pellets were suspended in ice-cold 70% ethanol and held at −20ºC for at least 12–18h. Following this incubation, preparation and staining of samples and appropriate controls were carried out as per manufacturer's instructions. Stained samples were settled onto poly-L-lysine coated glass slides, mounted in Prolong Gold Antifade Mountant, and visualized on a Leica DMi8 microscope with SOLA SE 365 light source and Chroma filters for FITC detection. Total cell counts and sperm morphology of the PFA fixed sperm was visualized by

differential Interference contrast microscopy at 63x. At least three fields of view and 200 sperm were scored for each sample to determine percent TUNEL positive.

2.2.6. Sperm RNA isolation

Approximately 10 million mature sperm per sample were lysed in 1mL TRIzol Reagent (catalog# 15596018, Thermo-Fisher, Waltham, MA, USA) plus 10 µl β-ME (catalog# M3148, Millipore-Sigma, St. Louis, MO, USA) using homogenizing pestles (catalog# 6478820, Electron Microscopy Sciences, Hatfield, PA, USA). Subsequently, 200µl of 1-Bromo-3-chloropropane (catalog# B9673, Millipore-Sigma, St. Louis, MO, USA) was added to separate the aqueous phase, which was collected and precipitated using an equal volume of isopropanol. After two ice-cold, 70% ethanol washes, RNA samples were reconstituted in RNase free water and stored at −80ºC.

2.2.7. Sperm RNA sequencing

Illumina single-end cDNA libraries were synthesized from size-selected RNAs (<50 bases) derived from 100 ng of sperm total RNA using the TruSeq Stranded mRNA kit. Four biological replicates per treatment group were multiplexed and sequenced on a single HiSeq2000 lane (Illumina) within the sequencing core of the Whitehead Institute. Using Bowtie2 (RRID:SCR_016368) and Tophat (RRID:SCR_013035), small RNA reads were aligned to the Mus musculus (UCSC version mm10) reference genome (Langmead and Salzberg, 2012). Small RNA reads with a single allowable mismatch were selected for further analysis. Small RNA annotation was performed by separately

aligning reads to the microRNA database(http://www.mirbase.org/), tRNA database (http://gtrnadb.ucsc.edu/), and piRNA database (http://pirnabank.ibab.ac.in/index.shtml), as described previously (Sharma et al., 2018). Differentially expressed microRNAs were quantified using the miRDEEP2 ver2.0.0.7 pipeline (Friedlander et al., 2012). The referenced tRNA database holds sequences for both tRNA anticodons and tRNA fragments (tRFs), which are selected as reads partially matching the tRNA anticodon but are less than 34 nucleotides in length (Sharma et al., 2016). To quantify differentially expressed tRFs, piRNAs, and tRNAs, total counts of mapped reads were calculated using the featureCounts pipeline (Liao et al., 2014) and then normalized to the total mapped reads of each class of small RNA species, as described previously (Sharma et al., 2016). Generated volcano plots contrast the differential enrichment of ncRNAs by raw p-value and not by FDR selection.

2.2.8. Data Handling and Statistical Analysis

For all experiments, measures were input into the statistical analysis program GraphPad (RRID:SCR_002798; GraphPad Software, Inc., La Jolla, CA, USA) and statistical significance was set at alpha = 0.05. For all datasets, normality was first verified using the Brown-Forsythe test. In this study, the effect of treatment was assessed using either an unpaired Student's t-test or two-way analysis of variance test (ANOVA), with differences among the means evaluated using Sidak's posthoc test of contrast. In all instances, we have marked statistically significant differences with an asterisk. For the comparisons of testicular, epididymal and seminal vesicle weights expressed as a

percentage of total paternal body weight, as well as the percentage of TUNEL and CMA3 positive sperm, data were arcsine transformed and an unpaired t-test with Welch's correction applied. To calculate the tRFs:piRNA ratio, the percentage of mapped tRFs per sample was divided by the percentage of mapped piRNAs and differences compared between treatments using an unpaired student's t-test.

2.3. Results

2.3.1. Daily ethanol exposures induce pharmacologically meaningful blood alcohol concentrations but do not impact paternal body weight

To define the long-term impact alcohol exposure has on both reproductive function and the male-inherited developmental program, we returned to our established mouse model of chronic alcohol exposure (Chang et al., 2017, 2019a). Here, postnatal day 90 adult males were provided limited access to either the ethanol or control preconception treatments during a four-hour window, that began one hour into the night cycle. Once consistent patterns of alcohol consumption were established, males were maintained on this protocol for a period of 70 days, which corresponds to the length of two complete spermatogenic cycles and ensures that sperm formed prior to alcohol treatment are not able to confound the resulting phenotypes. For each male, the amount of fluid consumed per day was recorded. No differences in fluid consumption between the two preconception treatment groups were observed (Figure 2.1 A).

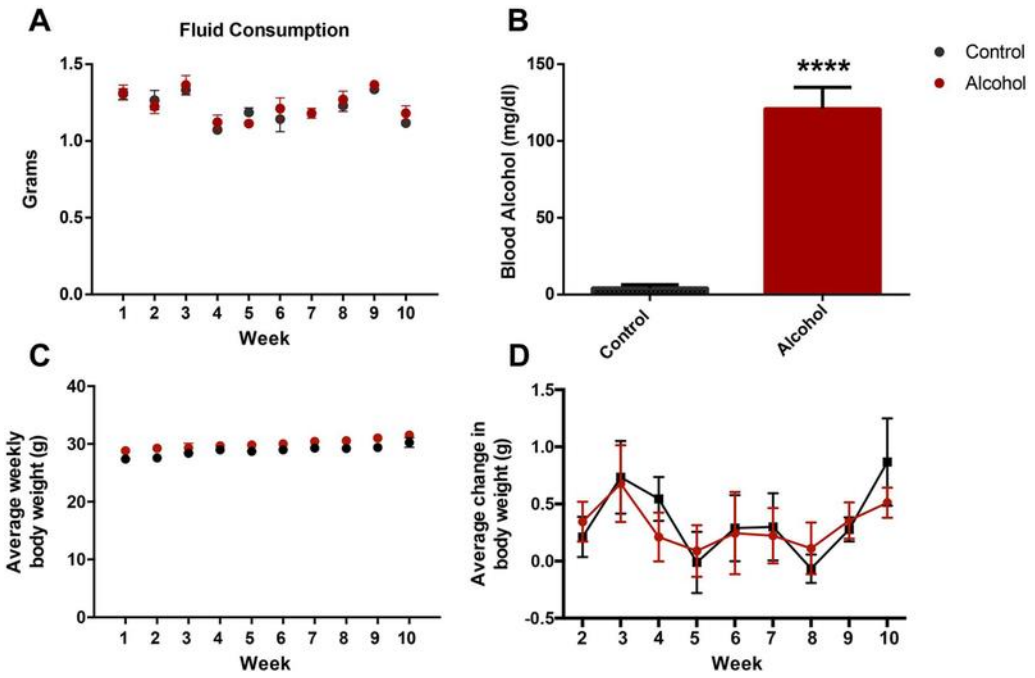

Figure 2.1 Chronic alcohol exposure using a limited access model induces physiologically relevant plasma alcohol levels but does not alter paternal weight. A) Average daily fluid consumption compared between the preconception treatment groups (n=11). B) Average plasma alcohol levels between preconception treatment groups, as measured one month after the beginning of treatment (n=9). C) Average weight of males in each treatment group over the experimental course (n=11). Average weekly weight gain of males in each preconception treatment group (n=11). Data were analyzed using an unpaired t-test, error bars represent the standard error of the mean (**** $p < 0.0001$). Reprinted with permission from "Alterations in sperm-inherited noncoding RNAs associate with late-term fetal growth restriction induced by preconception paternal alcohol use" by Bedi et al. 2019. Reproductive Toxicology, 87, pp. 14, Copyright [2019] by Bedi et al

The rodent model we employed (Drinking in the Dark) promotes the daily, voluntary consumption of ethanol in sufficient quantities to achieve pharmacologically meaningful blood alcohol concentrations, typically around 125 mg/dL or 1.5x the legal limit (Figure 2.1 B). In the United States, 16% of men report engaging in high-risk drinking, which is defined as exceeding five or more standard drinks on any day within a given week and importantly, 8.3% of men routinely consume more than two drinks per day (Grant et al., 2017). Therefore, the blood alcohol levels observed in our model of

preconception male alcohol exposure are physiologically relevant. Further, chronic, daily alcohol use among males is both prevalent and a significant health concern. During the treatment course, no differences in body weight or changes in the rate of weight gain were observed between the preconception treatment groups (Figure 2.1 C-D).

2.3.2. Chronic paternal alcohol exposure induces late-term fetal growth restriction and reductions in placental efficiency within the offspring

In our previous studies examining the offspring of alcohol-exposed males, we identified fetal growth restriction in only the female offspring at gestational day 14.5 (Chang et al., 2017), while at birth, both male and female offspring exhibited significant growth restriction (Chang et al., 2019a). Therefore, we examined fetal growth at day 16.5 of gestation, which corresponds to the period when the mouse fetus experiences a dramatic increase in growth rate (McCarthy, 1965). After 70 days of exposure, males undergoing the described preconception treatments were mated to unexposed females, and at gestational day 16.5, dams were sacrificed and offspring evaluated for growth. No differences in litter size were observed between the preconception treatment groups (Figure 2.2 A). At this developmental stage, the male and female offspring of alcohol-exposed sires displayed a ~15% reduction in fetal weight ($p < 0.01$), a ~10% reduction in crown-rump length ($p < 0.01$) and a respective 9% and 14% reduction in the weight of the gestational sac ($p < 0.05$) (Figure 2.2 B-D). These reductions in fetal growth were accompanied by an 18% increase in the placental weight of the male offspring of alcohol-exposed sires, while placental weights of the female offspring were identical to

the controls (Figure 2.2 D). Collectively, a respective 28% and 17% reduction in placental efficiency (grams of fetus produced per gram of placenta (Wilson and Ford, 2001)) was observed for the male and female offspring of the alcohol-exposed sires (Figure 2.2 E) . These observations indicate that the growth restriction associated with paternal alcohol use predominantly manifest during the later phases of pregnancy and correlate with reductions in placental efficiency.

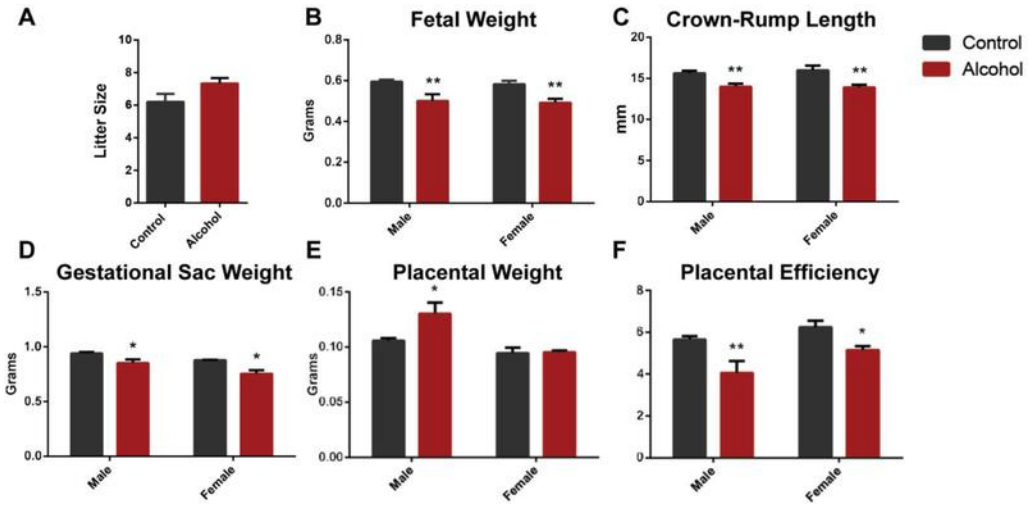

Figure 2.2 Chronic preconception paternal alcohol exposure induces fetal growth restriction and decreased placental efficiency in the offspring at gestation day 16.5. A) Comparison of litter size between matings sired by control and ethanol-exposed males (n=5 control 6 alcohol). Comparisons of B) fetal weight, C) crown-rump length, D) gestational sac weight and E) placental weights between male and female offspring sired by control and ethanol-exposed males (n=10 male and 12 female offspring). F) Placental efficiencies (gram of fetus produced per gram of placenta) compared between the male and female offspring of ethanol-exposed sires (n=10 male and 12 female offspring). Data were analyzed using either an unpaired t-test or a two-way ANOVA followed by Sidak's post hoc analysis. Error bars represent the standard error of the mean (* $p<0.05$, ** $p < 0.01$). Reprinted with permission from "Alterations in sperm-inherited noncoding RNAs associate with late-term fetal growth restriction induced by preconception paternal alcohol use" by Bedi et al. 2019. Reproductive Toxicology, 87, pp. 14, Copyright [2019] by Bedi et al

2.3.3. Chronic paternal alcohol use does not overtly impact male reproductive physiology

To better understand how the memory of chronic paternal alcohol use transmits to the offspring, we began by examining large-scale measures of male reproductive function. No differences in the absolute or proportional weights of the testis, epididymis or seminal vesicles, as well as the spleen or liver could be identified (Figure 2.3 A-E). Mean values and variations in serum testosterone levels we similar between the treatment groups and were consistent with established values (Bartke et al., 1973) (Figure 2.3 F). Histological examinations of testicular sections could not identify any overt morphological differences and no changes in the mean surface area of the seminiferous tubules could be identified between the preconception treatment groups (Figure 2.3 G-I). From these results, we conclude that the dose and duration of chronic alcohol exposure employed here do not overtly impact male reproductive physiology.

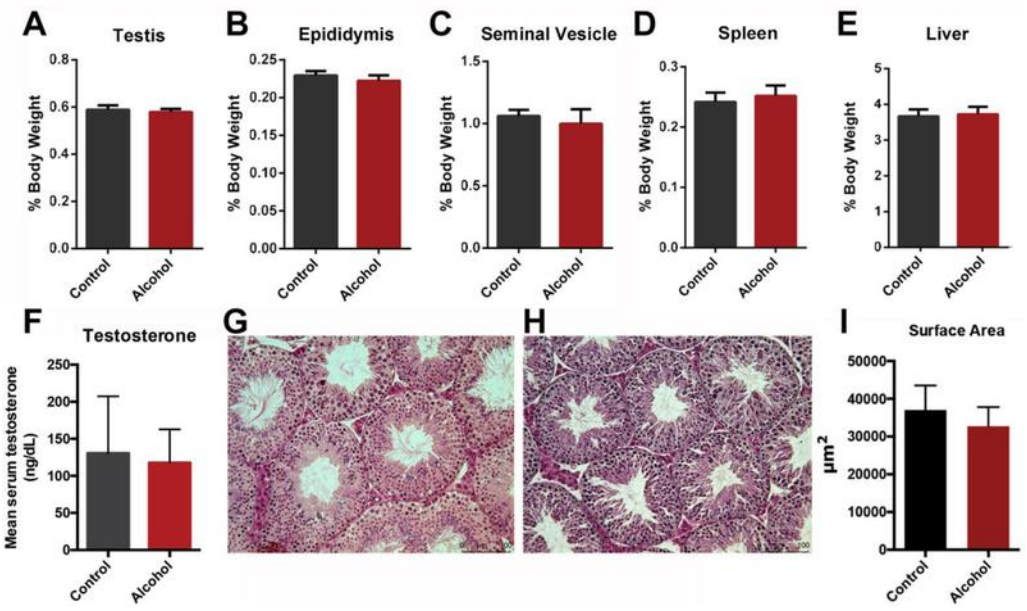

Figure 2.3 Chronic alcohol exposure does not impact macro measures of male reproductive physiology. Comparisons of proportional A) testicular, B) epididymal, C) seminal vesicle, D) spleen and E) liver weights between preconception treatment groups (n=11). F) Levels of plasma testosterone were compared between preconception treatment groups (n=6). Representative hematoxylin and eosin-stained sections of G) control and H) alcohol-exposed testes (n=3, with two, non-consecutive sections examined for each testis). I) Surface area of sectioned seminiferous tubules was determined using the LASX software package and compared between preconception treatment groups (n=3). Percent organ weights were arcsine transformed and an unpaired t-test with Welch's correction used to compare treatments. For all other comparisons, an unpaired t-test was applied. Error bars represent the standard error of the mean. Reprinted with permission from "Alterations in sperm-inherited noncoding RNAs associate with late-term fetal growth restriction induced by preconception paternal alcohol use" by Bedi et al. 2019. Reproductive Toxicology, 87, pp. 15, Copyright [2019] by Bedi et al

2.3.4. Chronic paternal alcohol use does not impact sperm production, morphology, viability or large-scale measures of chromatin structure

We next assayed the impact of chronic male alcohol use on sperm production. No differences in total sperm counts or changes in sperm morphology could be identified between treatment groups (Figure 2.4 A-B). Using the TUNEL assay, we were unable to identify any increases in sperm DNA fragmentation (Figure 2.4 C). Chromomycin A3

(CMA3) is a fluorochrome, which has been shown to compete with protamines for binding to the minor groove of DNA and is, therefore, indicative of compromised nuclear packaging. Using this stain, we could not detect any increases in the sperm of males chronically exposed to alcohol (Figure 2.4 D). Thus, we were unable to identify any large-scale changes in sperm production, DNA fragmentation (TUNEL assay) or nuclear packaging (CMA3 staining).

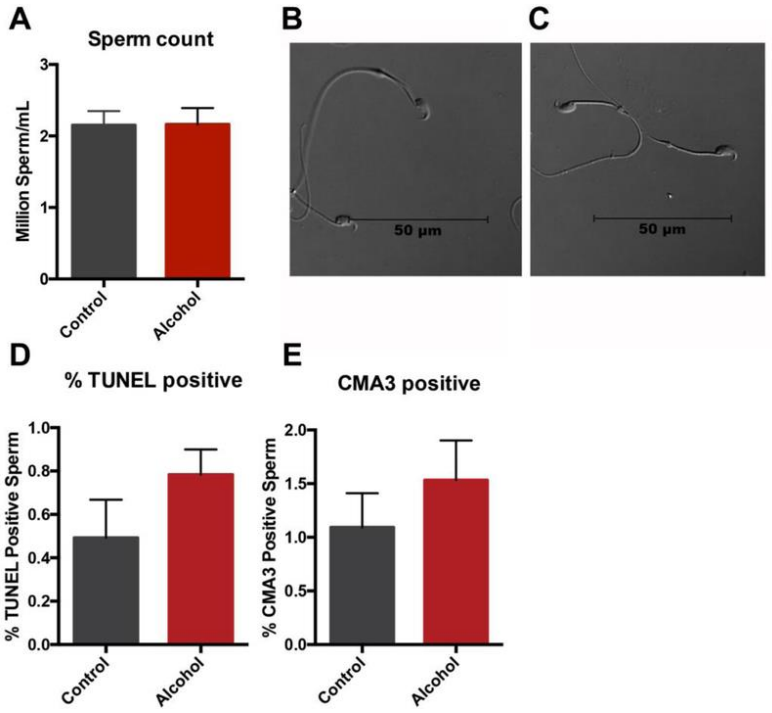

Figure 2.4 Chronic paternal alcohol exposures do not measurably impede sperm production or alter either sperm DNA fragmentation or nuclear packaging. A) Total sperm counts were compared between preconception treatment groups (n=11). Representative light micrographs comparing B) control and C) alcohol-exposed sperm (n=11). The percentage of D) TUNEL positive and E) CMA3 positive sperm were compared between preconception treatment groups (n=4). Data comparing the percentage of stained sperm were arcsine transformed and an unpaired t-test with Welch's correction applied. All other comparisons were conducted using an unpaired t-test. Error bars represent the standard error of the mean. Reprinted with permission from "Alterations in sperm-inherited noncoding RNAs associate with late-term fetal growth restriction induced by preconception paternal alcohol use" by Bedi et al. 2019. Reproductive Toxicology, 87, pp. 16, Copyright [2019] by Bedi et al

2.3.5. Chronic paternal alcohol alters the profile of sperm-inherited non-coding RNAs

Using an inhalation model of exposure, Rompala and colleagues recently described alterations in sperm derived ncRNAs induced by a 5-week exposure to alcohol (Rompala et al., 2018). These studies achieved similar blood alcohol levels (125–175mg/dL) to those observed in our model. However, whether these separate models of exposure and different durations induce similar or distinct impacts on the profile of sperm-inherited ncRNAs is unknown. To examine this further, mature sperm were collected from the cauda epididymides and vas deferens of the control and ethanol-exposed males used to sire the offspring analyzed in Figure 2.2 . The purity of sperm was judged to be greater than 99% as evaluated by microscopy. Similar to previous reports (Peng et al., 2012), isolated RNAs predominantly ranged from 20 to 40 nucleotides in length (Figure 2.5 A). Small RNAs from control and ethanol-exposed males were subjected to deep sequencing analysis, with an average of 25 million mappable reads obtained per sample (n=4). Similar to previous studies describing the small RNA profiles of mouse sperm (Peng et al., 2012; Rompala et al., 2018; Sharma et al., 2016), we found that the majority of small RNA reads mapped to transfer RNA-derived small RNAs (~60% tRFs) and Piwi-interacting RNAs (~30% piRNAs) (Figure 2.5 B). The remaining small RNAs predominantly mapped to transfer RNAs (~5% tRNAs) and microRNAs (~5% miRNAs) (Figure 2.5 B). A recent study by Sharma et al., described proportional changes in the ratio of tRFs and piRNAs as sperm undergo maturation in the epididymis (Sharma et al., 2018). Here, a progressive increase in tRFs

and a loss of piRNAs were observed as sperm mature. Although sperm derived from alcohol-exposed males tended to have proportionally fewer mappable tRFs and a greater abundance of piRNAs, individually, these trends did not reach statistical significance ($p=0.0552$ and $p=0.1086$) (Figure 2.5 C-D). However, a ratio comparing tRFs:piRNAs revealed a significant shift ($p<0.05$) between the two preconception treatment groups (Figure 2.5 E). Further, while populations of tRNAs were similar between treatments, we observed a significant ($p=0.03$), ~30% increase in the abundance of miRNAs in sperm derived from alcohol-exposed males (Figure 2.5 F-G). These observations reveal that chronic alcohol consumption shifts the profile of sperm-inherited non-coding RNAs, with miRNAs exhibiting the greatest change.

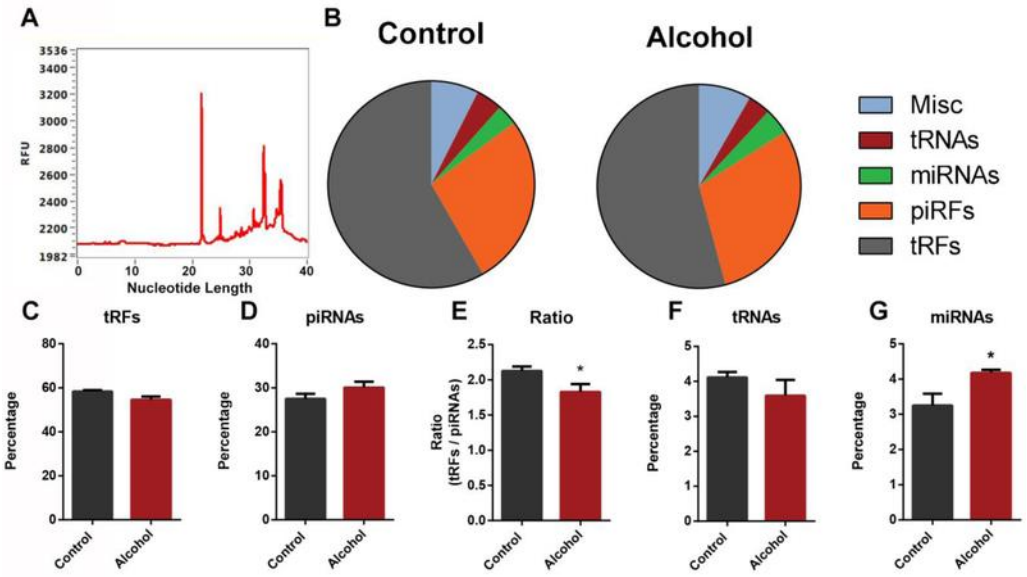

Figure 2.5 Alcohol-induced alterations to the profile of sperm-inherited non-coding RNAs. A) Representative graph depicting the size distribution of RNAs isolated from sperm. B) The proportional abundance of transfer RNA-derived small RNAs (~60% tRFs) Piwi-interacting RNAs (~30% piRNAs), transfer RNAs (~5% tRNAs) and microRNAs (~5% miRNAs) between sperm derived from the two preconception treatment groups (n=4). Individual comparison of the percentage of C) tRFs and D) piRNAs mapped between preconception treatment groups. E) The ratio of tRFs:piRNAs in sperm derived from control and alcohol-exposed males. Individual comparison of the percentage of F) tRNAs and G) miRNAs mapped between preconception treatment groups. For comparison of percentages mapped, data were arcsine transformed and an unpaired t-test with Welch's correction applied. All other comparisons were conducted using an unpaired t-test. Error bars represent the standard error of the mean (* $p<0.05$). Reprinted with permission from "Alterations in sperm-inherited noncoding RNAs associate with late-term fetal growth restriction induced by preconception paternal alcohol use" by Bedi et al. 2019. Reproductive Toxicology, 87, pp. 16, Copyright [2019] by Bedi et al

2.3.6. Alterations in the abundance of miR21, miR30, and miR142 in alcohol-exposed sperm

Using the Bowtie2 and miRDEEP2 pipelines, we compared the abundance of individual candidate small non-coding RNAs between control and alcohol-exposed sperm. No differentially enriched tRFs, piRNAs or tRNAs could be identified between treatment groups (Figure 2.6 A-C). In contrast, three differentially enriched miRNAs

could be identified between treatments (miR21, miR30, and miR142) (Figure 2.6 D). Of these, miR21 and miR142 were abundantly enriched in both treatment groups (miR21 500 (C) and 900 (A) fpkm, miR142 600 (C) and 300 (A) fpkm). However, differences in the abundance of these two candidates offset each other, and therefore, do not explain the 30% increase in miRNA enrichment observed in alcohol-exposed sperm (Figure 2.5 F). In contrast to these candidates, the remaining miRNAs identified displayed large variations both across and within treatment groups (Figure 2.6 E). Collectively, these observations indicate that the 30% increase in miRNA abundance represents a general increase and is not linked to any specific candidate. Recently, alterations in the profile of sperm-inherited miRNAs induced by chronic stress have been directly linked to increased circulating levels of corticosterone (Short et al., 2016). We, therefore, assayed the levels of this hormone in our model. No differences in corticosterone could be identified between preconception treatment groups (Figure 2.6 F). Therefore, the 30% increase in miRNA enrichment and differences in miR21, miR30 and miR142 cannot be linked to alcohol-induced changes in the profile of circulating corticosterone.

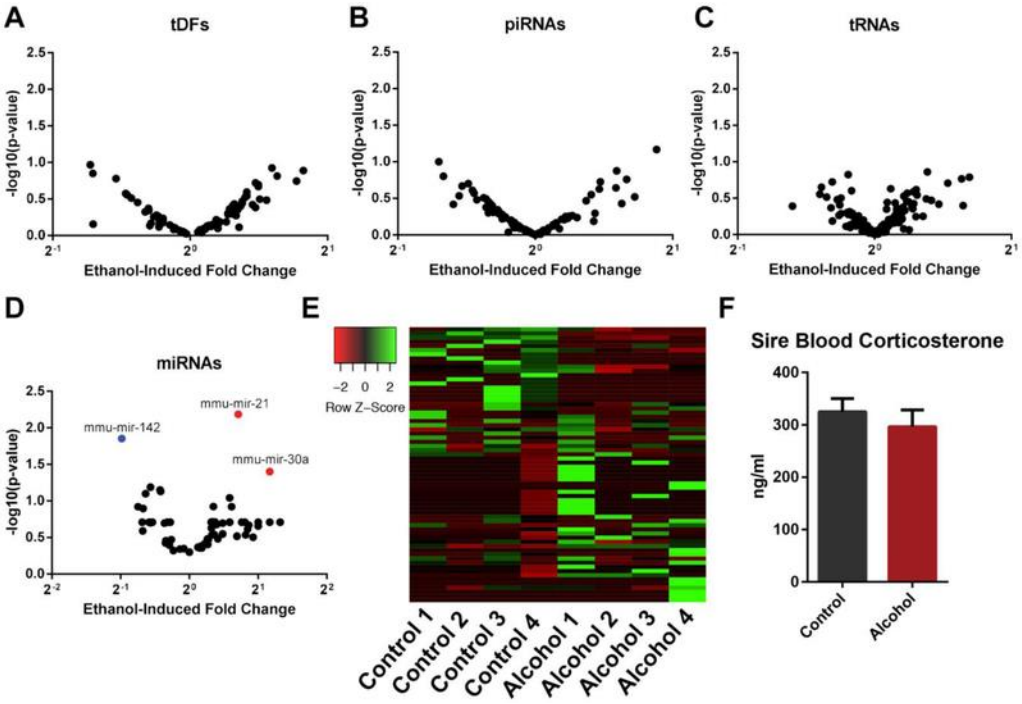

Figure 2.6 Alcohol-induced changes in the abundance of sperm-inherited miR21, miR30, and miR142. Volcano plots comparing the differential enrichment of candidate A) tRFs, B) piRNAs, C) tRNAs and D) miRNAs of sperm derived from the two preconception treatment groups. E) Heatmap comparing the variation of sperm derived miRNAs between treatment groups. F) Comparison of circulating levels of corticosterone between preconception treatment groups. An unpaired t-test was applied to compare the levels of corticosterone. Error bars represent the standard error of the mean, miRNAs identified with either blue or red dots were differentially enriched ($p<0.05$). Reprinted with permission from "Alterations in sperm-inherited noncoding RNAs associate with late-term fetal growth restriction induced by preconception paternal alcohol use" by Bedi et al. 2019. Reproductive Toxicology, 87, pp. 17, Copyright [2019] by Bedi et al

2.4. Discussion

Using a mouse model of voluntary alcohol consumption, our group recently described an association between chronic preconception paternal alcohol use and deficits in both placental function and fetal growth within the offspring (Chang et al., 2017). Subsequent studies revealed that these alcohol-induced growth phenotypes were accompanied by a prolonged period of fetal gestation and sex-specific patterns of

postnatal growth restriction (Chang et al., 2019a). These deficits in growth are similar to phenotypes described in long-term clinical studies of children with fetal alcohol spectrum disorders (Carter et al., 2013; Moore and Riley, 2015) and join a growing body of literature indicating preconception paternal alcohol use is a significant, yet under-recognized contributor to alcohol-induced growth defects (reviewed here (Day et al., 2016; Finegersh et al., 2015)). However, the question of how the memory of chronic alcohol use transmits from father to offspring remains unresolved.

The literature examining the impacts of chronic alcohol use on male reproductive physiology is varied and highly inconsistent (Condorelli et al., 2015; Van Heertum and Rossi, 2017). To this point, of three published studies using similar rodent models of exposure, two identified systemic decreases in testosterone concentrations (Anderson et al., 1980; Emanuele et al., 2001), while the third was unable to identify any reproducible changes (Salonen et al., 1992). Similarly, the human literature is equally varied, with studies describing both alcohol-associated decreases and increases in testosterone levels (Jensen et al., 2014; Muthusami and Chinnaswamy, 2005; Valimaki et al., 1990). However, combined with the negative correlations observed between alcohol use and successful outcomes in human in vitro fertilization (Klonoff-Cohen et al., 2003; Rossi et al., 2011), the prevailing feeling is that this teratogen exerts a negative effect on male reproductive function (Condorelli et al., 2015; Van Heertum and Rossi, 2017).

In this study, we returned to our voluntary model of alcohol consumption to determine the impact chronic ethanol use has on male reproductive physiology and the association of sperm-inherited noncoding RNAs with the transmission of alcohol-

induced growth defects. Here, we first confirmed that chronic preconception paternal alcohol exposure induced fetal growth restriction in the offspring and extended our previous findings by demonstrating that these deficits in growth primarily manifest during the later phase of pregnancy (Figure 2.2). We then assayed large-scale measures of male reproductive health, including testicular, epididymal and seminal vesicle weights, as well as testicular morphology and testosterone levels. However, we were unable to identify changes in any of these criteria. In addition, no differences in total sperm counts, sperm DNA fragmentation or sperm nuclear packaging were observed between the preconception treatment groups. Combined with the observed similarities in litter size between preconception treatments, we conclude that the dose and duration of alcohol exposure employed in our model do not impact macro-measures of male reproductive physiology.

As no observable changes in either sperm DNA methylation (Chang et al., 2017) or macro-measures of nuclear structure (Figure 2.4) could be observed, we examined alcohol-induced alterations in the profile of sperm-inherited noncoding RNAs. Using an inhalation model of exposure, Rompala and colleagues recently identified alcohol-induced changes in the profile of tRFs and miRNAs, as well as select mitochondrial small mRNAs in sperm (Rompala et al., 2018). In contrast to these observations, we were only able to identify differences in select miRNAs, none of which were consistent with this published study. Although both models result in sex-specific patterns of postnatal growth restriction (Rompala et al., 2017a), these two separate models of exposure may induce distinct epigenetic changes. However, we did observe some

similarities between our dataset and previous works examining the impact of paternal stress on offspring phenotype. Specifically, miR-30 and miR-21 were both up-regulated in the present study as well as in that of three previous reports examining stress-induced changes in sperm noncoding RNAs (Gapp et al., 2014a; Rodgers et al., 2013; Short et al., 2016). Although the levels of plasma corticosterone observed in our mice were higher than those reported by Rodgers et al. (Rodgers et al., 2013), we presume this difference is due to the techniques used to measure corticosterone levels and note that our results are consistent with those of two other publications employing ELISA-based measurements (Kim et al., 2013; Short et al., 2016). Regardless, we could not identify any changes in the levels of plasma corticosterone between treatment groups, indicating alcohol may alter sperm-inherited noncoding RNAs through distinct mechanisms. Importantly, the three differentially enriched candidate miRNAs identified in this study are all known to be modulated by alcohol exposure (Osterndorff-Kahanek et al., 2018; Saad et al., 2015).

Recent studies indicate that dynamic changes in the levels of tRFs, piRNAs, and miRNAs are a core feature of sperm maturation (Sharma et al., 2018). Specifically, progressive increases in tRFs are observed during epididymal transit, while conversely, piRNAs become reduced. These changes are hypothesized to be integral to sperm maturation and the reproductive success of the conceptus (Sharma et al., 2018). In this study, we observed a shift in the ratio of tRFs and piRNAs indicating that the sperm of alcohol-exposed males has proportionally fewer tRFs and more piRNAs. This may indicate that the complement of non-coding RNAs in alcohol-exposed sperm are less

mature than the controls. Of note, miR21, which is comparatively rare in testicular sperm populations, is nearly absent in the in the epididymal soma but is highly abundant in epididymosomes of the caput region of the epididymis (Belleannee et al., 2013; Nixon et al., 2015; Reilly et al., 2016). This suggests that the alcohol-induced shifts in noncoding RNAs may primarily be mediated by effects on epididymal trafficking. However, further studies are needed to confirm this hypothesis.

At this point, we do not know if the modest changes in noncoding RNA abundance identified in this study are directly linked to the alcohol-induced growth restriction phenotypes observed in the offspring. The comparative contribution of sperm-inherited RNAs to the vast repertoire found in the early conceptus is negligible (Yang et al., 2016) and further, no mechanisms have been identified by which this small contribution could stably alter the gene expression profile of the early embryo and the long-term health of the offspring. In light of this, it is challenging to see how modest changes (50% decrease in miR142, 1.5-fold increases in miR21 and miR30) in the identified candidates could induce fetal growth restriction with the consistency observed in our model, as well as mediate the long-term impacts on offspring metabolic health. One possibility is that the paternally-inherited RNAs are post-transcriptionally modified to confer dramatically enhanced stability, which may potentiate their impacts beyond preimplantation development and influence the processes of lineage specification (Chen et al., 2016b). It may also be that unrelated alterations in sperm histone retention and chromatin looping mediate the observed effects or a combinatorial interaction between multiple epigenetic mediators. Finally, we have not ruled out the possibility that these

phenotypes may be due to alcohol-induced changes in the seminal plasma. In previous studies, ablating the seminal vesicle gland induced placental hypertrophy in late gestation and sex-specific effects on the long-term growth and metabolic health of the offspring (Bromfield et al., 2014). Although the effects on offspring growth were opposite to those observed in our model, the impact on placental growth is compelling. Future studies using IVF will be necessary to determine the impact of male seminal plasma in mediating the effects of paternal alcohol use on the offspring.

3. PRECONCEPTION PATERNAL ALCOHOL EXPOSURE INDUCES SEX-SPECIFIC CHANGES IN PLACENTAL GENE EXPRESSION AND ALTERED CTCF LOCALIZATION ACROSS MULTIPLE GENE CLUSTERS

3.1. Introduction

Although cited as the consequence of maternal drinking, emerging preclinical research demonstrates that male alcohol use before conception also associates with fetal alcohol spectrum disorder (FASD) phenotypes. Similar to other models of altered paternal epigenetic programming, preconception male alcohol exposures result in behavioral, growth, metabolic, and physiologic effects in the offspring (Rompala et al., 2019). Collectively, these studies indicate that paternal alcohol use before conception is a significant contributing factor to the incidence and variation of FASD phenotypes. Further, they reveal that, in addition to acute toxicity, heritable alterations in the developmental program also drive the development of alcohol-induced structural and behavioral defects. However, the mechanisms by which alcohol heritably alters the developmental program, transmitting the memory of exposure across life stages, remain unknown.

Although perceived as a childhood disorder, FASD growth deficits are, in fact, lifelong and associate with long-term immune dysfunction, hyperinsulinemia, and other endocrine disruptions (Carter et al., 2013; Castells et al., 1981; Day et al., 2002; Moore and Riley, 2015). Despite more than fifty years of study, the breadth and developmental origins of these defects remain poorly described. However, like other models of altered

developmental programming, disruptions in placental morphogenesis and function are suspected of playing a significant role (Kalisch-Smith et al., 2019).

Parental exposure history, external stressors, and genetic susceptibilities all converge to negatively influence placental growth and function (Nugent and Bale, 2015; Rosenfeld, 2015). Notably, despite a wide range of exposures, multiple, divergent models of altered developmental programming exhibit many similar patterns of placental dysfunction, which correlate with related patterns of behavioral, and metabolic defects later in life. In addition, researchers postulate that variance in the patterns of fetal-placental growth between males and females underly the emergence of sex-specific phenotypic differences in adult offspring (Kalisch-Smith et al., 2017; Rosenfeld, 2015). Therefore, understanding how altered developmental programming, either before conception or during early life, influences the formation and function of the placenta is crucial to defining the developmental basis of multiple exposure-associated phenotypes.

Previous studies from our lab indicate that preconception male drinking is associated with fetal growth restriction, placental overgrowth, and sex-specific patterns of postnatal growth restriction and metabolic dysfunction (Bedi et al., 2019; Chang et al., 2017, 2019a, 2019b). These observed differences in placental growth and gene expression, through altered placental-endocrine signaling, may program some of the sex-specific growth and metabolic defects we observe in adulthood (Chang et al., 2019a, 2019b). Several tissues exhibit sex-biased gene expression patterns, including the brain, liver, kidney, and immune system (Mayne et al., 2016; Qu et al., 2015; Rinn et al., 2004). Significantly, sex-specific differences in the gene expression profiles of these

tissues underly variations in xenobiotic metabolism, cancer aggression, and the incidence of autoimmune disease between males and females (Ruggieri et al., 2010; Waxman and Holloway, 2009). However, few studies have examined sexually dimorphic changes in placental gene expression or correlated these differences with sex-specific phenotypic outcomes.

Differential patterns of gene expression observed between males and females are the consequence of sex-specific enhancer-promoter interactions (Matthews and Waxman, 2020; Sugathan and Waxman, 2013). Enhancers are short DNA elements that bind large conglomerates of transcription factors and regulate the transcription of genes located several kilobases or even megabases away (Reiter et al., 2017). The folding of nuclear DNA into organized loops bridges the large gaps between gene promoters and gene enhancers, enabling clusters of genes to be regulated by a common set of enhancers. Chromatin architectural proteins, including the zinc finger proteins CCCTC-Binding Factor (CTCF) and the Cohesin complex, organize and facilitate inter-loop bridges between genes and their respective enhancers (Handoko et al., 2011; Ji et al., 2016; Kagey et al., 2010; Rao et al., 2014; Whalen et al., 2016). Significantly, CTCF also plays a role in folding the sperm genome, and CTCF binding site accessibility transmits to the early embryo (Arpanahi et al., 2009; Jung et al., 2017, 2019). Thus, if alcohol induces alterations in CTCF localization during spermatogenesis, these abnormalities may transmit to the early offspring and stably alter chromatin looping in the developing conceptus. Therefore, we hypothesized that differences in placental

growth and gene expression induced by preconception paternal alcohol exposure would correlate with alterations in CTCF localization.

Here, we report that both the male and female progeny of alcohol-exposed sires displayed altered expression of similar cohorts of genes but that the direction of change was diametrically opposite between males and females. Notably, many of these candidate genes localized to co-regulated gene clusters, suggesting a higher order of transcriptional control was perturbed. In focusing on the male offspring, we find that, similar to previous studies examining transcriptional control across gene clusters (Espitia Jaimes et al., 2018; Handoko et al., 2011; Mishiro et al., 2009), disrupted gene expression patterns correlate with reductions in CTCF occupancy at gene promoters and putative enhancers. Unexpectedly, altered CTCF occupancy does not correlate with changes in placental DNA methylation. These data reveal that paternally inherited, DNA methylation-independent epimutations induced by alcohol alter the positioning of CTCF chromatin boundary elements, which correlate with the emergence of sexually dimorphic changes to a common set of genes.

3.2. Materials and Methods

3.2.1. Animal Studies and Tissue Collection

All experiments were conducted under AUP 2014-0087 and approved by Texas A&M University IACUC. In the outlined experiments, the male mice were of a C57BL/6(Cast7) background, while female mice were C57BL/6J (RRID: IMSR_JAX:000664). We obtained the C57BL/6(Cast7) strain of mice from the

Bartolomei laboratory, the derivation of which is described here (Mann et al., 2003). We have previously described the preconception paternal alcohol exposures, animal breeding, and tissue collections for the samples used here (Chang et al., 2017). Briefly, on postnatal day 90, we provided adult C57BL/6(Cast7) males with limited access to ethanol (EtOH) during a four-hour window, immediately after the initiation of their sleep cycle. During this time, we provided experimental males access to either a solution of 10% (w⁄v) EtOH and 0.066% (w⁄v) Sweet'N Low (Cumberland Packing Corp, Brooklyn NY, USA) (experimental), while we exposed control males to 0.066% (w⁄v) Sweet'N Low alone. After 70 days of exposure, we paired exposed C57BL/6(Cast7) males with naive C57BL/6J dams and collected fetal-placental tissues on day 14.5 of gestation (GD14.5).

3.2.2. Sex Determination

We isolated genomic DNA using the DNeasy Blood and Tissue Kit (catalog # 69504; Qiagen, Germantown MD, USA) and carried out PCR amplification of the *Zfy* and *Xist* genes. Primers are listed in Table 1.

3.2.3. RNA sequencing and Data processing

We isolated total RNA from GD14.5 fetal placentae using the RNeasy Plus Mini Kit (catalog # 74134; Qiagen, Germantown MD, USA), according to the manufacturer's instructions. We generated RNA-libraries using the Illumina RNA-seq preparation kit followed by pooling and high-throughput sequencing on an Illumina HiSeq 2500

(Genomic Core at Whitehead Institute for Biomedical Research, Cambridge, MA, USA). We mapped the raw reads to the mm10 database using tophat (Trapnell et al., 2012) and then assembled reads using cufflinks. We then used Cuffdiff to assign each gene an expression value in FPKM and report the statistical significance using an FDR-corrected p-value of $q<0.05$ (Trapnell et al., 2012). Finally, we performed functional analysis of differentially expressed genes using the Ingenuity Pathway Analysis (IPA) version 2.0 (Jiménez-Marín et al., 2009).

3.2.4. Analysis of gene expression using Reverse Transcription Quantitative Polymerase Chain Reaction (RT-qPCR)

We isolated RNA from placental tissues using Trizol (catalog# 15596026; Thermo-Fisher, Waltham, MA, USA) and treated 1ug RNA with DNAase I (catalog# AMPD1; Sigma, St. Louis MS, USA) according to the recommended protocols. We mixed isolated RNAs with 1µL 10mM dNTP (catalog # 18427-013; Thermo-Fisher, Waltham, MA, USA), 1µL random hexamer oligonucleotides (catalog# 48190011; Thermo-Fisher), 11µL water and incubated at 70℃ for 5min. After cooling on ice, we added SuperScriptII reaction buffer, DTT, and SuperScriptII, according to the SuperScriptII system (catalog# 18064-071; Thermo-Fisher). We then incubated samples at 25℃ for 5 minutes, 42℃ for 50 minutes, 45℃ for 20 minutes, 50℃ for 15 minutes and finally 70℃ for 5 minutes. We measured the relative abundance of individual genes using the Dynamo Flash master mix (catalog# F-415XL; Thermo Scientific), according

to the manufacturer's protocol, on a Bio-Rad CFX38 PCR system. Primers are listed in Table 1.

3.2.5. Chromatin Immunoprecipitation (CHIP) Analysis

We dispersed placentas into single-cell suspensions using 100μm cell strainers (catalog # 352360; Corning Life Sciences, Corning, NY, USA), as described previously (Veazey et al., 2015). We performed Chromatin Immunoprecipitations (ChIP) as previously described (Chang et al., 2019b). We purified eluted DNA using Qiaquick PCR Cleanup kit (catalog# 28106; QIAGEN). The antibodies we used include: anti-H3K4me1 (catalog# 39297; Active Motif, Carlsbad, CA, USA); anti-H3K27ac (catalog# 39133; Active Motif); anti-CTCF (catalog# 07-729, Millipore-Sigma, Burlington, MA, USA); anti-Rad 21 (catalog# ab992; Abcam, Cambridge, MA, USA). All antibodies were used at 1 ug/reaction, including the negative control IgG (catalog# SC-2027; Santa Cruz Biosciences, Santa Cruz, CA, USA). After purification, we shipped a portion of the purified ChIP DNA samples to the Whitehead Genomic Services (Cambridge, MA), where 200-400 bp size selected DNA libraries were generated using the Swift 2S DNA Library prep kit (catalog# 44384; Swift Biosciences, Ann Arbor, MI, USA). The libraries were sequenced as single-end 50-bp reads with an average depth of 35 million reads per sample. Finally, using qPCR, we assayed precipitated DNAs for relative enrichment using the Dynamo Flash supermix (catalog# F-415XL; Thermo Scientific) on a Bio-Rad CFX38 PCR system. Primer sequences are listed in Table 2.

3.2.6. ChIP-Sequencing Data Processing

We uploaded all sequence files to the Galaxy server (Afgan et al., 2018) (usegalaxy.org) for further processing. We then used Trimmomatic (Bolger et al., 2014) to trim FASTQ files for end quality and remove adapters. We then mapped trimmed reads to the mouse reference genome (mm10) using the Burrows-Wheeler Alignment tool BWA (Li and Durbin, 2009), and we only retained reads with a minimum MAPQ score of 20 for downstream analysis as BAM files.

3.2.6.1. Peak calling and differential peak analysis

We used MACS2 (Feng et al., 2012) to analyze CTCF ChIP-seq datasets and to call peaks enriched against mapped reads obtained from Input files with an FDR threshold of 0.1. We determined the fragment size 'd' from alignment results using the MACS2 predictd tool, and we used this data as the extension size for the MACS2 callpeak tool. We converted Bedgraph treatment file outputs to BigWig files for visualization in Integrative Genomics Viewer (IGV) (Thorvaldsdóttir et al., 2013). We extracted peaks from the narrowpeaks outputs common to all Control samples and all Treatment samples using BEDTools (Quinlan and Hall, 2010). We only considered intersecting peaks if at least a 0.25 fraction of the genomic intervals overlapped in both samples. We characterized the peaks unique to the Treatment group as "gained peaks" while those found only in Control samples were "peaks lost". We used the bdgdiff function in MACS2 to identify differential peaks with likelihood ratio > 1000.

3.2.6.2. DNA sequence motif analysis

We extracted genomic DNA sequences from the resulting datasets into a fasta file. Next, we analyzed these large nucleotide datasets sequences for Motif discovery, enrichment analysis, and clustering using MEME-ChIP (Ma et al., 2014). We then compared the resulting enriched motif sequences to known motifs in the HOCOMOCO Mouse motif database using the motif comparison tool Tomtom (Gupta et al., 2007).

3.2.6.3. Visualization of peaks and regions of interest

We converted all peak files to BigWig files and visualized the separate tracks in IGV. We then loaded the BED files marking genomic intervals of peaks gained or lost directly from Galaxy to IGV. Finally, we downloaded and visualized the published annotation BED file ENCSR121NJX demarcating known candidate cis-regulatory elements in the C57BL6 placenta, which we obtained from the ENCODE portal (https://www.encodeproject.org/) (Consortium et al., 2020).

3.2.7. Data treatment and Statistical analysis

For analysis of gene expression, the replicate cycle threshold (Ct) values for each transcript were compiled and normalized to the geometric mean of the three reference genes including, succinate dehydrogenase complex, subunit A (Sdha NM_023281), mitochondrial ribosomal protein L1 (Mrpl1 NM_053158) and hypoxanthine-phosphoribosyl transferase (Hprt NM_013556) (Carnahan et al., 2013). We calculated normalized expression levels using the ddCt method described previously (Schmittgen

and Livak, 2008). We then transferred the derived relative fold change values from each biological replicate into the statistical analysis program GraphPad (GraphPad Software, Inc., La Jolla, CA), where we then verified data for normality using a Shapiro-Wilk test. We set significance at p-value < 0.05 and utilized a two-way analysis of variance (ANOVA), followed by Tukey's HSD analysis, to contrast the effects of sex and preconception treatment. In all instances, we have marked statistically significant differences with an asterisk.

For qPCR-based analysis of candidate gene regulatory region enrichment, we first normalized ChIP samples to 1% input, using the formula previously described (Mukhopadhyay et al., 2008). Next, to independently examine alterations in each post-translational modification, we normalized the means from each independent sample to the control average. We then tabulated the results of 3 independent experiments and calculated the cumulative means and standard error of the mean. Finally, the Values from each biological replicate were transferred into the statistical analysis program GraphPad (GraphPad Software, Inc., La Jolla, CA). We verified normality using a Shapiro-Wilk test and then used a student's unpaired t-test to assess differences.

3.2.8. Reduced Representation Bisulfite Sequencing (RRBS) and Data Processing

For each sample, we digested 300 ng of placental DNA with MSP1 (2 hours, enzyme 20U/sample) at 37°C followed by TaqαI (2 hours, 20U/sample) at 65°C. We then size-selected the digested DNA for fragments larger than 300 bp and subjected samples to bisulfite treatment using the Methylamp DNA Bisulfite Conversion Kit

(catalog# P-1001; Epigentek, Farmingdale, NY, USA). We verified that the DNA was >99% converted, then performed library preparation by DNA end polishing and adaptor ligation followed by library amplification using indexed primers. We eluted the purified library in 12 µl and verified integrity using a Bioanalyzer and KAPA Library Quantification. We sequenced 10 nM of sample libraries on an Illumina HiSeq 2500 (EpigenTek Farmingdale, NY, USA). We merged replicate Fastq files into a single fastq file and performed quality analysis using Fastqc. We trimmed the reads using TrimGalore (-q 20, adapter AGATCGGAAGAGC, --length 20, --rrbs) and processed the sequences using the Babraham Bioinformatic's program, Bismark (www.bioinformatics.babraham.ac.uk/projects/bismark/Bismark_User_Guide.pdf). The reference bisulfite genome was produced via "bismark_genome_preparation", and "bismark" was run against the converted genome (--non_directional, --bowtie1, -n 1, -q). We sorted and indexed the resulting BAM files using the "samtools sort" and "samtools index" programs. We converted the sorted/indexed BAM files into SAM files using the "samtools view" program. We performed the remaining analysis using MethylKit in RStudio.

3.2.9. Western Blot

Placentas were homogenized in pH 7.5 Tris lysis buffer including 50mM Tris, 1mM EGTA, 150mM NaCl, 1% Triton X-100, 1% β-mercaptoethanol, 50mM NaF and 1mM Na3VO4. Samples were separated on 8% sodium dodecyl sulfate-polyacrylamide gels by electrophoresis and then transferred to PVDF membranes. Primary antibodies

used in this study were anti-CTCF (catalog# 07-729, Millipore); anti-beta actin (catalog# ab8227, Abcam). We visualized blots using secondary antibodies conjugated to horseradish peroxidase (Life Technologies, Waltham, MA) and an enhanced chemiluminescence detection system (Pierce, Rockford, IL). We determined the relative expression of CTCF as a ratio to β -actin by quantifying band intensities using ImageJ (National Institutes of Health, Bethesda, MD). Each experimental group contains eight different animals (n = 8).

3.3. Results

3.3.1. The placentae of offspring sired by alcohol-exposed males exhibit sex-specific changes to a common cohort of genes.

To better understand alterations in placental physiology induced by paternal alcohol exposure, we returned to the RNA-sequencing data sets generated from placental samples isolated on gestational day 14.5 (Chang et al., 2017). This stage represents the earliest phase at which we can detect alterations in fetal growth and placental efficiency. Using more current informatic tools and a more robust FDR-corrected p-value of $q<0.05$, we reanalyzed these data and identified a higher-confidence set of differentially expressed genes. Specifically, we identified 287 differentially expressed genes between placentae derived from the male offspring of control and alcohol-exposed males, with 283 displaying decreased expression and only 4 displaying an increased expression (Figure 3.1 A). In the female offspring of alcohol-exposed sires, we identified 265 differentially expressed genes, with 12 downregulated and 153 upregulated genes

(Figure 3.1 A). Out of the 387 significantly altered genes in male placentas and 357 in females, 218 genes were common to both groups. Unexpectedly, most of these candidate genes displayed diametrically opposite patterns of change in male offspring (downregulation) compared to the female offspring (upregulation) (Figure 3.1 B). From these observations, we conclude that although a similar cohort of genes become misregulated in the placental tissues of offspring sired by alcohol-exposed sires, the direction is sex-specific.

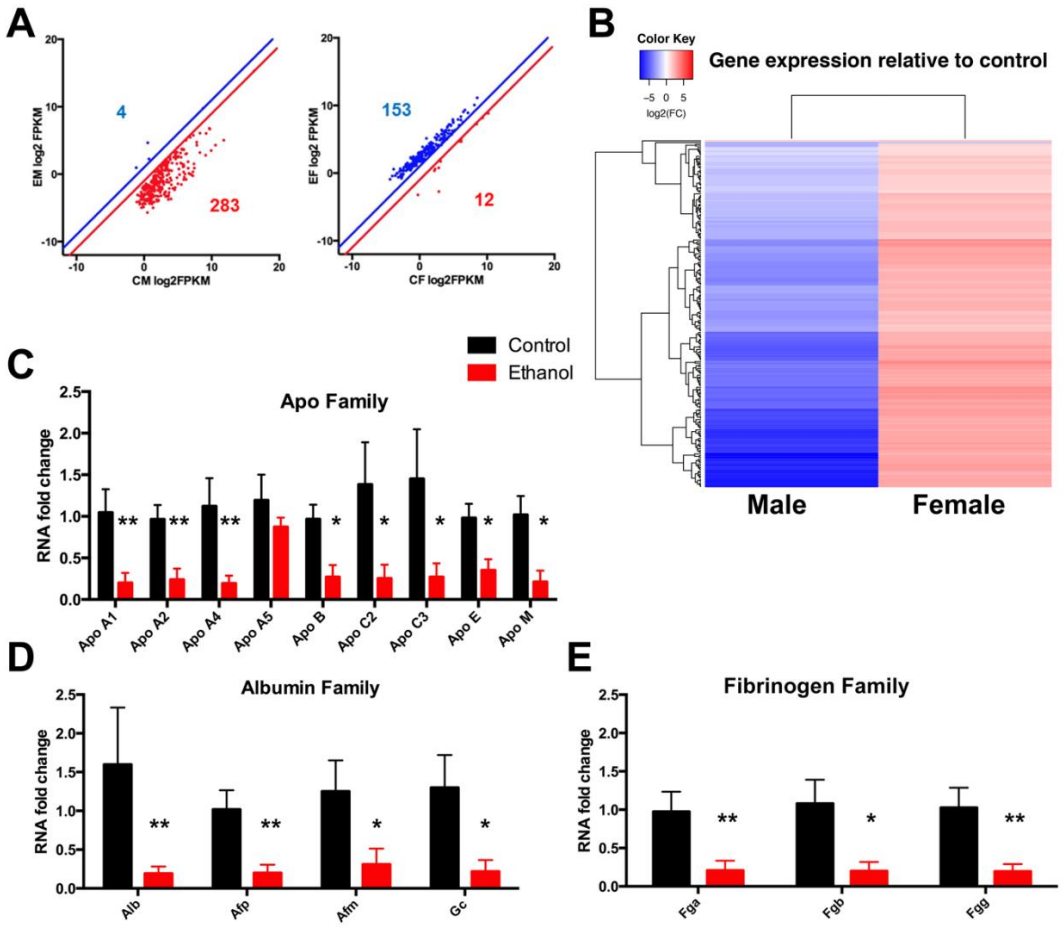

Figure 3.1 Preconception paternal alcohol exposure induces sexually dimorphic changes to a common cohort of genes, including candidates located in the albumin, apolipoprotein, and fibrinogen gene clusters. A) Comparison of the placental transcriptome between male (left) and female (right) offspring sired by males exposed to the control and ethanol preconception treatments. Analysis produced using cuffdiff, with an FDR-corrected p-value ($q<0.05$; n=2). B) Heatmap comparing the differential expression of candidate genes between placentae derived from the male and female offspring of control and ethanol-exposed sires. Using RT-qPCR, we assayed the expression of candidate genes belonging to the C) apolipoprotein, D) albumin, and E) fibrinogen gene families. Gene expression was normalized to the geometric mean of transcripts encoding Sdha, Mrpl1, and Hprt. (n=8) Error bars represent the standard error of the mean, * $P < 0.05$, ** $P < 0.01$. Note: Apoa1, Apo3c, Apoa4, and Apoa5 all localize to the apolipoprotein gene cluster on mouse chromosome 9.

3.3.2. Dysregulated genes localize to gene clusters

In both males and females, the top five scored molecular and cellular functions of the identified differentially expressed genes were molecular transport, protein synthesis, lipid metabolism, small molecule biochemistry, and vitamin and mineral metabolism, which all play important roles in placental function during development. In addition to the emergence of these functional groups, several gene families colocalizing to gene clusters all displayed changes in gene expression. Therefore, we assayed the expression of genes within three of the identified clusters. Given that placental growth phenotypes induced by paternal alcohol exposure are more severe in the male offspring (Bedi et al., 2019; Chang et al., 2017), we focused our validation analysis on male placentae. Consistent with our revised RNA-seq analysis, transcript levels of multiple apolipoproteins, including Apoa1, Apoa2, Apoa4, Apob, Apoc2, Apoc3, Apoe, and Apom were significantly reduced in male offspring sired by alcohol-exposed sires (Figure 3.1 C). Interestingly, Apoa1, Apo3c, and Apoa4, which all localize to the apolipoprotein gene cluster located on mouse chromosome 9, were downregulated, while in contrast, the lone remaining gene in this cluster, Apoa5 remained unchanged. Unlike the other genes in this cluster, Apoa5 is not regulated by the centrally located apoCIII enhancer (Gao et al., 2005). In addition to the apolipoproteins, we also observed reduced transcription of other critical transport proteins, including Alb, Afp, Afm, Gc, and Ttf, and finally, the fibrinogen proteins Fga, Fgb, and Fgg (Figure 3.1 D-E). Notably, the transcriptional dysregulation we observed in these candidate genes impacted most, if not all, of the genes located in their respective clusters, with nearly the entire complement of

the albumin, apolipoprotein, and fibrinogen gene clusters demonstrating simultaneous down-regulation. These reductions are similar to observations reported in experiments examining changes in gene expression induced by depletion of chromatin factors facilitating enhancer-promoter looping (Handoko et al., 2011; Mishiro et al., 2009).

3.3.3. Alterations in CTCF binding within the placentae of the male offspring sired by alcohol-exposed sires

To determine if alterations in the localization of chromatin-binding proteins contribute to alterations in placental gene expression observed in the offspring of alcohol-exposed sires, we used chromatin immunoprecipitation followed by deep sequencing of isolated DNAs (ChIP-seq). In human cells, CCCTC-binding factor (CTCF) facilitates the chromatin organization required to control the expression of genes within the apolipoprotein and fibrinogen gene clusters (Espitia Jaimes et al., 2018; Mishiro et al., 2009). Significantly, deletion of either the CTCF sites within these loci or RNA-interference mediated depletion of CTCF protein simultaneously reduces gene expression across these gene clusters by half. As we observed a similar phenomenon in placentae derived from the male offspring of alcohol-exposed sires, we focused our analysis on CTCF localization in male placentae.

Our sequencing experiments yielded a good correlation between experimental replicates (Figure 3.2 A). The identified peaks demonstrated strong enrichment of the consensus CTCF binding site (Figure 3.2 B; p=1.1e-1146), and principal component analysis identified a clear separation between samples derived from the different

preconception treatment groups (Figure 3.2 C). Consistent with previous studies examining CTCF localization, 30% of reads mapped to distal intergenic regions while the remainder mapped to gene bodies (45%) and promoters (25%) (Figure 3.2 D). Using MACS2 with a minimal intersection of 100bp, we identified 6,252 high-confidence peaks in all samples derived from the offspring of control males and 7,072 in offspring sired by alcohol-exposed males (Figure 3.2 E). Notably, 99% of identified peaks mapped to placental regulatory regions identified by the ENCODE consortium (Consortium et al., 2020).

Of the high-confidence CTCF peaks we identified, 4366 were consistent between both treatment groups. However, compared to placental tissues isolated from the offspring of controls, the male offspring of alcohol-exposed sires lost 1916 peaks and gained 2711 unique peaks (Figure 3.2 E). When we mapped these peaks to the nearest gene and examined this list using IPA, we identified an enrichment of pathways participating in molecular transport, cellular movement, and tissue morphology (Figure 3.2 F). We then directly contrasted differential patterns of CTCF binding to the 287 differentially expressed transcripts we identified in Figure 3.1 above, 203 of which mapped to known genes. Of these differentially expressed genes (DEGs), 25% exhibited altered CTCF binding within 100kb of their transcriptional start sites (TSS); 44 (15%) exhibited increased CTCF binding, and 30 (10%) displayed reductions. These data are consistent with recent studies examining RNAi-depletion of CTCF, demonstrating that 25% of differentially expressed genes are directly bound by this protein (Khoury et al., 2020; Nora et al., 2017; Ren et al., 2017; VonHandorf et al., 2018).

Interestingly, while the overall proportion of peaks gained or lost were evenly distributed across gene bodies, a higher proportion of DEGs corresponded to increased CTCF binding 1-5 and 5-10 kb away and reduced CTCF occupancy 10-50 and 50-100 kb away from the affected gene TSS (Figure 3.2 G). These observations suggest that an increase in CTCF binding has a more significant effect on gene regulation within 10 kb, and a reduction in CTCF strength affects genes located more distally.

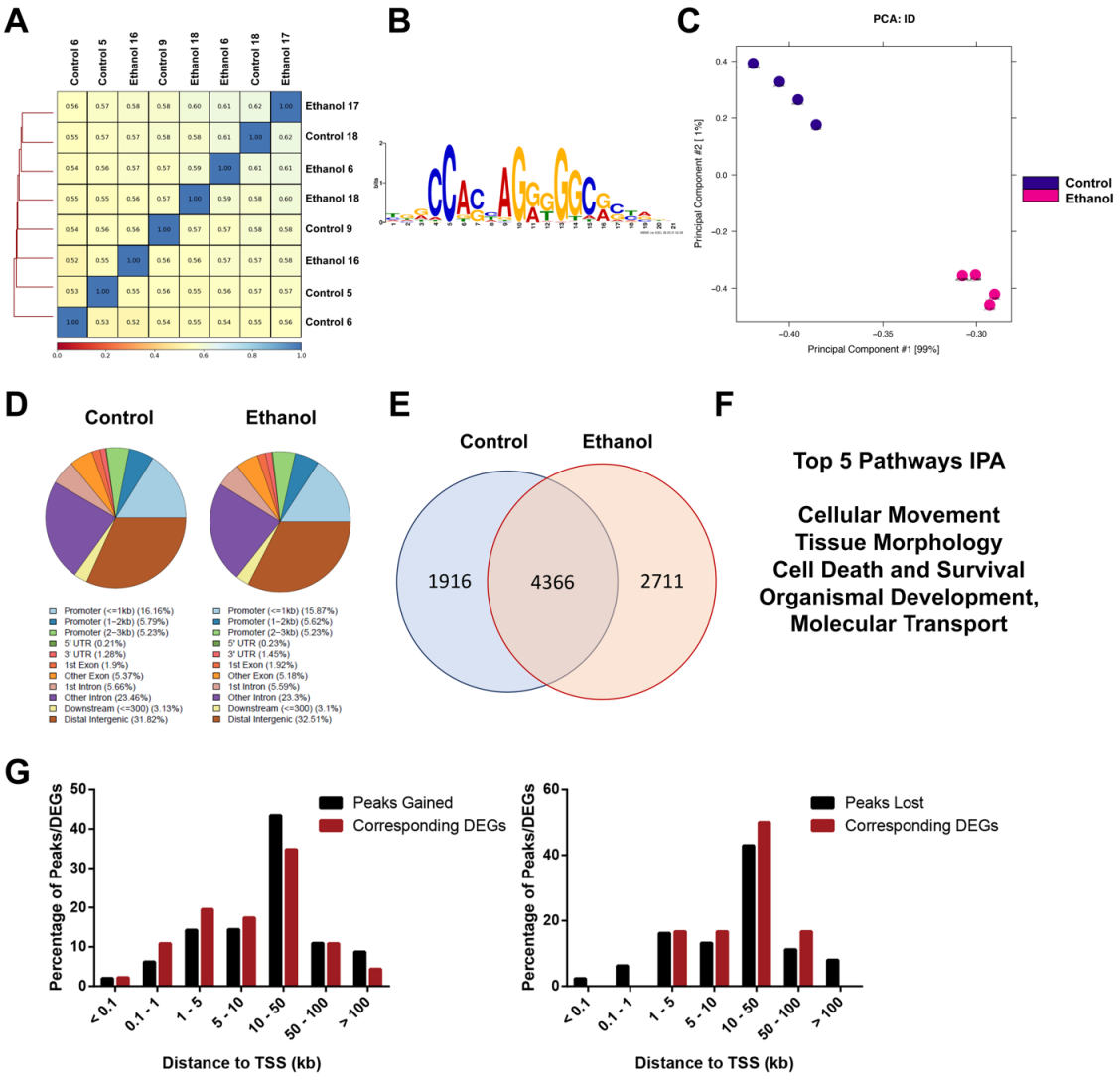

Figure 3.2 Chromatin immunoprecipitation analysis reveals preconception paternal alcohol exposure induces alterations in placental CTCF localization. A) Correlation analysis between placental samples derived from the male offspring of control and ethanol-exposed sires (n=4). B) Strong enrichment of the consensus CTCF binding site in precipitated DNA. C) Principle component analysis and D) genomic distribution of CTCF precipitated fragments compared between the preconception treatment groups. E) Venn diagram and F) Integrated Pathway Analysis comparing differential patterns of CTCF binding between male placentae derived from control and ethanol-exposed sires. G) Correlation of CTCF peaks gained (left) and lost (right) with the transcriptional start sites of the differentially expressed genes identified in Figure 3.1.

Similar to previous studies, we observed alterations in CTCF peak height and width across multiple loci corresponding to regulatory regions shared among multiple

tissue types (Figure 3.3). Importantly, in further support of a role for altered CTCF binding in modifying the expression of our identified candidate genes, we identified altered CTCF enrichment at multiple loci across the identified gene clusters (representative peaks from the albumin and apolipoprotein gene clusters shown below).

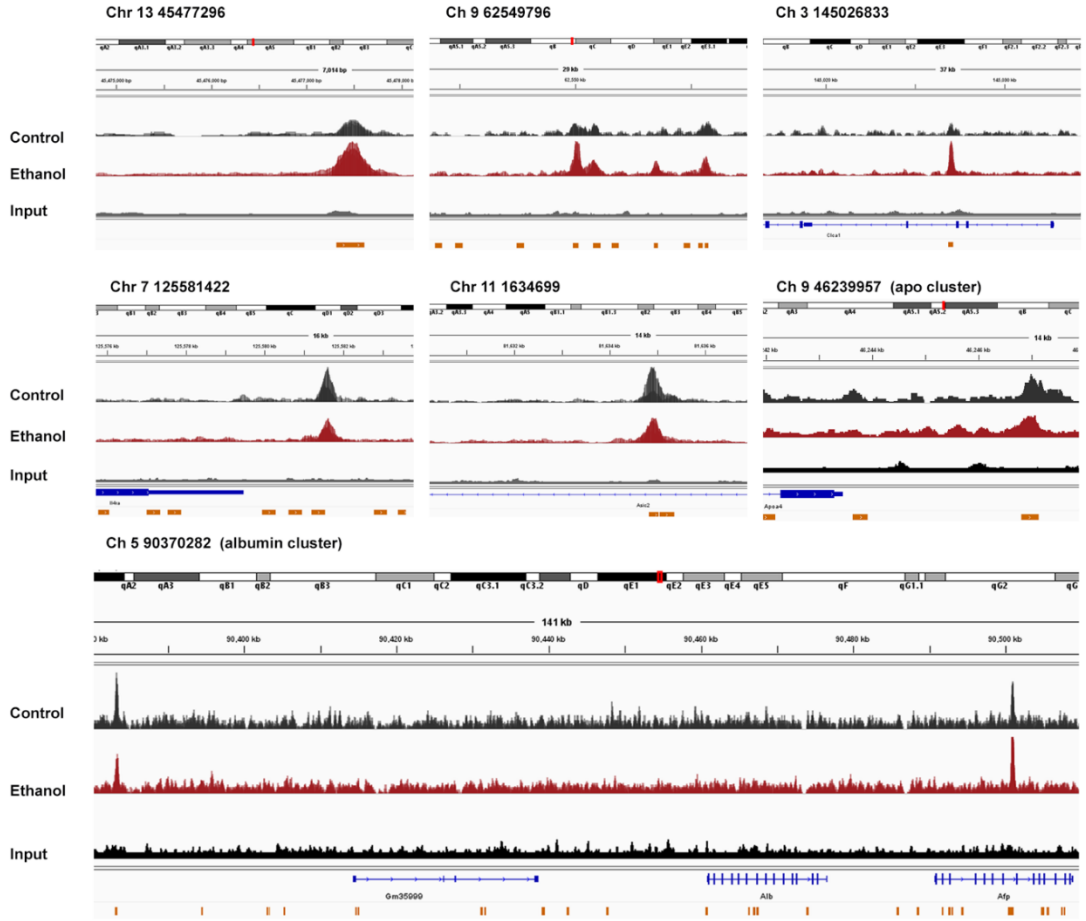

Figure 3.3 Altered placental CTCF enrichment between the offspring of control and ethanol-exposed sires. Integrative Genome Viewer tracks of chromosomal regions exhibiting differential CTCF enrichment. Regions include the apolipoprotein cluster on chromosome 9 (middle right) and the albumin cluster located on chromosome 5 (bottom panel).

3.3.4. Reductions in CTCF occupancy within candidate gene clusters

We returned to the apolipoprotein, albumin, and fibrinogen gene clusters to validate our ChIP-seq studies, as these regions all displayed altered CTCF binding and co-incident patterns of transcriptional dysregulation. Using qPCR, we assayed the enrichment of CTCF at select regions across these gene clusters (representative map of the albumin cluster is presented in Figure 3.4 A). We selected candidate enhancers (**E**) and candidate insulators (**I**) based on the enrichment of CTCF from our datasets, recent studies of these gene clusters in mouse and human liver (Espitia Jaimes et al., 2018; Matthews and Waxman, 2018; Mishiro et al., 2009), as well as published profiles of H3K27ac and H3K4me1 derived from CHIP-seq profiles in trophectoderm stem cells (Shen et al., 2012). These studies identified altered enrichment of CTCF across multiple distal enhancer and promoter regions within loci across all three of the examined gene clusters (Figure 3.4 B-D). Interestingly, most of these changes localized to promoter regions or tissue-specific enhancers. Using the albumin cluster as an example, the large enhancer located upstream of the albumin gene (Matthews and Waxman, 2018) is absent in placental cells, as is the upstream CTCF peak. However, the region upstream of alpha-fetoprotein contains multiple CTCF binding sites, which are reduced in placentae derived from alcohol-exposed males. In contrast, one of the CTCF peaks located within the gene body of alpha-fetoprotein, present in both liver and placental cells, increased in placentae derived from alcohol-exposed males (Figure 3.3 bottom panel). These results indicate that select CTCF sites across these gene clusters display altered enrichment in placentae derived from the offspring of ethanol-exposed males.

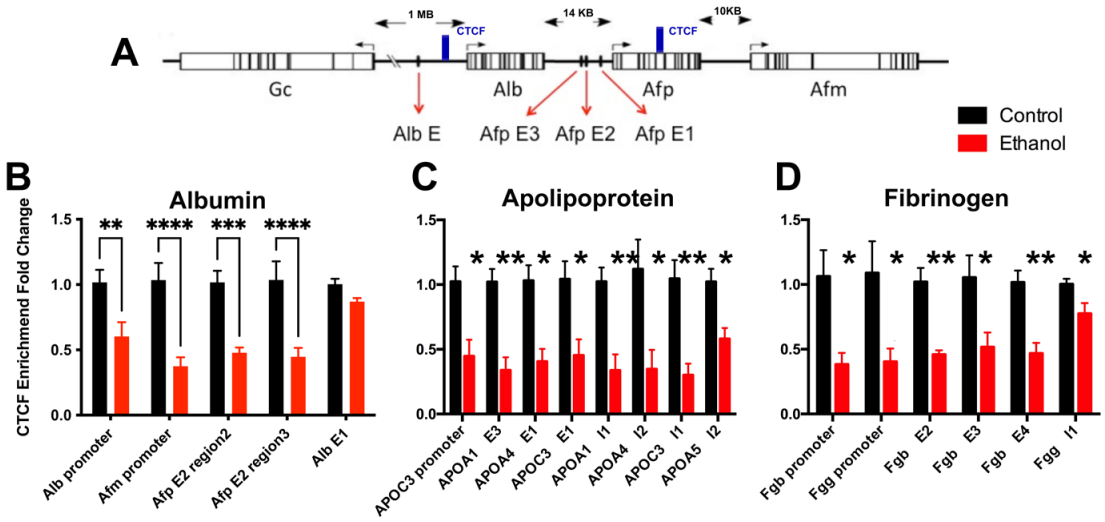

Figure 3.4 Validation of altered CTCF binding within candidate gene clusters. A) Map of the albumin gene cluster with known CTCF peaks previously identified in mouse liver 53 demarcated in blue, and enhancer regions upstream of alpha-fetoprotein (Afp) identified in red. Altered CTCF enrichment within the (B) albumin, (C) apolipoprotein, and (D) fibrinogen gene clusters. We performed chromatin Immunoprecipitation (ChIP) analysis on cellular extracts derived from GD14.5 placentae using antibodies recognizing CTCF. We assayed precipitated extracts for the enrichment of promoter regions, candidate Enhancers, or Insulators within the indicated loci. ChIP experiments were performed on a total of 8 placentae across five different litters, and data analyzed using a two-way ANOVA followed by Uncorrected Fisher's LSD. Error bars represent the standard error of the mean, * P < 0.05, ** P < 0.01, **** P < 0.0001.

3.3.5. Alterations in CTCF occupancy do not correlate with changes in the Cohesin complex member Rad21 or broad changes in enhancer associated histone posttranslational modifications

CTCF and the cohesion complex are both required for DNA looping (Nora et al., 2017), which form insulated loops, a subset of which facilitate promoter-enhancer interactions (Ren et al., 2017; VonHandorf et al., 2018). Importantly, Cohesin lacks sequence-specific DNA binding activity and requires DNA binding factors, like CTCF, to be loaded onto chromatin (Ciosk et al., 2000). Therefore, altered CTCF binding would be expected to influence both CTCF binding and enhancer function. Using ChIP, we

examined placental extracts for the enrichment of Cohesin complex member Rad21. In addition, we also examined the enrichment of histone H3, lysine four monomethylation (H3K4me1), and histone H3, lysine 27 acetylation (H3K27ac), given their association with poised and active gene enhancers, respectively (Creyghton et al., 2010).

Unexpectedly, using primers targeting the candidate regions exhibiting altered CTCF enrichment within the albumin, apolipoprotein, and fibrinogen gene clusters above, we did not observe any alterations in Rad21 binding, which was constant across all examined loci (Figure 3.6). Further, only one region displayed a decrease in H3K27ac enrichment, while we observed reduced H3K4 me1 at seven out of the 43 loci examined (Figure 3.5). From these data, we conclude that altered CTCF localization does not influence Rad21 enrichment or consistently alter colocalizing post-translational histone modifications.

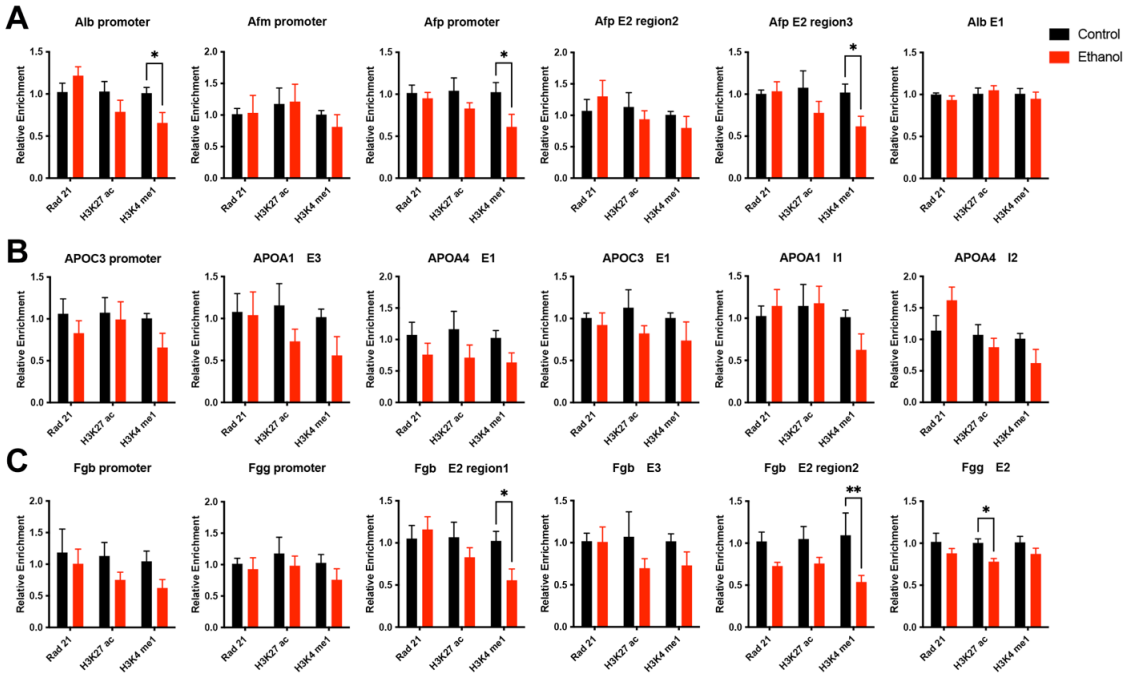

Figure 3.5 Consistent Rad21 binding and modest alterations in enhancer-associated histone posttranslational modifications in placentae derived from the male offspring of alcohol-exposed sires. We used ChIP qPCR to assay the enrichment of the Cohesin component Rad21 and histone h3 lysine four mono-methylation (H3K4 me1) and lysine 27 acetylation (H3K27 ac) in the (A) albumin, (B) apolipoprotein, and (C) fibrinogen gene clusters. In these studies, we selected candidate loci exhibiting altered CTCF enrichment. ChIP experiments were performed on a total of 8 placentae across five different litters, and data analyzed using a two-way ANOVA followed by Uncorrected Fisher's LSD. Error bars represent the standard error of the mean, * $P < 0.05$, ** $P < 0.01$.

3.3.6. Changes in DNA methylation do not correlate with alterations in gene expression and CTCF binding.

To further investigate the basis to altered CTCF enrichment, we examined placental DNA methylation. Cell-specific CTCF occupancy correlates with DNA methylation patterns (Bell and Felsenfeld, 2000; Fedoriw et al., 2004; Stadler et al., 2011; Wang et al., 2012; Xu and Corces, 2018). Similarly, patterns of altered DNA methylation associate with programmed changes in placental gene expression (Susiarjo

et al., 2013). Therefore, we utilized bisulfite mutagenesis and second-generation deep sequencing to determine if changes in CTCF occupancy and gene expression correlated with alterations in DNA methylation. Using DNA samples isolated from 2 male and two female placentae from each treatment, we achieved an average of 112 million reads for each sample, each with Q30 scores over 90%. Using Babraham Bioinformatic's program Bismark, we mapped reads against a converted mouse genome and used the RStudio Bioconductor package methylkit to analyze mapped reads. Consistent with previous studies, we identified similar placental DNA methylation profiles between sexes (Decato et al., 2017; Price et al., 2012).

As previously reported, placental samples exhibited a reduced global methylation profile, displaying 56% (+/- 0.7) CpG methylation as compared to the ~70% commonly observed in somatic tissues (Eckhardt et al., 2006; Hon et al., 2013; Schroeder et al., 2013). Similar to our studies of alcohol-exposed sperm, we could not detect any differences in global levels of DNA methylation between the preconception treatment groups in any of the CpG, CHG, or CHH contexts (Figure 3.6 A). Further, informatic analysis of mapped reads identified a strong correlation between treatment groups, and clustering analysis failed to separate placental samples by preconception treatment (Figure 3.6 B-C).

To identify differentially methylated regions of the genome, we analyzed our datasets for alterations in individual CpGs, as well as between non-overlapping 1000 base pair windows or 'tiles' of the genome (Lister et al., 2009). Setting rigorous cutoff values of 30x coverage, a minimal change in DNA methylation of 20%, a q-value of

0.01, and p-value of less than 0.05 (Ziller et al., 2015), (http://www.roadmapepigenomics.org/protocols), we were unable to identify any high-confidence differentially methylated regions. As global levels of DNA methylation are lower in the placenta (Eckhardt et al., 2006; Hon et al., 2013; Schroeder et al., 2013), we reduced the stringency of our analysis in the hopes of identifying more modest changes. When we lowered these criteria to include values of 5x coverage, a minimal change in DNA methylation of 5%, a q-value of 0.05, and a p-value of less than 0.05, we identified 19 differentially methylated CpGs (Table) and 26 differentially methylated tiles Table). These same regions emerged when we analyzed male and female samples separately (data not shown).

The individual CpGs predominantly mapped to intergenic regions (57%), with 30% mapping to gene bodies and only 14% mapping to promoter regions (Figure 3.6 D). Similarly, 82% of the differentially methylated tiles mapped to intergenic regions, 13% mapping to gene bodies, while none of the identified tiles fell within promoter regions. These results are entirely consistent with other genome-wide studies of DNA methylation, which demonstrate that DNA methylation predominantly maps to gene bodies and intergenic regions (Eckhardt et al., 2006; Edwards et al., 2010; Lister et al., 2009). Of the 45 loci identified using this strategy, 80% displayed an increase in methylation, while only nine displayed reductions. Here, individual CpGs displayed more significant % change (+17% / -28%) versus the more modest (+/- ~10%) differences observed in the tiling analysis.

Interestingly, 70% of the differentially methylated features (9 of the 19 identified differentially methylated CpGs and 23/26 of the differentially methylated tiles) fell directly into an integrated transposable element, endogenous retrovirus, or some other class of repetitive sequence (Table and Table). These observations could be significant, as previous studies examining the epigenetic inheritance of the agouti locus have revealed alcohol-induced changes in patterns of DNA methylation within an integrated IAP element, which associate with heritable alterations in the transcriptional control of this locus (Kaminen-Ahola et al., 2010). However, none of the identified differentially methylated loci mapped to within +/- 1 million base pairs of either the promoter regions or gene bodies of the differentially expressed candidates identified in Figure 3.1. Similarly, only one of the 45 differentially methylated regions mapped to a CTCF peak. This region, located on chromosome 17, falls within the gene encoding the Rn45s ribosomal RNA. Although not the same specific CpG, we also identified this general locus in our studies of differentially methylated sperm (Chang et al., 2017). Further, this region has emerged from other studies examining altered developmental programming, suggesting the epigenetic modification of this locus may associate with programmed alterations in fetal growth (Holland et al., 2016; Sánchez-Martín et al., 2015). However, in each instance, our experiments identified single CpGs, not large regions, and none of the differentially methylated sites we identified fell within recognized CTCF binding sites.

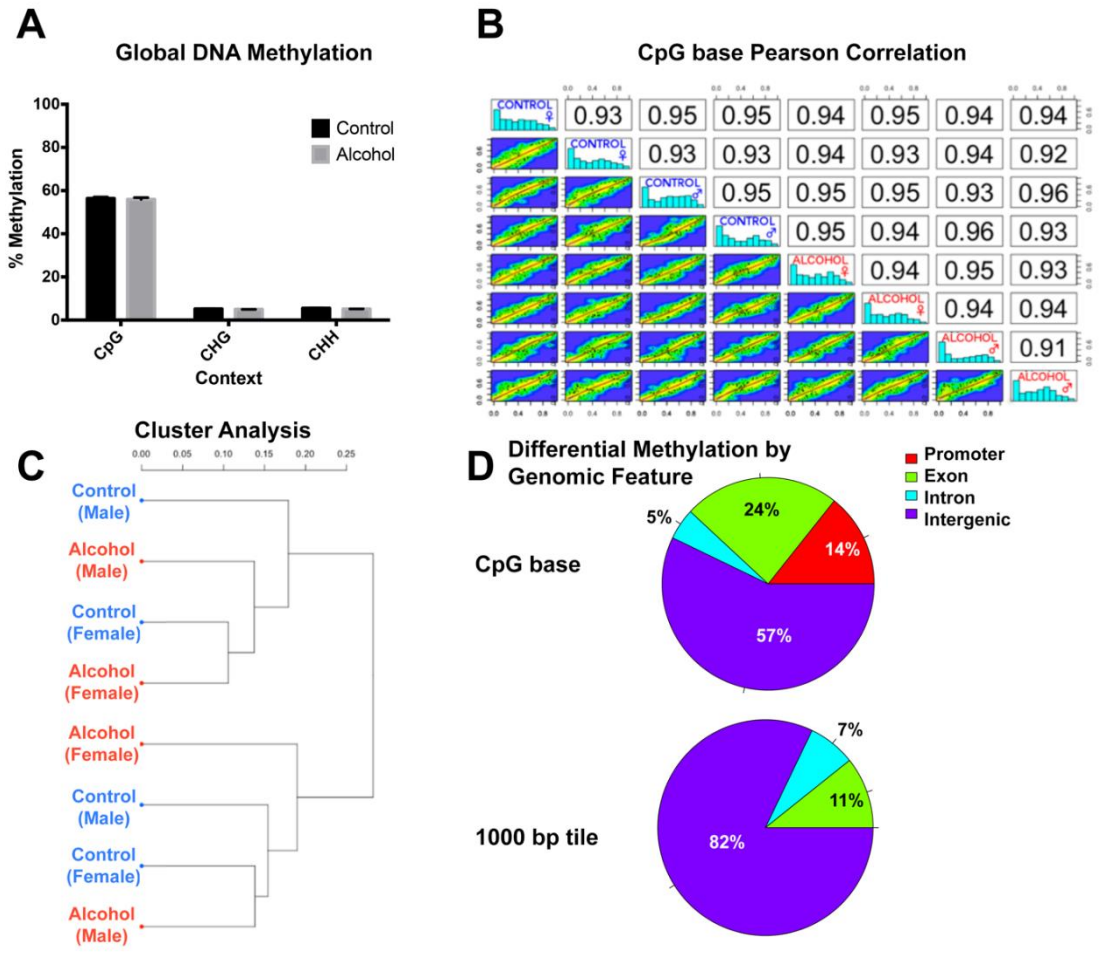

Figure 3.6 Preconception male alcohol exposure does not impact the global DNA methylation profile of the offspring placentae. (A) Global DNA methylation profiles of placental tissues derived from control and alcohol-exposed males across CpG, CHG, and CHH contexts (n=4). (B) Pearson correlation analysis between genomic DNA methylation profiles of offspring placentae (n=4). (C) Clustering analysis between the DNA methylation profiles of offspring placentae sired by control and alcohol-exposed males. (D) Association of differentially methylated CpGs (top) and non-overlapping 1000 base pair tiles (bottom) with genomic features.

3.4. Discussion

Analysis of placentae derived from the offspring of alcohol-exposed sires identified sex-specific changes to a common cohort of genes, with widespread changes in expression across the albumin, apolipoprotein, and fibrinogen gene clusters. Our

previous studies observed fetal-placental growth deficits that cumulatively associated with a 10% increase in gestational length (Chang et al., 2019a). However, we were unable to identify the underlying cause of the delayed parturition. Here, we report the misregulation of multiple genes involved in growth factor signaling and fetal maturation.

We observed altered expression of Alb, Afp, Afm, and Gc, located within the albumin cluster, all highly expressed in the placenta and fetal liver (McLeod and Cooke, 1989). Albumin (Alb) and the other serum transport protein identified, transferrin (Trf), are both synthesized by trophoblast cells and serve functions integral to the transport of thyroid hormones during pregnancy (McKinnon et al., 2005). In mice, defects in thyroid hormone transport have well-characterized impacts upon fetal growth and maturation (Beamer et al., 1981), which primarily manifest later in development (Adams et al., 1989) and are associated with delayed maturation of the lungs (deMello et al., 1994). Within this same gene cluster, Gc (vitamin D binding protein) is also expressed in trophoblast cells and serves to move vitamin D into fetal circulation (Dror, 2011). Disruptions in vitamin D transport impair fetal growth, and in both humans and mice, also delay the maturation of the lungs (Saadoon et al., 2017). Genes within the apolipoprotein gene cluster play central roles in cholesterol homeostasis, which is crucial to both the endocrine function of the placenta as well as lung maturation (Rooney, 1989). In humans and rodents, glucocorticoid signaling increases the cholesterol content of the fetal lung as part of the maturation process (Aszterbaum et al., 1993), and both low- and high-density lipoproteins are required by alveolar cells within the fetal lung to produce pulmonary surfactant (Rooney, 1989). In both mice and humans, induction of

lung surfactant proteins during maturation is a major milestone promoting the initiation of parturition (Ratajczak and Muglia, 2008).

Finally, during pregnancy, multiple genes within the fibrinogen gene cluster exhibit up-regulation proportional to advancing gestational age, support proper development of fetal-maternal vascular communication, and are induced as part of the inflammatory process associated with parturition (Fuller and Zhang, 2001; Iwaki et al., 2002; Manten et al., 2004; Palumbo et al., 2004). Therefore, we posit that, alterations in placental gene expression across these three clusters collectively delay maturation of the fetal lungs, extending the length of gestation. Future studies will examine the offspring of alcohol-exposed sires for progressive increases in pulmonary surfactant protein A and other contractile protein factors to verify this assertion.

Altered expression across the *albumin*, *apolipoprotein* and *fibrinogen* gene clusters prompted us to consider that preconception paternal alcohol exposure had altered CTCF localization. Within these gene clusters, genomic DNA folds into a complex three-dimensional loop, which moves the promoter regions of co-regulated genes into the proximity of cluster-specific regulatory elements (Espitia Jaimes et al., 2018; Matthews and Waxman, 2018; Mishiro et al., 2009). Significantly, using cultured human cells, researchers have demonstrated that depleting CTCF protein using siRNAs or deleting individual CTCF binding sites using Cas9 causes the loop structures of the apolipoprotein and fibrinogen gene to collapse, reducing the expression of multiple genes spanning across these clusters (Espitia Jaimes et al., 2018; Mishiro et al., 2009).

Based on these studies, we hypothesized that male placentae derived from the offspring of alcohol-exposed sires would display altered CTCF occupancy.

We focused our analyses on male placentae, as the overgrowth phenotypes were more consistent in males than females (Bedi et al., 2019; Chang et al., 2017, 2019a). Our ChIP-seq analysis and qPCR validation confirmed altered CTCF enrichment at multiple loci, including within these three gene clusters. Consistent with recently published studies of the albumin cluster in mouse liver (Matthews and Waxman, 2018), we were able to identify CTCF enrichment within the Afp gene body, which demonstrated 37% increased enrichment in samples derived from the alcohol treatment group (Figure 3.3, bottom; likelihood ratio of 2,829,863). However, the previously described CTCF peak located ~55kb upstream of the Alb promoter in the liver was absent in the placenta, with the next closest peak ~75kb upstream. This more upstream peak exhibited reduced enrichment in the placenta derived from alcohol-exposed sires. These observations indicate that the liver and placenta share some common CTCF binding sites, as well as tissue-specific ones, many of which are influenced by preconception alcohol exposures. These data are also consistent with recent reports indicating CTCF exerts a powerful impact on localized gene expression within the domain but that most impacted genes are not directly bound by this protein (Khoury et al., 2020; Nora et al., 2017; Ren et al., 2017). Finally, they reinforce the assertion that environmental exposures can influence CTCF localization (VonHandorf et al., 2018).

During spermatogenesis, CTCF plays a major role in organizing the sperm genome (Arpanahi et al., 2009; Jung et al., 2017, 2019). Thus, if alcohol induces

alterations in CTCF localization during spermatogenesis, these abnormalities may transmit to the offspring and stably alter chromatin looping on the paternally inherited allele. In support of this assertion, CTCF exclusively binds the maternal allele of the IGF2-H19 imprint control locus, while the paternal allele remains unbound. Importantly, this pattern is independently established during the respective production of the sperm and egg and is maintained into adulthood of the offspring (Fedoriw et al., 2004).

Based on these published works, it is tempting to speculate that alcohol exposure disrupts CTCF-localization in the sperm-inherited genome, which transmits to the offspring and disrupts gene-chromatin looping on paternal-inherited chromosomes. However, we could not identify any changes in DNA methylation within alcohol-exposed sperm (Chang et al., 2017), nor could we identify any correlation between altered placental DNA methylation and CTCF binding, even at low stringency. Thus, whether the observed alterations in CTCF localization are truly causal in programming gene expression, or merely another symptom of altered developmental programming, remains unknown. From our perspective, the induction of diametrically opposite gene expression patterns in males and females is more suggestive of sex-specific adaptations rather than the direct inheritance of altered programming. Future studies will examine CTCF localization in alcohol-exposed sperm, determine if affected loci transmit to the offspring and if these changes impact patterns of chromatin looping between affected gene promoters and enhancers.

4. ENHANCER-ASSOCIATED HISTONE MODIFICATIONS ARE REMODELED DURING THE EPIDIDYMAL MATURATION OF MOUSE SPERM

4.1. Introduction

Although gestational stressors have well-established effects on offspring growth and development, preconception exposures have only recently emerged as having a critical influence on the health and fitness of the next generation. Indeed, an increasing number of studies now reveal the potential of parental lifestyle choices and exposure history to impart inter- or transgenerational phenotypic changes to the offspring (Fleming et al., 2018). Therefore, understanding how and when germline programming occurs is essential to deciphering the developmental origins of disease and, concerning preconception male exposures, addressing a major blind spot in the field of developmental toxicology.

Male germ cell specification and differentiation are characterized by dramatic changes in chromatin structure, ranging from erasure and re-establishment of DNA methylation during the embryonic phases to the critical role of post-translational histone modifications during meiosis (Reviewed (Larose et al., 2019)). During sperm production, stage-specific alterations in chromatin structure are accompanied by the trafficking of multiple histone variants, many of which are unique only to sperm, that prepare the sperm nucleus for transcriptional quiescence and nuclear compaction (Le Blévec et al., 2020). Finally, during the late stages of spermatogenesis, where germ cells

differentiate into round spermatids (spermiation), the majority of histones are evicted and replaced with protamines (Gatewood et al., 1987).

Despite the essential role of protamines in nuclear compaction, a small subset of the paternal genome remains packaged in nucleosomes. Depending on the method of analysis, these nucleosome enriched regions co-localize with regulatory regions of developmentally crucial genes (Arpanahi et al., 2009; Brykczynska et al., 2010; Erkek et al., 2013; Gardiner-Garden et al., 1998; Hammoud et al., 2009; Royo et al., 2016; Yamaguchi et al., 2018; Yoshida et al., 2018) and gene-poor domains enriched in repetitive elements (Carone et al., 2014; Samans et al., 2014; Sillaste et al., 2017; Yamaguchi et al., 2018; Zalenskaya et al., 2000). The retention of nucleosomes, along with region-specific patterns of post-translational modifications are hypothesized to contribute to the establishment of the embryonic transcriptional program (Du et al., 2017; Flyamer et al., 2017; Jung et al., 2017). In support of this assertion, markers of poised chromatin can be traced from the establishment of the male germline during early embryonic development through meiosis into fertilization-competent sperm (Lesch et al., 2013).

Notwithstanding the recent discovery that sperm pick up additional epigenetic information in the form of secreted noncoding RNAs during maturation (Chen et al., 2016a), the established dogma has long been that all facets of chromatin-based epigenetic programming are complete before exiting the testis (Kota and Feil, 2010; Larose et al., 2019; Rando, 2016). In large part, this dogma has persisted because the nuclear compaction established during spermiation is thought to physically exclude

enzyme complexes involved in chromatin modification. However, studies in rodents (Ariel et al., 1994; Skinner et al., 2019) and recent clinical data (Donkin et al., 2016) suggest that patterns of DNA methylation are subject to change during epididymal maturation. These observations raise the prospect that histone post-translational modifications may also be modified during sperm maturation. Large-scale proteomic studies have reported changes in select histone post-translational modifications between elongating spermatids and mature sperm (Luense et al., 2016). However, this previous study never determined whether these changes occurred in the testis or during epididymal transit. This question is significant as it would imply that periconceptional male exposures could alter chromatin-based epigenetic programming.

Using a mouse model, we investigated the hypothesis that sperm chromatin post-translational modifications are subject to change during epididymal transit. To avoid the bias associated with antibody-based methods, we utilized nano-liquid chromatography, triple quadrupole mass spectrometry (nanoLC-MS) to characterize 80 different histone variants and post-translational modifications. We find that multiple post-translational modifications change between the caput and cauda regions of the epididymis and that the majority of these differentially enriched modifications are associated with gene enhancers. Using western blotting of sperm extracts, we confirm that changes in histone H3 lysine 27 and lysine 64 and di methylation of histone H3 lysine 9 occur between the caput and cauda portions of the mouse epididymis, and that these changes correlate with the presence of Class I histone deacetylase enzymes HDAC1 and HDAC3. These observations raise the prospect that paternal stressors immediately before conception

may alter chromatin-based epigenetic programming of enhancers, influencing the transcriptional program of the early embryo.

4.2. Materials and Methods

4.2.1. Mouse Sperm Isolation and Histone Acid Extraction

Experiments involving mice were conducted under AUP 2017-0308 and approved by the Texas A&M University IACUC. We obtained postnatal day 90 adult C57BL/6N (RRID:IMSR_JAX:005304) males from the Texas A&M Institute for Genomic Medicine. We maintained males on a standard diet (catalog# 2019, Teklad Diets, Madison, WI, USA) and 12-hour light/dark cycle. After dissection, we separately placed the initial segment of the caput and the entire portion of the cauda, plus approximately 1 cm of vas deferens, into 12 well plates containing 500 µL of pre-warmed (37 °C) Human Tubal Fluid medium (catalog# ZHTF-100, Zenith Biotech, Blue Bell, PA, USA). We then made four or five incisions to each separated section of the epididymis to allow sperm to swim out. We incubated plates at 37°C for 30 min, collected sperm and diluted a 10 µL aliquot 1:50 in diH2O to count cells using a Neubauer chamber slide. We washed the samples in PBS, then incubated sperm in somatic cell lysis buffer (0.1 % SDS, 0.5 % Triton- X-100) for thirty minutes on ice, confirmed purity using microscopy, then centrifuged and washed samples in PBS, snap froze the sperm pellets and stored them at -80°C.

We acid extracted histones using a modified version of the previously described procedure (Garcia et al., 2007). We resuspended frozen sperm pellets in Nuclei Isolation

Buffer-250 with 0.3% NP-40 (15mM Tris-HCl (pH 7.5), 60mM KCl, 15mM NaCl, 5mM MgCl2, 1mM CaCl2, 250mM Sucrose, 1mM DTT, 10mM sodium butyrate, and 1:100 Halt protease inhibitor (Cat# PI78437, Thermo Fisher Scientific, Pittsburgh, PA, USA)) and rotated them at 4°C for 30 minutes. We verified sperm lysis using microscopy and then centrifuged samples at 600g for five minutes. We washed the samples twice using Nuclei Isolation Buffer-250 with no NP40 and after the second centrifugation, resuspended the pellet in five volumes of 0.2M H2SO4, then rotated the samples overnight at 4°C. We then centrifuged samples at 4,000 x g for 4 minutes, transferred histone-enriched supernatant to new tubes and added Trichloroacetic Acid to a final concentration of 20% by volume, then incubated samples for two hours on ice. We centrifuged samples at 10,000 x g for five minutes at 4°C, discarded the supernatant and resuspend the pellet in 1mL cold acetone/0.1% HCl. We then washed the pellet twice with 100% acetone, air dried the sample and resuspended the pellet in water.

4.2.2. Ram Sperm Isolation and Histone Acid Extraction

Experiments utilizing rams were conducted under AUP 2017-0210 and approved by the Texas A&M University IACUC. After euthanasia, we isolated the reproductive track from 14-month-old rams. We made large incisions all across the proximal and distal loops of the caput, as well as the entire cauda, then separately placed the caput and cauda into 50ml conical tubes filled with warmed PBS, and then incubated the tubes in a 37°C water bath for 30 minutes to allow sperm to swim out. We washed sperm twice in fresh PBS, then incubated the sperm in somatic cell lysis buffer (0.1 % SDS, 0.5 %

Triton- X-100) for thirty minutes on ice. We washed cells in PBS, incubated sperm in 50mM DTT for 30 minutes at room temperature, then sonicated cells for five minutes (five 30 second pulses) using a Bioruptor sonication system (Diagenode, Denville, NJ, USA). We pelleted cells by centrifugation, resuspended the pellet in Nuclei Isolation Buffer-250 with no NP40, and incubated the samples at 4°C with constant rotation for 30 minutes. We pelleted cells by centrifugation, resuspended the pellet in 0.2M H2SO4, sonicated the samples again for five minutes (five 30 second pulses), and then incubated the samples overnight at 4°C with constant rotation. We then added Trichloroacetic Acid to the supernatant to a final concentration of 20% by volume, and incubated samples on ice for two hours. We centrifuged samples at 10,000 x g for five minutes at 4°C, discarded the supernatant and washed the pellet twice in ice cold acetone. We let the samples air dry for 20 minutes and then resuspend the pellet in water.

4.2.3. Mass Spectrometry

We assayed the profile of sperm histones using the ModSPec service from Active Motif (Carlsbad, CA, USA). Pelleted histone peptides were resuspended in 0.1% TFA in water and analyzed on a TSQ Quantiva triple quadrupole (QqQ) mass spectrometer directly coupled with an UltiMate 3000 Dionex nano-liquid chromatography system (Thermo Fisher Scientific, Pittsburgh, PA, USA). Peptides were first loaded onto an in-house packed trapping column (3cm×150μm) and then separated on a New Objectives PicoChip analytical column (10 cm×75 μm). Both columns were packed with New Objectives ProntoSIL C18-AQ, 3μm, 200Å resin. The chromatography gradient was

achieved by increasing percentage of buffer B from 0 to 35% at a flow rate of 0.30 µl/min over 45 minutes. Solvent A: 0.1% formic acid in water, and B: 0.1% formic acid in 95% acetonitrile. The QqQ settings were as follows: collision gas pressure of 1.5 mTorr; Q1 peak width of 0.7 (FWHM); cycle time of 2 s; skimmer offset of 10 V; electrospray voltage of 2.5 kV. Targeted analysis of unmodified and various modified histone peptides was performed. This entire process was repeated three separate times for each sample.

4.2.4. Total Protein Isolation and Western Blotting

We homogenized fresh sperm in Tris-lysis buffer (50 mM Tris, 1 mM EGTA, 150 mM NaCl, 1% Triton X- 100, 1% b-mercaptoethanol, 50 mM NaF, 1 mM Na3VO4; at pH 7.5). We separated protein extracts (either sperm total protein or acid extracted histones) on 10% sodium dodecyl sulfate polyacrylamide gels and transferred proteins to PVDF membranes. Blots represent pooled caput spermatozoa collected from eight to ten males, while cauda sperm consist of mature sperm isolated from one or the pooled sperm from two males. The primary antibodies we used in this study are as follows: antiH3K9me2 (Cat# 39240, Active Motiff Carlsbad, CA, USA), antiH3K27me3 (Cat# 07-449; RRID:AB_310624; Millipore-Sigma, St. Louis, MO, USA), antiH3K27ac (cat# ab4729; RRID:AB_2118291; Abcam, Cambridge, MA, USA), antiH3K64ac (Cat# ab214808, Abcam) antiH3K36ac (Cat# ab177179, Abcam), antiH4K20me3 (Cat# ab9053; RRID:AB_306969; Abcam), anti-panacetyl-Histone H3 (Cat# 06-599; RRID:AB_2115283; Millipore-Sigma) and antiH3 (Cat# ab1791; RRID:AB_302613;

Abcam). We visualized blots using secondary antibodies conjugated to horseradish peroxidase (catalog no. sc-2004; RRID:AB_631746; Santa Cruz Biotechnology, Santa Cruz, CA, USA) and an enhanced chemiluminescence detection system (LI-COR, Lincoln, Nebraska USA).

4.2.5. Data analysis

Raw mass-spec files were imported and analyzed in Skyline with Savitzky-Golay smoothing (MacLean et al., 2010). All Skyline peak area assignments for monitored peptide transitions were manually confirmed. A minimum of 3 peptide transitions were quantified for each modification. For each monitored amino acid residue, each modified (and unmodified) form was quantified by first calculating the sum of peak areas of corresponding peptide transitions, then the sum of all modified unmodified forms determined. Finally, each modification is then represented as a percentage of the total pool of modifications. This process was carried out for each of the three separate mass spec runs, and the raw data imported into Excel to calculate the mean and standard deviation for each modified and unmodified form of the corresponding amino acid residue.

For the analysis of western blots, we quantified band intensities using the densitometry feature of ImageJ (RRID:SCR_003070; National Institutes of Health, Bethesda, MD, USA) and after importing the obtained values into Excel, derived a ratio of the intensity of the modified histone divided by the intensity for total histone H3. We imported these ratios into the statistical analysis program GraphPad

(RRID:SCR_002798; GraphPad Software, Inc., La Jolla, CA, USA) and set statistical significance at alpha = 0.05. We verified all datasets for normality using the Brown-Forsythe test, then compared histone ratios using an unpaired student's t-test.

4.2.6. Sperm Chromatin Immunoprecipitation sequencing (ChIP-seq)

Sperm histone ChIP was carried out using a previously published protocol (Hisano et al., 2013). Briefly, for each individual biological rep, sperm collected from the Caputs and Cauda of 10-15 mice were pooled, purified and pre-treated with 50μM DTT for 2h at RT to open sperm chromatin. Cell suspensions were split into roughly 15-20 million sperm aliquots per IP and treated with 90 U of MNase (New England Biolabs, #M0247S) for 5 min at 37C. MNase-digested chromatin was then pre-cleared with blocked A/G Sepharose beads for 1h at 4C. For IP, 5 μg of antibody (H3K27ac or H3K9me2) was added to the pre-cleared chromatin overnight followed by 50 μL of blocked beads for 4 h at 4C. Beads were washed and DNA was then eluted in elution buffer. Following RNase A and proteinase K treatment, DNA was purified using phenol/chloroform isolation and ethanol precipitation and resuspended in 40 μL ultrapure water.

Library preparation using 10ng of DNA and 75 bp paired-end sequencing with at least 50 million reads per samples was carried out at the UT Health Cancer Genomics Center, Houston. Raw fastq reads were trimmed for adapters and quality and then mapped to the mm10 reference genome using BWA-MEM.

Peaks were called using MACS2 for either narrow or broad regions with an FDR of 0.05. Bedgraph files were used to produce bigwig files for visualization using IGV.

4.3. Results

4.3.1. Sperm histone variants and post-translational modifications in the caput and cauda portions of the mouse epididymis

To achieve an unbiased assessment of changes in chromatin structure, we separately isolated sperm from head caput and cauda portions of epididymides taken from 6- to 8-week-old C57BL/6N males and acid extracted histones (Figure 4.1 A-B). Using nano-liquid chromatography, triple quadrupole mass spectrometry (nanoLC-MS), we measured histone composition and abundance in pooled samples isolated from at least 10 million caput and cauda sperm. We then calculated the sum of peak areas for each peptide transition and determined the total pool of modifications for each residue. We used this value to normalize the data and calculate the relative abundance of each modification across three independent runs (all modifications + unmodified peptides = 100%). A complete list of the evaluated histone isoforms and the relative abundance of each post-translational modification within the total peptide pool is available in Table . Our analyses quantified the post-translational modifications at 30 different residues across histones H2A, H2A1 H2A3, H3.1, H3.3, and H4. We find that most of the residues examined (19/30) are unmodified in both caput and cauda sperm (Table). Notable exceptions were histone H3 lysine 9 (H3K9) histone H3.1 and H3.3 lysine 27 and lysine 36 (H3K27 and H3K36), as well as histone H4 lysine 20 (H4K20), which

were all at least 50% modified. Consistent with previous reports examining human and mouse sperm (Luense et al., 2016), we were only able to identify trace amounts of histone H1.4.

To determine if alterations in chromatin structure occur during sperm maturation, we examined changes in the relative abundance of the measured post-translational modifications between caput and cauda sperm. These analyses identified 12 different residues that exhibited either a ~5-fold or greater difference in relative abundance or a shift of greater than ~10% within the peptide pool (Figure 4.1 C). These included changes at histone H3, lysine 4 (H3K4), lysine 9 (H3K9), lysine 14 (H3K14), lysine 23 (H3K23), lysine 27 (H3K27), lysine 36 (H3K36), lysine 56 (H3K56), lysine 64 (H3K64), lysine 79 (H3K79), and lysine 122 (H3K122), as well as histone H4 lysine 16 (H4K16), and lysine 20 (H4K20). We did not observe any changes for the isoforms of histone H2.

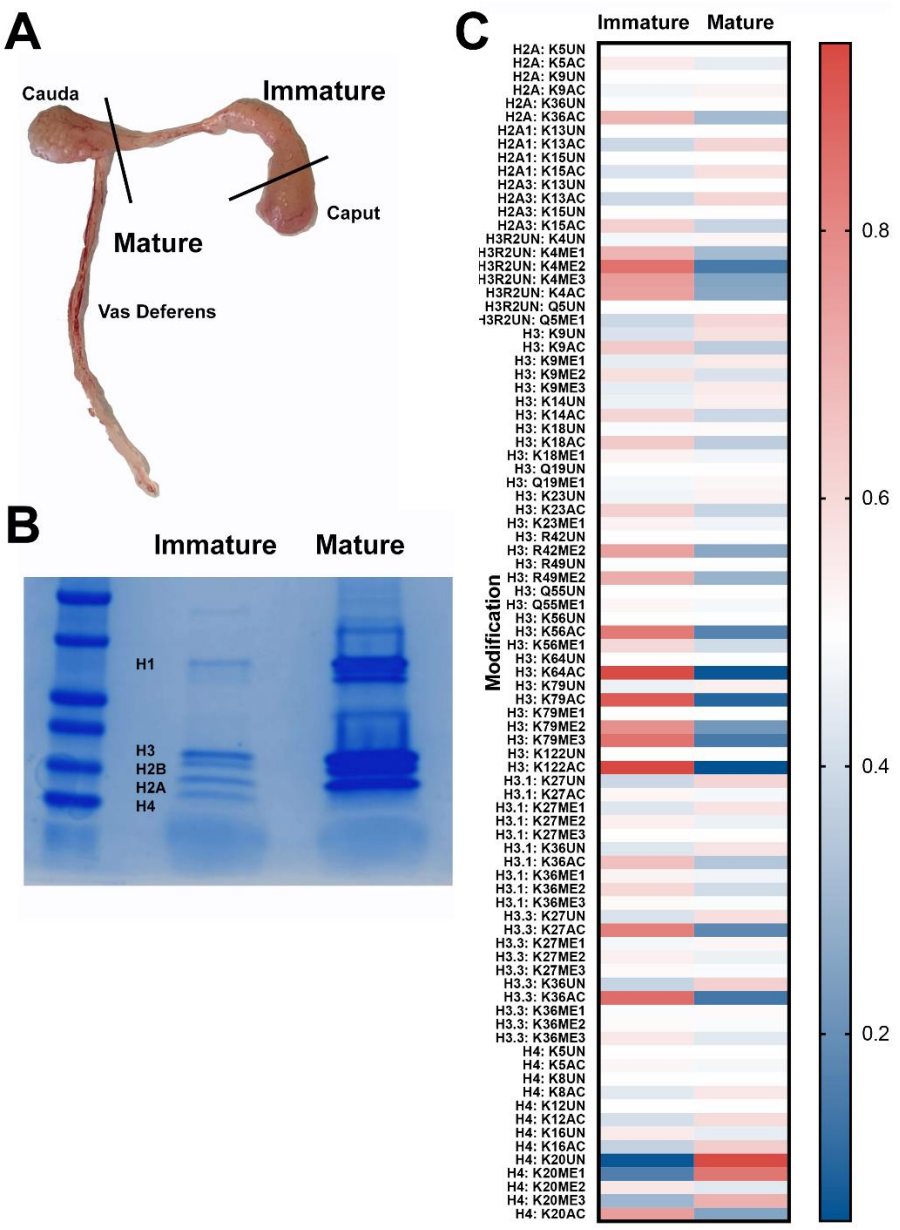

Figure 4.1 Alterations in histones posttranslational modifications between caput derived spermatozoa and cauda derived sperm. (A) We acid extracted histones from ten million cells isolated from the caput and cauda regions of the epididymis (B) and ran proteins on a polyacrylamide gel and stained with Coomassie blue (left). Using LC/MS, we compared the histone posttranslational modification profiles of caput spermatozoa and mature sperm. (C) Heatmap comparing the calculated percentage of each individual peptide transition as a fraction of the total peptide pool (all modifications + unmodified peptides = 100%). Data represent the average of three independent runs obtained from a pooled sample of 10 million caput and cauda sperm.

In the transition from caput spermatozoa to cauda sperm, decreases in most posttranslational modifications were balanced by equivalent gains in the unmodified form of the histone (Figure 4.2). As examples, between caput and cauda sperm, we observed an ~8% decrease in H3K4 monomethylation, which was offset by an 8% increase in unmodified H3K4 and a ~10% decline in H3K9 dimethylation equipoised by a near equivalent increase in unmodified H3K9 (Figure 4.2A-B). Similarly, for histone H3 lysines 14, 23, and 27, ~5% to 13% decreases in acetylation were accompanied by equivalent increases in the unmodified forms of these residues within the peptide pool (Figure 4.2C-E). The more substantial magnitude shifts in the acetylation of H3K27 appeared on histone H3.3, and not the H3.1/H3.2 isoforms (LC/MS analysis cannot distinguish H3.1 or H3.2). In contrast, acetylation of histone H4 lysine 16 (H4K16ac) increased 13%, while unmodified H4K16 decreased by 13% (Figure 4.2H). The remaining changes in histone posttranslational modifications represented shifts in distributions between multiple posttranslational modifications. As examples, H3K36 and H3K79 exhibited losses in both acetylation and methylation, which were accompanied by an increased abundance of the unmodified peptide (Figure 4.2F-G). At the same time, H4K20 displayed an 18% decline in the dimethylated form and an equivalent increase in the trimethylated form (Figure 4.2I). Although less than 1% of the peptide pool, we observed 5 to 15-fold decreases in the acetylation of histone H3, lysine 56, 64, and 122 (H3K56, H3K64, and H3K122, Figure 4.2J-L). Interestingly, trimethylation of histone H3 lysine 4 (H3K4me3) and lysine 27 (H3K27me3) were constant during the transition from the caput to caudal region of the epididymis (Figure 4.1).

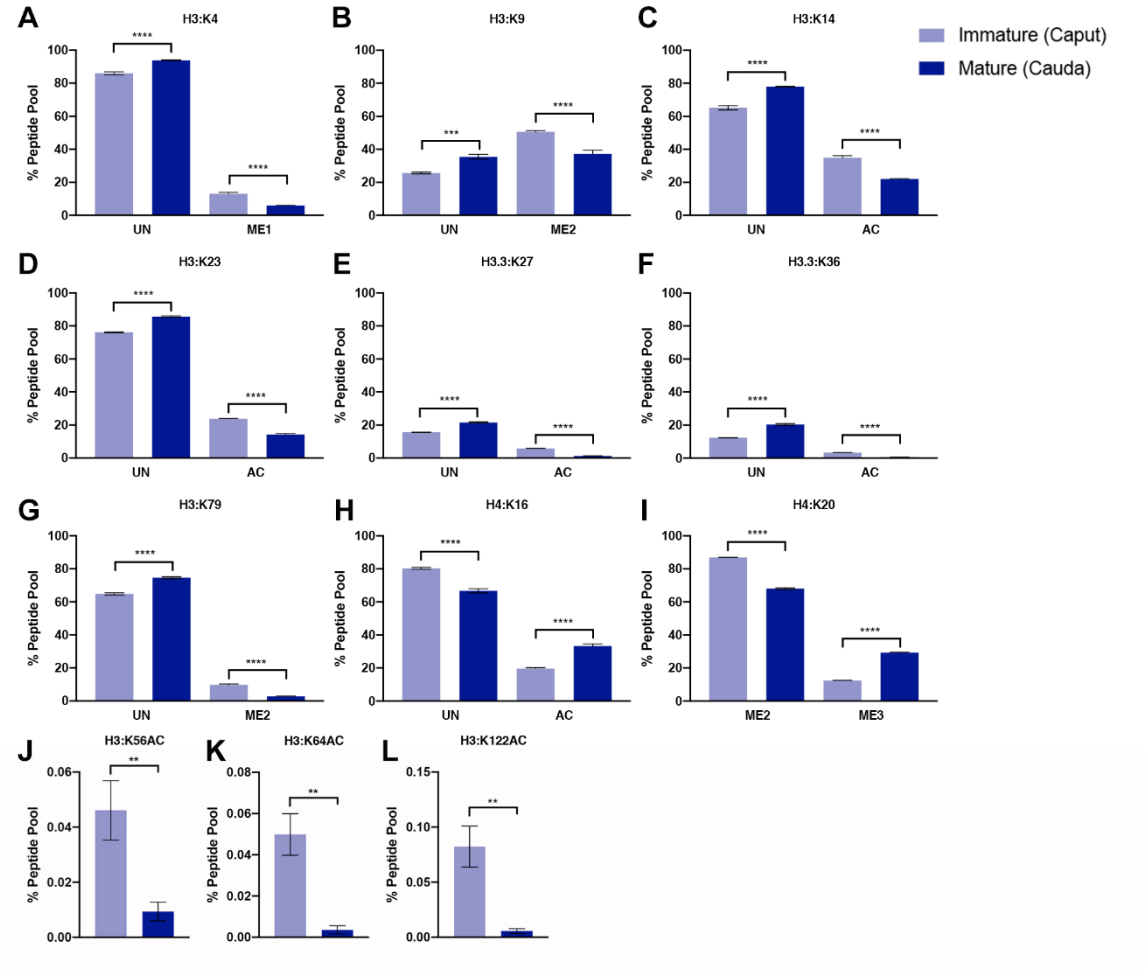

Figure 4.2 Gains and losses of select histone posttranslational modifications during epididymal maturation of mouse sperm. Bar graphs contrasting gains and losses of unmodified (UN) histones with the levels of lysine acetylation (AC), monomethylation (ME1) dimethylation (ME2), and trimethylation (ME3) in sperm isolated from the caput and cauda portions of the epididymis. Error bars represent the SEM, n = 3 replicates, ** $p < 0.01$, *** $p < 0.001$, **** $p < 0.0001$.

4.3.2. Changes in the profile of post-translational modifications associated with enhancer function during epididymal maturation

To validate our mass spectrometry analysis, we acid extracted histones from ~7.5 million caput and cauda sperm and, using western blotting, examined changes in six of the post-translational modifications identified above (Figure 4.3). Consistent with the

mass spec analysis, levels of H3K27 trimethylation were identical between caput and cauda sperm, while levels of H3K27 acetylation and H3K9 dimethlyation decreased during epididymal maturation ($p < 0.05$). Despite representing a small fraction of the peptide pool, we also confirmed decreased enrichment of H3K64 acetylation between immature and mature sperm. Although decreases in the acetylation of H3K36 and increases in the trimethylation of H4K20 tended to be similar to those observed in our proteomic analysis, these differences did not reach statistical significance of p less than 0.05 (specific p-values were 0.09830 and 0.1743 respectively). We suspect differences in the sensitivity and variability of western blotting compared to nanoLC-MS explain these discrepancies (Zheng et al., 2013). Importantly, several of the post-translational modifications validated here associate with gene enhancer activity. These include histone H3 lysine 27 acetylation (H3K27ac), lysine 64 acetylation, and H3K9 dimethylation (H3K9me2) (Creyghton et al., 2010; Higashijima et al., 2020; Pradeepa et al., 2016). These observations suggest that gene enhancer-associated posttranslational modifications may be specifically targeted during epididymal transit.

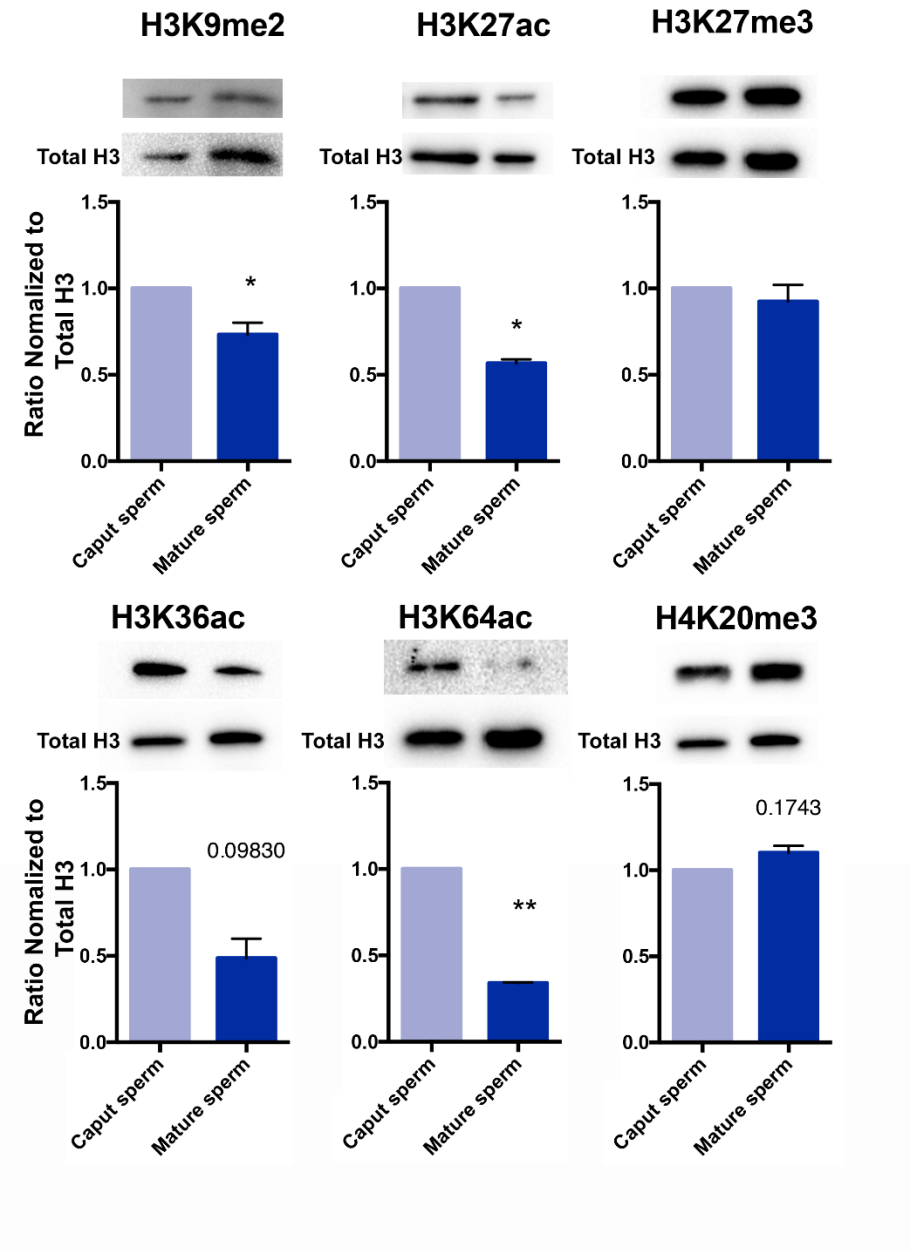

Figure 4.3 Changes in select histone posttranslational modifications between mouse caput spermatozoa and cauda sperm. Comparison of select histone posttranslational modifications between immature and mature sperm was conducted using western blotting. Blots of each histone modification were quantified using ImageJ and normalized to levels of total histone H3. This normalized ratio was compared between caput and cauda sperm. Error bars represent the SEM, n = 3 replicates, * $p < 0.05$, ** $p < 0.01$

4.3.3. Alterations in Histone H3 lysine 9 dimethylation and lysine 27 acetylation during epididymal maturation

To better understand the dynamics of histone structure during epididymal transit, we focused on H3K9me2 and H3K27ac and used chromatin immunoprecipitation followed by deep sequencing (ChIP-seq) to monitor changes in enrichment during sperm maturation. Our analysis of H3K9me2 revealed a strong correlation between biological replicates and between caput and cauda sperm samples (Figure 4.4 A). Consistent with our LCMS and western blotting, MACS2 identified decreased enrichment of both broad and narrow peaks between caput and cauda samples, with 6,768 broad regions in caput samples decreasing to 3,489 broad peaks in cauda (Figure 4.4 B) and 3,950 narrow peaks in caput samples decreasing to 2,164 narrow peaks in cauda sperm (Figure 4.4 C). These changes reflected a general thinning of H3K9me2 enrichment (Figure 4.4 D), with the majority of H3K9me2 enriched regions mapping to distal intergenic (65%) and intronic regions (25%); consistent between caput and cauda-derived samples. (Figure 4.4 E-F). In support of this observation, regions enriched in H3K9me2 were generally depleted of CpG islands and did not correlate with gene transcriptional start sites (Figure 4.4 G-H). However, when we broke CpG enrichment into clusters, we observed a slight (968 out of 16014; 6%) increase in H3K9me2 enrichment centered at CpG islands within cauda-derived samples. Notably, most of these regions were centered on promoter regions (representing 2% of regions described in Figure 4.4 E) with GO pathway analysis identifying enrichment of processes involved in chiasma assembly, synaptonemal complex assembly, chromosome organization, and male gametogenesis. In contrast to

CpG islands and transcriptional start sites, we observed strong enrichment of distal enhancer-like sequences for a subset of H3K9me2 enriched regions (Figure 4.4 I). From these data, we conclude that H3K9me2 enriched regions of the sperm genome predominantly map to distal intergenic regions, some of which associate with enhancer-like sequences. Interestingly, promoter regions of genes driving sperm production progressively increase in H3K9me2 during epididymal maturation.

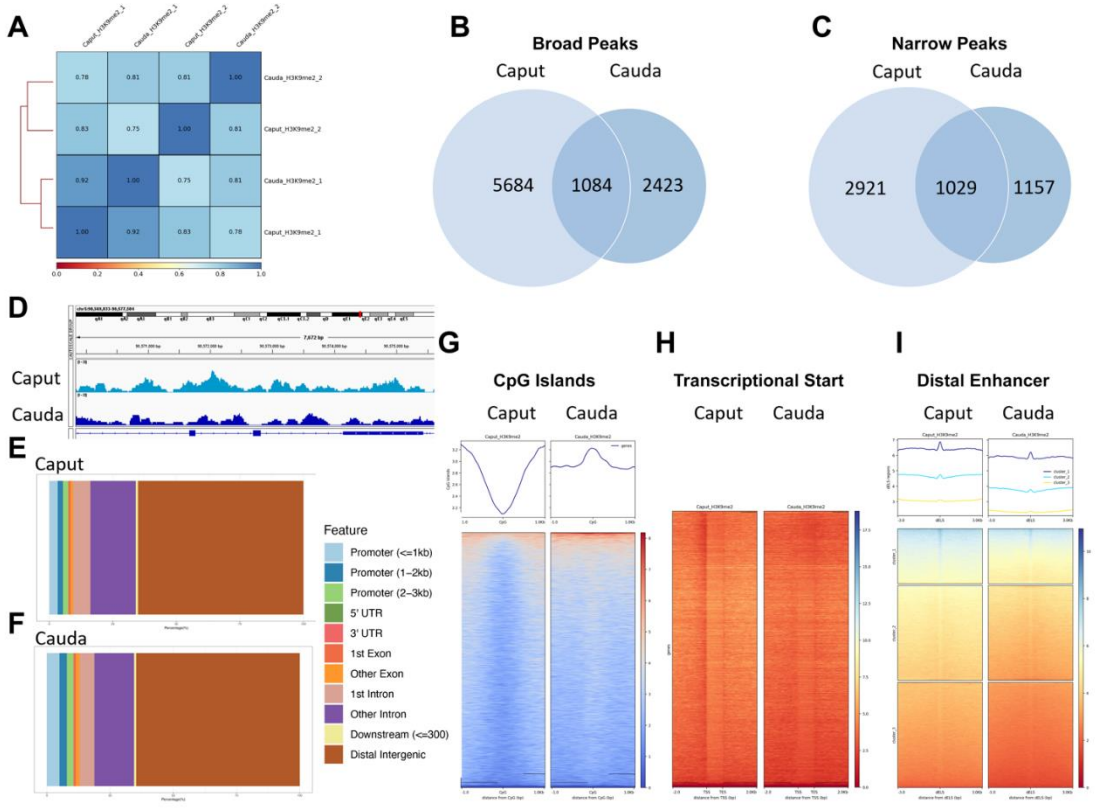

Figure 4.4 ChIP-sequencing identifies decreased enrichment of H3K9me2 at distal intergenic regions during the transition of mouse caput spermatozoa to cauda sperm. (A) Correlation analysis between H3K9me2 ChIP-seq signals derived from sperm isolated from the caput and cauda regions of the epididymis (n=2). Venn diagrams comparing changes in (B) broad and (C) narrow peaks between caput and cauda-derived sperm. (D) Integrative Genome Viewer tracks of chromosomal regions exhibiting differential H3K9me2 enrichment between caput and cauda-derived sperm. Bar chart representation of the distribution of H3K9me2 across key genomic features between (E) caput and (F) cauda-derived samples. Heatmaps displaying the enrichment of H3K9me2 signals across (G) CpG islands, (H) gene bodies, or (I) regions exhibiting a signature of distal enhancers.

Our studies of H3K27ac enriched regions identified several significant contrasts with the patterns identified for H3K9me2. First, although cauda-derived samples correlated with each other, caput samples were much more variable (Figure 4.5 A). Second, consistent with H3K9me2, MACS2 identified a reduction in broad peaks (Figure 4.5 B; caput sperm exhibited 7904 broad peaks, which decreased to 5144 regions in cauda-derived sperm), while in contrast, we identified an increase in narrow peaks (Figure 4.5 C; 14,976 enriched regions in caput sperm, which increased to 18,110 regions in cauda-derived samples). Interestingly, these changes primarily reflected a sharpening of broad domains into focused peaks (Figure 4.5 D). Third, unlike H3K9me2, which primarily associated with distal intergenic regions in both caput and cauda-derived sperm, H3K27ac shifted from distal intergenic (21%) and intronic regions (48%) in caput-derived samples to primarily localizing to gene promoters (72%) and distal intergenic regions (12%) in cauda-derived sperm (Figure 4.5 E-F). Finally, consistent with increased enrichment at gene promoters, we identified a significant shift towards the enrichment of H3K27ac to CpG islands (Figure 4.5 G) and gene transcriptional start sites (Figure 4.5 H). For the gene promoters, pathway analysis identified genetic processes involved in histone modification, embryo development, and multiple aspects of reproductive biology. We also observed a dramatic sharpening of H3K27ac signals at distal enhancer-like sequences (Figure 4.5 H). For the top cluster of regions exhibiting increased peak sharpening in cauda-derived sperm (9879 of the 209041 enhancer regions), pathway analysis identified processes involved in embryo development, pattern specification, embryonic morphogenesis, and CNS development.

Collectively, these observations indicate that during epididymal transit, H3K27 transitions from broad domains to sharp, focused peaks centered on gene promoters and distal enhancers driving early embryonic development. Interestingly, we observed a weak negative correlation between H3K9me2 and H3K27ac, suggesting these marks may oppose each other.

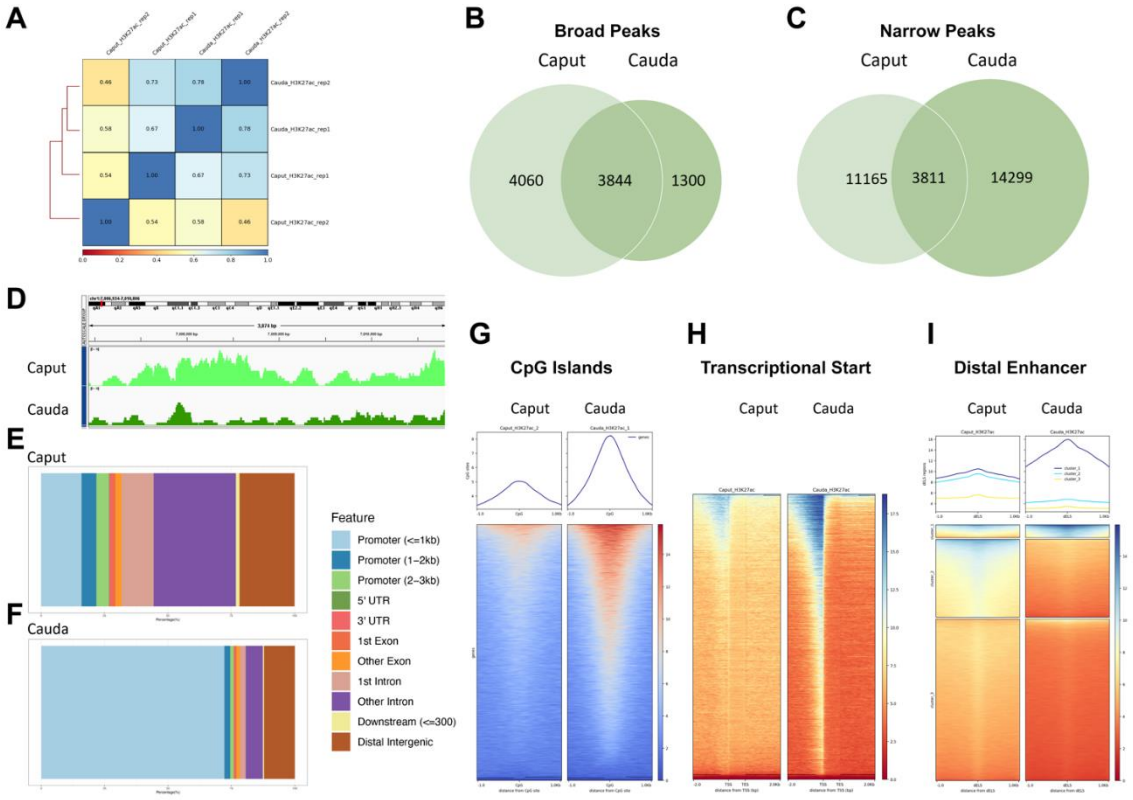

Figure 4.5 During epididymal maturation, broad H3K27ac peaks sharpen and transition from intronic and distal regions to gene promoters and enhancers driving embryo development. (A) Correlation analysis between H3K27ac ChIP-seq signals derived from sperm isolated from the caput and cauda regions of the epididymis (n=2). Venn diagrams comparing changes in (B) broad and (C) narrow H3K27ac peaks between caput and cauda-derived sperm. (D) Integrative Genome Viewer tracks of chromosomal regions exhibiting the transition from diffuse broad peaks to more focused enrichment between caput and cauda-derived sperm. Bar chart representation of the distribution of H3K27ac across key genomic features between (E) caput and (F) cauda-derived samples. Heatmaps displaying the enrichment of H3K27ac signals across (G) CpG islands, (H) gene bodies, or (I) regions with a distal enhancer-like signature.

4.3.4. Reduced levels of histone H3 lysine 27 acetylation between mouse embryonic stem cells and mature sperm.

Our data indicate that histone posttranslational modifications associated with gene enhancers are selectively reduced during epididymal transit. However, recent studies employing chromatin immunoprecipitation followed by genome-wide sequencing (ChIP-seq) have identified H3K27ac-enriched regions within the sperm genome (Jung et al., 2017). To explore this discrepancy, we compared the datasets derived from sperm to the well-characterized H3K27ac enhancer profiles identified in mouse embryonic stem cells (mESCs) (Shen et al., 2012). We processed these published datasets following ENCODE3 guidelines, mapped sequence reads using MACS2 with p-value cutoff of 0.01 and identified the closest gene to each peak using bedTools. After filtering out peaks within 1000 base pairs of transcriptional start sites, we identified 21,139 sperm and 33,254 mESC unique peak sets. In mESCs, 54% of peak heights exhibited more than a 5-fold enrichment over background and 13% were greater than 10-fold. In contrast, of the peak sets identified in sperm, only 18% displayed a 5-fold enrichment over input reads, while less than one percent surpassed a 10-fold enrichment (Figure 4.6). Although challenges remain when comparing published ChIP-seq datasets produced by different labs (Meyer and Liu, 2014), our analysis indicates that H3K27ac peak heights are broadly reduced in sperm when compared to mESCs ($p<0.0001$).

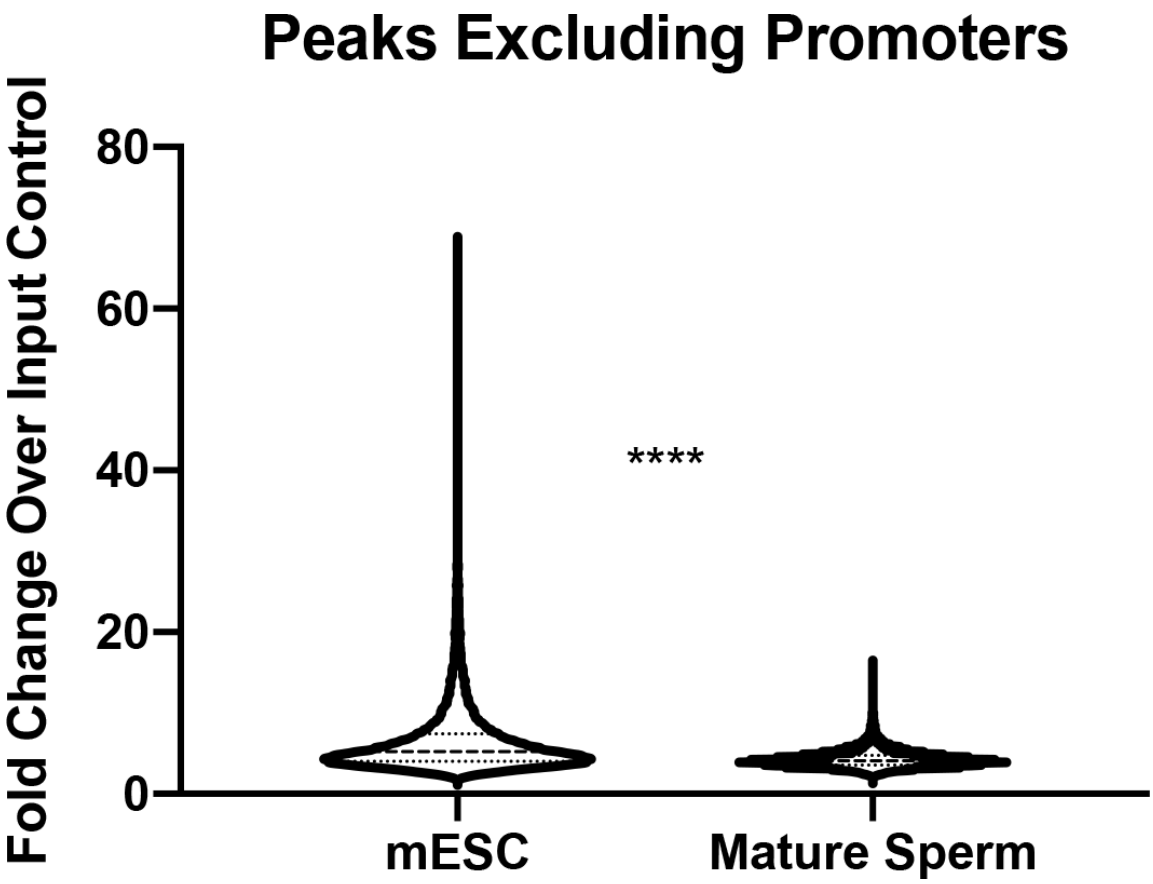

Figure 4.6 The profile of global H3K27ac enrichment in sperm is reduced compared to the profile observed in mESCs. Published chromatin immunoprecipitation datasets were used to compare the global profiles of H3K27ac enrichment. The violin plots compare global fold enrichment of H3K27ac over the input control between mouse embryonic stem cells (mESCs) and mature sperm.

4.3.5. Histone deacetylase expression in sperm isolated from the head caput and cauda portions of the mouse epididymis

In somatic cells, the histone deacetylase family of enzymes carry out removal of acetyl groups from lysine residues on histone tails. This family is divided into three classes based on their exclusive localization to the nucleus (Class I), their ability to shuttle between the cytoplasm and the nucleus (Class II) and if they require the cofactor NAD+ for deacetylase activity (Class III) (Johnstone, 2002). Of these three, Class I

deacetylases frequently associate with transcription factors and drive the decommissioning of gene enhancers (Qiao et al., 2020; Whyte et al., 2012). Given that the majority changes identified by our nanoLC-MS involve histone deacetylation, we examined sperm for the presence of Class I HDACS. Using RIPA buffer, we isolated protein extracts from ~7.5 million caput and cauda sperm, then examined the expression of HDAC1, HDAC2, and HDAC3 using western blotting. We were able to detect both HDAC1 and HDAC3 in spermatozoa isolated from the caput portion of the epididymis (Figure 4.7). When we increased the number of mature sperm five-fold to 38 million (isolated from four mice), we detected both HDAC1 and HDAC3 in mature sperm (Figure 4.7). We were unable to detect HDAC2 in any sperm samples. From these data, we conclude that HDAC1 and HDAC3 are present in both immature and mature mouse sperm.

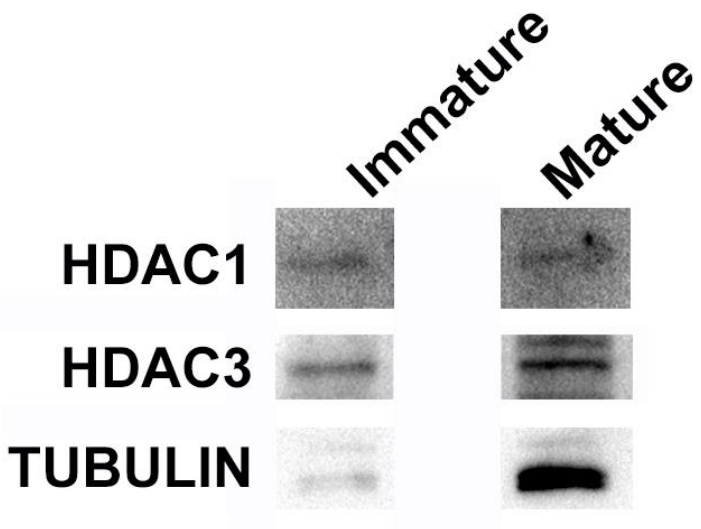

Figure 4.7 Identification of Class I Histone Deacetylase enzymes HDAC1 and HDAC3 in mouse sperm. Expression of HDAC1 and HDAC3 was assayed in immature and mature sperm using western blotting. Protein extracts were derived from 7.5 million caput spermatozoa and 38 million cauda sperm.

4.3.6. Differences in histone posttranslational modifications during epididymal maturation of ram sperm

Finally, we sought to determine if changes in histone posttranslational modifications are a common feature of mammalian epididymal maturation. To this end, we assayed patterns of histone structure between immature and mature sperm isolated from Ovis aries (Rambouillet Merino). Similar to mouse sperm, less than 5% of the ruminant genome retains histones (Champroux et al., 2016), and both species exhibit an extended (10 to 14 day) epididymal transit time compared to humans (Robaire and Hinton, 2015). After euthanasia, we dissected the ram reproductive track and separately isolated sperm from the caput and cauda regions of the epididymis. Using western blotting, we assayed changes in histone structure between caput spermatozoa and cauda sperm. Similar to mice, we did not observe any significant changes in the levels of H3K27me3 between caput spermatozoa and mature sperm, while levels of H3K36ac diminished during epididymal transit (Figure 4.8). Although blots using H3K27ac and H3K64ac antibodies failed to identify appropriately sized bands for histone H3 (data not shown), we detected a significant reduction in pan-histone H3 acetylation between caput and cauda sperm. These data indicate that, in addition to mice, rams also exhibit changes in histone posttranslational modifications during epididymal maturation.

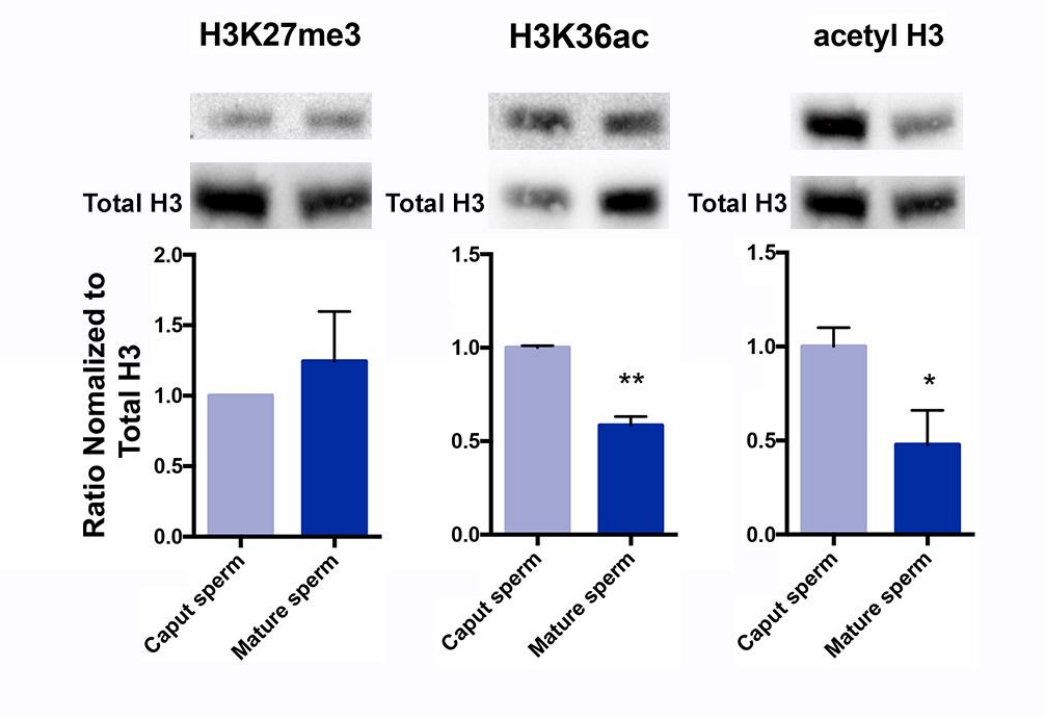

Figure 4.8 Changes in histone posttranslational modifications during the epididymal maturation of ram sperm. Comparison of histone posttranslational modifications between immature and mature sperm using western blotting. Blots of each histone modification were quantified using ImageJ and normalized to levels of total histone H3. This normalized ratio was compared between caput and cauda sperm. Error bars represent the SEM, n = 3 males, * $p < 0.05$, ** $p < 0.01$.

4.4. Discussion

This study's core finding is that posttranslational histone modifications in the sperm epigenome change during epididymal transit. Previous studies examining chromatin structure in mature sperm have primarily focused on modifications associated with gene promoters, including H3K4me3 and H3K27me3 (Lesch et al., 2013). Our study did not observe differences in either of these chromatin states, suggesting that bivalent chromatin modifications centered on gene promoters are stable during epididymal maturation. Significantly, of the twelve posttranslational modifications

exhibiting either the most significant fold change or most substantial shifts within the peptide pool, seven are directly linked to gene enhancer function. These include histone H3 lysine 4 monomethylation (H3K4me1), lysine 27 acetylation (H3K27ac) lysine 79 dimethylation (H3K79me2), lysine 64 acetylation (H3K64ac), lysine 122 acetylation (H3K122ac), and histone H4 lysine 16 acetylation (H4K16ac), which demarcate active or poised enhancers (Creyghton et al., 2010; Godfrey et al., 2019; Pradeepa et al., 2016; Rada-Iglesias et al., 2011; Taylor et al., 2013), as well as H3K9 dimethylation (H3K9me2), which localizes to silent enhancers (Higashijima et al., 2020). In point, with the exception of increased H4K16ac, our LC-MS comparisons of caput spermatozoa and cauda sperm identified decreases in all the histone posttranslational modifications associated with enhancer activity characterized to date, as well as selective increases in modifications hypothesized to oppose enhancer chromatin topology directly (Pradeepa et al., 2016). Specifically, acetylation of H4K16 maintains an open state by impeding the ability of chromatin to form cross-fiber interactions and is directly opposed by methylation histone H4K20 (Lu et al., 2008; Shogren-Knaak et al., 2006). Both of these modifications increase during epididymal transit and are in the top twelve differentially enriched posttranslational modifications. Future studies are needed to determine if these opposing modifications colocalize to the same loci and if the remaining four modifications we identified, including acetylation of histone H3 lysine14, 23, 36, and 56, associate with gene enhancers in sperm.

Based on our observations, we postulate that gene enhancers are selectively targeted and decommissioned during epididymal transit. Although not conclusive,

identification of HDAC1 and HDAC3 here in mouse sperm, and by others in human sperm (Kim et al., 2014), suggest Class I HDACS may direct this process. In embryonic stem cells, Class I HDACs complex with lysine-specific demethylase 1 (also known as KDM1A) to demethylate histone H3 on Lys 4 and Lys 9 (H3K4/ K9). During stem cell differentiation, the cooperative interaction of these chromatin modifiers within the nucleosome remodeling and histone deacetylase (NuRD) complex is essential for the decommissioning of enhancers driving pluripotency (Whyte et al., 2012). In addition to reductions in enhancer-associated histone acetylation, our nanoLC-MS data also identified reductions in both H3K4me1 and H3K9me2, indicating the NuRD complex could be present in maturing sperm.

In further support of our hypothesis that enhancers are selectively decommissioned during epididymal transit, reduction of lysine 27 acetylation was only observed on the histone H3.3 variant, and not H3.1/3.2. Histone H3.3 specifically incorporates into enhancer regions, and similar to acetylation of H4K16, impedes intrafiber folding, maintaining the open conformation necessary to bind cofactors required to activate transcription (Chen et al., 2013). While histone variants H3.1 and H3.2 incorporate during S-phase, H3.3 incorporates outside of DNA replication (Henikoff and Ahmad, 2005). Significantly, the H3.3 variant persists though the transition from the sperm genome to the paternal pronucleus after fertilization (Van Der Heijden et al., 2008). The selective targeting of histone H3.3 in maturing sperm provides further support to the H3 barcode hypothesis, positing that region-specific incorporation of histone variants serves as a backup for less stable posttranslational modifications and

represents the first layer of epigenetic memory (Hake and Allis, 2006). We suspect that the ability of H3.3 to maintain an open conformation allows the selective targeting of loci in the compacted sperm nucleus and, to be preferentially identified by oocyte-derived factors directing the establishment of the embryonic epigenome. Alternatively, the open confirmation conferred by histone variant H3.3 may predispose enhancer regions to protamine replacement, which recent studies suggest continues during epididymal maturation (Yoshida et al., 2018). Future studies will determine whether the targeted removal of histone posttranslational modifications associated with enhancer function erase remnant transcriptional memories leftover from sperm production or play a larger role in transmitting epigenetic information to the embryo

In mice, sperm production consists of a 34.5-day spermatogenic wave followed by functional maturation during a 10-day epididymal transit; taking approximately 45 days in total. (Meistrich et al., 1975; Oakberg, 1956). To date, the established dogma remains that select aspects of epigenetic programming are confined to specific windows (Le Blévec et al., 2020; Rousseaux et al., 2005). Patterns of sperm DNA methylation primarily occur in spermatogonial stem cells and their derived meiotically dividing spermatocytes, while the final remodeling of histones takes place during spermiation (Gatewood et al., 1987; Rousseaux et al., 2005). Although still emerging, the processes of sperm ncRNA trafficking largely appear to take place during epididymal transit (Sharma et al., 2018). Most studies examining perturbations to the paternally-inherited epigenetic program employ exposures longer than 45 days, which ensures coverage of the entire duration of sperm production and maturation (Bedi et al., 2019; Carone et al.,

2010; de Castro Barbosa et al., 2016; Chang et al., 2019a; Fullston et al., 2013; Gapp et al., 2014b; Morgan et al., 2020; Rodgers et al., 2015; Rompala et al., 2018; Vassoler et al., 2013). Therefore, these long-term exposures make it reasonable to suspect all facets of postnatal paternal epigenetic programming, including changes in sperm-inherited DNA methylation, post-translational histone modifications, and noncoding RNAs.

However, a limited number of studies have identified paternally inherited changes arising from acute exposures. For example, three weeks after the initiation of a high-fat diet, the female offspring of exposed males exhibit reduced glucose tolerance (Stanford et al., 2018). After fourteen days of either daily stress induced by prolonged restraint or direct glucocorticoid injections, the offspring of exposed males display persistent hyperglycemia (Wu et al., 2016). Finally, after only seven days of prolonged exposure to cold temperatures, offspring sired by exposed males displayed improved glucose metabolism and increased brown adipose tissue (Sun et al., 2018). Based on established dogma, the relatively short duration of these acute exposures implicates altered epigenetic programming during the final phases of sperm maturation, which are more likely to involve changes in the profile of sperm-inherited noncoding RNAs than alterations in DNA methylation or histone posttranslational modifications. However, clinical studies have identified changes in sperm DNA methylation as little as seven days after bariatric surgery (Donkin et al., 2016) and although not associated with an overt phenotypic change, exposing rodents to either cannabinoids or tetrahydrocannabinol for twelve days also influences this epigenetic modification in sperm (Acharya et al., 2020; Murphy et al., 2018). These data support the assertion that programming of DNA

methylation occurs during epididymal transit as well as during spermatogenesis (Ariel et al., 1994; Skinner et al., 2019). Building on these studies, we find that select histone posttranslational modifications also change during sperm maturation. Given that multiple studies can track sperm-inherited histones into the embryonic genome (Bui et al., 2011; van der Heijden et al., 2006; Van Der Heijden et al., 2008; Ihara et al., 2014; Van De Werken et al., 2014), we must now consider the possibility that acute environmental exposures may alter multiple aspects of the paternally-inherited epigenetic program and influence embryonic development. However, it remains to be determined if sperm-inherited changes in either DNA methylation or histone posttranslational modifications are drivers of altered developmental programming or additional symptoms.

5. ALCOHOL ALTERS THE ABUNDANCE AND ENRICHMENT OF POSTTRANSLATIONALLY MODIFIED HISTONES IN SPERM CHROMATIN

5.1. Introduction

For decades, research into the effects of pre- and peri-conceptional exposures on the health of the growing fetus and mature offspring have focused on the singular role of the mother. However, recent studies show that paternal lifestyle and preconception exposures have pronounced effects on placental and fetal markers of growth and development, inflammation and embryonic gene expression (Fleming et al., 2018). In the offspring, these effects persist into adulthood and have shown to be mediated by epigenetic mechanisms (Acharya et al., 2020; Chang et al., 2019b; Ng et al., 2010). Our understanding now is that sperm possess a wide suite of environmentally modifiable epigenetic marks, including DNA methylation, histone modifications, and small and long noncoding RNAs, that appear to influence gene expression in the early embryo (Marcho et al., 2020; Meyer et al., 2017; Sharma, 2019).

Owing to the retention of parental allele-specific imprinting via DNA methylation from gametes, beyond fertilization, into the genome of the developing embryo, sperm DNA methylation has been almost exclusively investigated as a mechanism for carrying the memory of environmental influences to the zygote. However, the contribution of changes in sperm DNA methylation to these phenotype-modifying epimutations in fetal, placental and adult tissue is debatable (Bedi and Golding, 2019). For example, studies examining the effects of different paternal dietary

regimens on offspring health find stable cytosine methylation in sire sperm DNA (Carone et al., 2010; Shea et al., 2015), while detecting reproducible changes in offspring liver methylation. Similarly, we found that paternal preconception ethanol intake affects fetal and placental growth with long-lasting consequences on adult metabolism (Chang et al., 2019b), yet no correlative alterations in sperm DNA methylation were observed (Chang et al., 2017). On the other hand, a recent study found that paternal cold exposure prior to conception resulted in improved metabolic outcomes for the offspring and this correlated with the presence of roughly 2500 differentially methylated regions (DMRs) in sire sperm (Sun et al., 2018). Out of the 11,000 genes expressed in the target, interscapular brown adipose tissue (iBAT), about 10% had overall shifts, compared to control, that inversely correlated with the altered methylation status of those genes in sire sperm after cold exposure. However, whether and how these methylation patterns from sperm persist in offspring iBAT is not known. Furthermore, research into transgenerational effects of paternal exposures to environmental toxicants shows that while differential sperm methylation as a result of ancestral exposures correlates with disease outcomes (Ben Maamar et al., 2019), there is little to no concordance of these differentially methylated sites across the male germline of each affected generation (McBirney et al., 2017).

New studies indicate that histone retention in the mouse sperm genome is higher (~8%) (Jung et al., 2017) than previously believed (~1%) (Erkek et al., 2013). Programming of the paternal genome at fertilization leads to widespread erasure of the histone marks carried by sperm (Zheng et al., 2016). However, recent evidence shows

that a fraction of modified histones in sperm escape this reprogramming and, in fact, mark developmental genes and influence their expression in the early embryo (Oikawa et al., 2020). Analyses of sperm histone retention using different techniques of Chromatin immunoprecipitation (ChIP) and different levels of enzymatic digestion reveal a highly complex organization of sperm chromatin. Initial MNase digestion studies, pointed towards enrichment in either gene deserts, devoid of promoters (Carone et al., 2014), or in gene rich regions (Erkek et al., 2013). Crosslinking ChIP analyses revealed that Histones not only enriched at promoters but also marked enhancer and super-enhancer regions in sperm (Jung et al., 2017). Subsequent studies showed that different regions of sperm chromatin are less accessible and only solubilize after extensive digestion (Yamaguchi et al., 2018). Different histone modifications also specifically enrich at certain genomic regions in chromatin; for e.g. H3K4me3 enriches at promoters (Yamaguchi et al., 2018) and our own analyses reveal that H3K27ac in mature sperm from cauda epididymides enriches at promoters while H3K9me2 is found at distal intergenic regions (4.3.3).

Evidence is now accumulating that can link paternal exposures with influences on sperm chromatin (Meyer et al., 2017; Rando, 2016; Siddeek et al., 2018). A recent study determined that paternal diet influences fetal skeletal development via the altered inheritance of sperm H3K4me3 (Lismer et al., 2021). Importantly, alterations in H3K4me3 in sperm impact its enrichment in the 8-cell embryos produced by these gametes as well, suggesting that these marks either partially escape erasure or influence their abundance in offspring cells. Similar studies analyzing low-protein (Yoshida et al.,

2020) or high fat diets (Claycombe-Larson et al., 2020) in rodents reveal plausible mechanisms that link these dietary regimens with reduced H3K9me2 at target genes or at a global level and mediate adverse metabolic outcomes in the fetus.

Alcohol is a widespread toxin that is well known for having teratogenic effects on the growing fetus when exposed *in utero* and a whole spectrum of growth, structural and central nervous system defects in the offspring that have mostly been linked to maternal exposures (Carter et al., 2013). Research from our lab and others has shown that paternal preconception alcohol consumption is linked to fetal growth deficits (Chang et al., 2017), behavioral defects (Rompala et al., 2017b) and adverse long-term metabolic programming (Chang et al., 2019b).

Having observed minimal effects of chronic alcohol use on sperm DNA methylation (Chang et al., 2017) and a substantial effect on the sperm small noncoding RNA profile (Bedi et al., 2019) in our mouse model, in the following analysis, we address the hypothesis that alcohol alters the abundance or regions of genomic enrichment of histone modifications in sperm. We use Mass Spectrometry-based analysis to first identify the global histone profile in sperm exposed to alcohol and select candidates to verify by western blot. Using ChIP-seq, we then identify differences in the genomic regions of enrichment of H3K4me3 and H3K9me2. These analyses reveal a considerable reduction in histone protein levels for at least one histone modification, H3K4me3, globally, as a consequence of alcohol exposure. Also, we identify differences in H3K4me3 and H3K9me2 occupancy distally from and at promoters of genes whose

regulation is critical for proper embryo development, neurodevelopment and cell-cell adhesion.

5.2. Materials and Methods

5.2.1. Animal Work and Tissue Collection

All experiments were conducted under AUP 2017–0308 and approved by the Texas A&M University IACUC. Individually caged C57BL/6J (RRID: IMSR_JAX:000664) postnatal day 90 adult males were obtained and housed in the Texas A&M Institute for Genomic Medicine, fed a standard diet (catalog# 2019, Teklad Diets, Madison, WI, USA) and maintained on a 12-hour light/dark cycle. In this study, we employed a voluntary model of alcohol exposure known as Drinking in the Dark. This model of exposure avoids the stress associated with forced feeding and mitigates the known impact of stress on the sperm-inherited epigenetic program (Gapp et al., 2014a). Using methods described previously (Chang et al., 2017), males were provided limited access to ethanol during a four-hour window, beginning one hour after the initiation of the dark cycle. During this four-hour window, experimental males were provided access to a solution of 10% (w⁄v) ethanol (catalog# E7023, Millipore-Sigma, St. Louis, MO, USA) and 0.066% (w⁄v) Sweet'N Low (Cumberland Packing Corp, Brooklyn NY, USA). Control males received a solution of 0.066% (w⁄v) Sweet'N Low alone. Mice were maintained on this regimen for ten weeks. After 70 days of exposure, we paired exposed males with naive C57BL/6J dams and collected fetal-placental tissues on day 16.5 of gestation (GD14.5).

5.2.2. Mouse Sperm Isolation

Mice were sacrificed under standard CO_2 asphyxiation protocols followed by cervical dislocation. After dissection, we placed the entire portion of the cauda, plus approximately 1 cm of vas deferens, from each animal, into one well of a 12-well plate containing 1 mL of pre-warmed (37 °C) PBS. We then squeezed sperm out of the vas with forceps and made four or five incisions to the cauda epididymis to allow sperm to swim out. We incubated plates at 37°C for 30 min, collected sperm and diluted a 10 μL aliquot 1:50 in diH2O to count cells using a Neubauer chamber slide. We washed the samples in PBS, then incubated sperm in somatic cell lysis buffer (SCLB: 0.1 % SDS, 0.5 % Triton- X-100) for 30 min on ice followed by another wash in SCLB, confirmed purity using microscopy, then centrifuged at 3000g for 5 min, washed samples in PBS, and either proceeded to the ChIP protocol or snap froze the sperm pellets and stored them at -80°C for acid extraction.

5.2.3. RNA sequencing and Data processing

We isolated total RNA from GD16.5 fetal placentae using the RNeasy Plus Mini Kit (catalog # 74134; Qiagen, Germantown MD, USA), according to the manufacturer's instructions. We generated RNA-libraries using the Illumina RNA-seq preparation kit followed by pooling and high-throughput sequencing on an Illumina HiSeq 2500 (Genomic Core at Whitehead Institute for Biomedical Research, Cambridge, MA, USA).

We mapped the raw reads to the mm10 mouse genome using RNA STAR v2.7.8a (Dobin et al., 2013) and counted sequences that mapped to exons using

featurecounts (Liao et al., 2014). We then carried out differential expression analysis using DESeq2 (Love et al., 2014) to determine significantly altered genes (FDR = 0.05).

5.2.4. Sperm Histone Acid Extraction

We acid extracted histones using a modified version of the previously described procedure (Garcia et al., 2007). We resuspended frozen sperm pellets in Nuclei Isolation Buffer-250 with 0.3% NP-40 (15mM Tris-HCl (pH 7.5), 60mM KCl, 15mM NaCl, 5mM MgCl2, 1mM CaCl2, 250mM Sucrose, 1mM DTT, 10mM sodium butyrate, and 1:100 Halt protease inhibitor (Cat# PI78437, Thermo Fisher Scientific, Pittsburgh, PA, USA)) and rotated them at 4°C for 30 minutes. We verified sperm lysis using microscopy and then centrifuged samples at 600g for five minutes. We washed the samples twice using Nuclei Isolation Buffer-250 with no NP40 and after the second centrifugation, resuspended the pellet in five volumes of 0.2M H2SO4, then rotated the samples overnight at 4°C. We then centrifuged samples at 4,000 x g for 4 minutes, transferred histone-enriched supernatant to new tubes and added Trichloroacetic Acid to a final concentration of 20% by volume, then incubated samples for two hours on ice. We centrifuged samples at 10,000 x g for five minutes at 4°C, discarded the supernatant and resuspend the pellet in 1mL cold acetone/0.1% HCl. We then washed the pellet twice with 100% acetone, air dried the sample and resuspended the pellet in water.

5.2.5. Sperm chromatin immunoprecipitation and sequencing analysis

Sperm histone ChIP was carried out using a previously published protocol (Hisano et al., 2013). Briefly, for each individual biological rep, sperm collected from the Caputs and Cauda of 10-15 mice were pooled, purified and pre-treated with 50μM DTT for 2h at RT to open sperm chromatin. Cell suspensions were split into roughly 15-20 million sperm aliquots per IP and treated with 90 U of MNase (New England Biolabs, #M0247S) for 5 min at 37C. MNase-digested chromatin was then pre-cleared with blocked A/G Sepharose beads for 1h at 4C. For IP, 5 μg of antibody (H3K27ac or H3K9me2) was added to the pre-cleared chromatin overnight followed by 50 μL of blocked beads for 4 h at 4C. Beads were washed and DNA was then eluted in elution buffer. Following RNase A and proteinase K treatment, DNA was purified using phenol/chloroform isolation and ethanol precipitation and resuspended in 40 μL ultrapure water.

Library preparation using 10ng of DNA and 150 bp paired-end sequencing with 30 million reads per samples was carried out at the Quick Biology, Pasadena, CA. Raw fastq reads were trimmed for adapters and quality and then mapped to the mm10 reference genome using BWA-MEM.

Peaks were called using MACS2 for either narrow or broad regions with an FDR of 0.05. Bedgraph files were used to produce bigwig files for visualization using IGV.

5.3. Results

5.3.1. Increased global Histone H3 lysine 4 trimethylation levels in chromatin of alcohol-exposed sperm

To address the hypothesis that alcohol leads to changes in the abundance of modified histones in sperm, we first employed a mass spectrometry-based technique as in the previous chapter (Active Motif, Carlsbad, CA, USA). We could not identify any significantly altered histones (Figure 5.1 A-E) except for a reduction in H3K4me3 that approached statistical significance ($p=0.0859$, Figure 5.1 A). To preserve statistical power of separate biological replicates, we analyzed total sperm from individual animals ($n=3$), typically between 10-20 million spermatozoa per animal, which was less than the numbers we used for mature sperm in the analysis in the previous chapter (~80 million). Perhaps, due to technical limitations of profiling histones from the reduced numbers of spermatozoa, the data were not considered entirely reliable by the mass-spec technician. Nevertheless, we proceeded to measure total H3K4me3 in the sperm of a separate cohort of animals. Contrary to the identified trend, we observed a significant and robust increase (~45%) in global H3K4me3 in sperm exposed to alcohol (Figure 5.1).

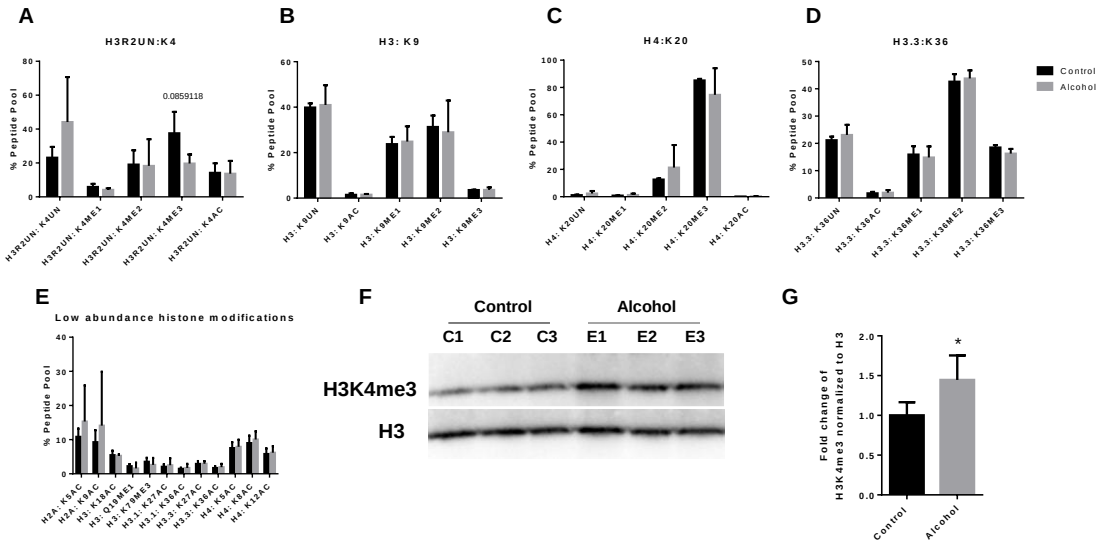

Figure 5.1 Sperm retained histones in alcohol treated males. (A-E) Bar charts depicting abundance of modified histones as a percentage of the peptide pool of (A) H3R2UN:K4 (B) H3:K9 (C) H4:K20 and (D) H3.3:K36, and (E) modified histones as percentages of their respective histone totals (only low abundance modifications that were less than 15% of their totals are shown). (F) Representative western blot of H3K4me3 and its (G) densitometry (n=4 control, 5 alcohol-exposed sperm). UN: unmodified histone, ME1,2,3: mono-, di- and tri-methylation, AC: acetylation, H3R2UN: Modification levels for H3K4 are only measured from peptides where R2 (Arginine in position 2 from N-terminal of H3 peptide) is unmethylated due to assay limitations. * $p < 0.05$

5.3.2. Alterations in the abundance of Histone H3 lysine 4 trimethylation and Histone H3 lysine 9 dimethylation in alcohol exposed sperm chromatin

After identifying increased H3K4me3 in acid-extracted histones from alcohol-exposed sperm, we wanted to better understand how the enrichment of this histone modification is altered in chromatin itself. We used ChIP-seq in sperm chromatin and identified narrow regions of enrichment, typical for canonical H3K4me3, using MACS2 (Feng et al., 2012). Our analysis revealed that this modification is largely concentrated in promoter regions (~74%) with the next most abundant H3K4me3 enrichment found in distal intergenic regions (~15%) (Figure 5.2 A). Although distribution remained broadly

similar in alcohol-exposed sperm, we identified an additional 1266 regions of enrichment. In contrast, only 256 regions were lost with chronic alcohol treatment (Figure 5.2 B). Interestingly, a larger proportion of the peaks gained could be located at gene promoters (29% v/s 20% of peaks lost) while a larger share of the peaks lost was from distal intergenic regions (45% v/s 35% in gained peaks) (Figure 5.2 C). TSS and CpG enrichment profiles revealed a very similar score for a large share of genes or CpG sites, respectively (Figure 5.2 F-G). A small subset of CpG sites which had a higher enrichment almost exclusively localized to promoters (95%, data not shown). GO analysis on genes associated with altered regions of enrichment revealed several pathways related to neuronal development such as synapse assembly (p-value 6.56E-06), synapse organization (p-value 7.36E-05), axonogenesis (p-value 7.30E-05) and neuron differentiation (p-value 1.46E-04). Other major networks were actin cytoskeleton reorganization (p-value 9.41E-05) and embryo development (p-value 2.86E-05). Many important epigenetic regulators were found in the list of embryo development pathway related genes that had altered H3K4me3 with alcohol exposure (Figure 5.2 E), for e.g., Dnmt3a (DNA (cytosine-5)-methyltransferase 3A), Kmt2d (Histone-lysine N-methyltransferase 2D) and Kdm4c (Lysine-specific demethylase 4C, distal intergenic) had increased H3K4me3, while Kdm1a had reduced H3K4me3 with alcohol.

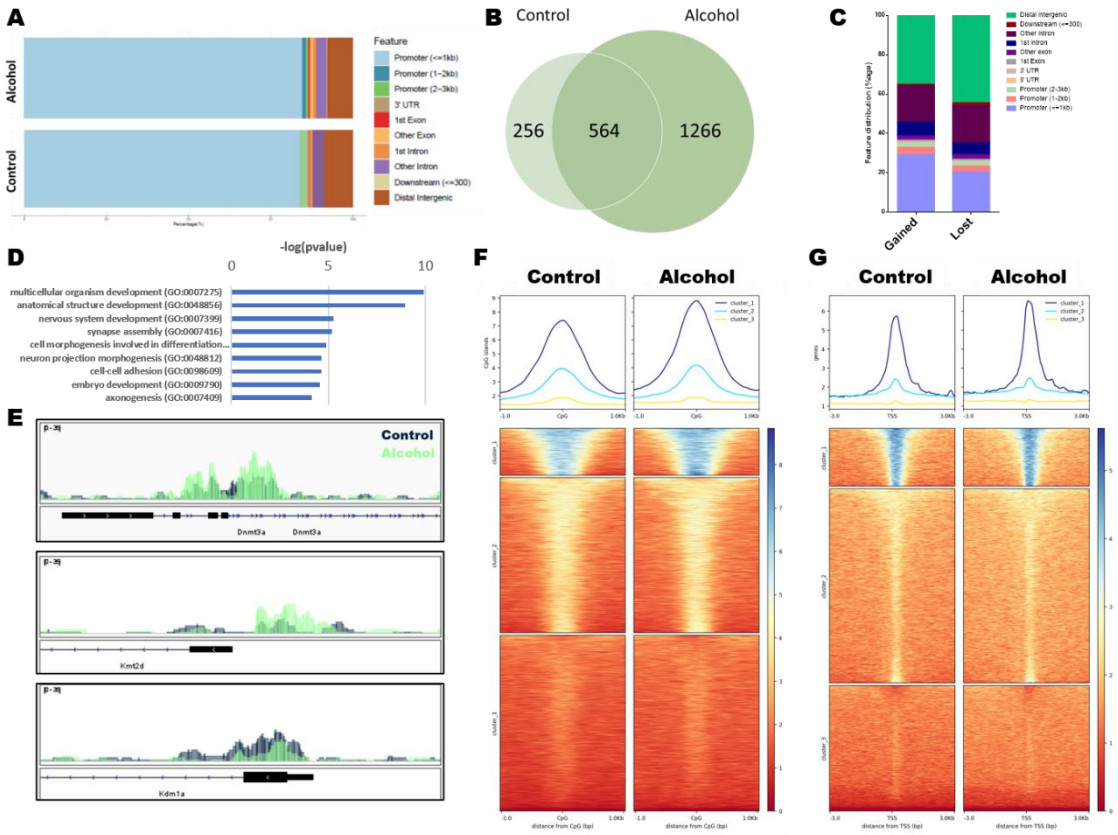

Figure 5.2 Alcohol exposure leads to altered H3K4me3 abundance at key genes involved in embryo development. (A) Genomic feature distribution of H3K4me3 in Control and Alcohol-exposed sperm. (B) Venn diagram showing overlap of peaks identified in control and alcohol exposed sperm. (C) Distribution of genomic features of regions where H3K4me3 was gained or lost with alcohol treatment. (D) Pathway analysis of genes associated with altered H3K4me3. (E) Integrative Genome Viewer tracks showing altered H3K4me3 at promoters or genes involved in embryo development; *Dnmt3a*, *Kmt2d* and *Kdm1a*. Heatmaps displaying enrichment of H3K4me3 signals across(F) CpG islands and (G) Transcription start sites.

Two studies in the last year that examined the effects of paternal diet on offspring health revealed reductions in global H3K9me2 in sire sperm in response to a low protein (Yoshida et al., 2020) or a high fat diet (Claycombe-Larson et al., 2020) indicating that this is a highly malleable histone mark that is responsive to more than one type of paternal exposure. In addition, it also undergoes dynamic shifts during the course of epididymal maturation (4.3.3), implying that short-term exposures limited to the

window of epididymal maturation may also affect its abundance or positioning. To determine if H3K9me2 underwent any changes in enrichment in sperm chromatin as a result of alcohol exposure, we carried out a similar ChIP-seq analysis as we did for H3K4me3. Our analysis revealed that, similar to findings in mature sperm, a large fraction of H3K9me2 enriched DNA is found in distal intergenic regions (Figure 5.3 A) and a sizeable portion of regions associated with alcohol exposure exclusively (333/743) while a smaller fraction was exclusive to controls (123/533). Trends for CpG enrichment were similar between both treatments (Figure 5.3 F). While a major share of alteration occurs at distal intergenic regions (Figure 5.3 C), there is evident loss of enrichment specifically at distal enhancers (Figure 5.3 G). Pathway analysis of genes associated with altered H3K9me2 reveled fewer pathways but the theme of neuronal development emerged again with regulation of presynapse assembly (p-value 3.14E-06), behavior (p-value 1.17E-05) and neurogenesis (p-value 2.36E-05) amongst the top 10 affected pathways. Other pathways converged around cell adhesion (p-value 7.99E-06), which was also enriched in H3K4me3 alteration associated pathways.

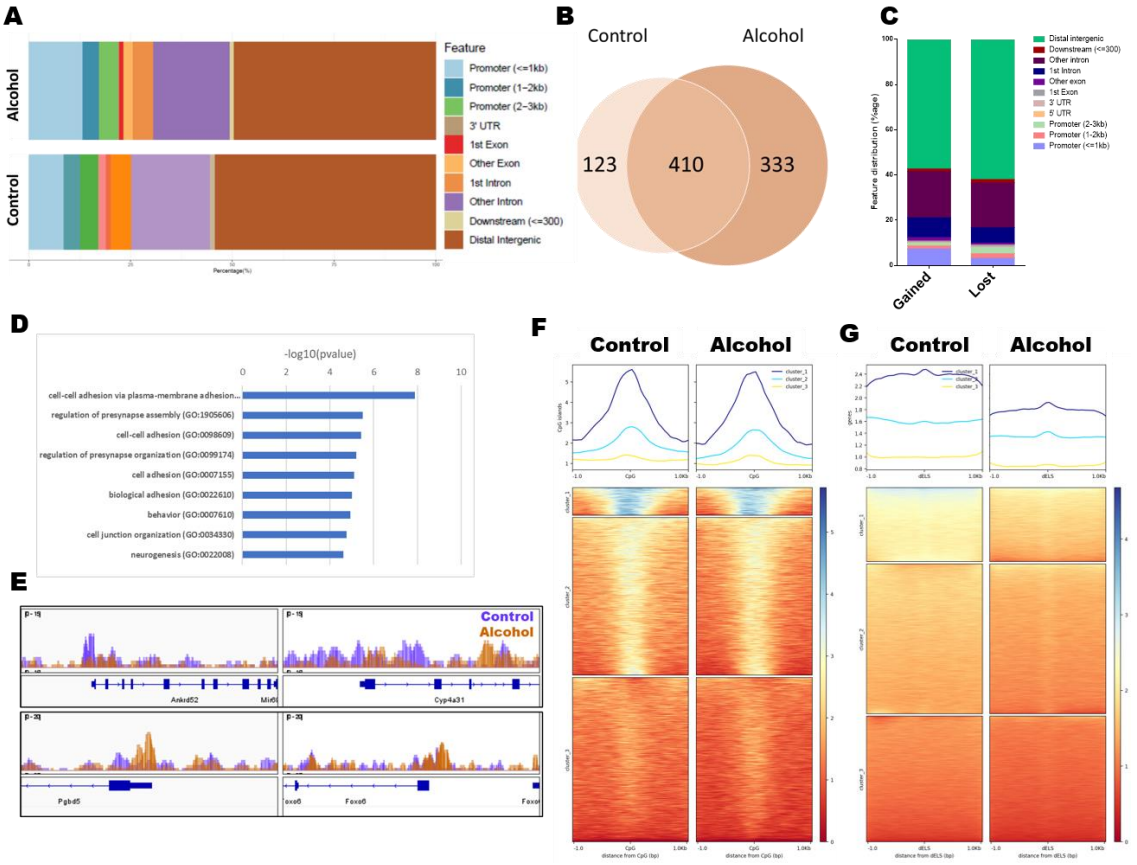

Figure 5.3 Alcohol exposure leads to altered H3K9me2 abundance at distal intergenic regions. (A) Genomic feature distribution of H3K9me2 in Control and Alcohol-exposed sperm. (B) Venn diagram showing overlap of peaks identified in control and alcohol exposed sperm. (C) Distribution of genomic features of regions where H3K9me2 was gained or lost with alcohol treatment. (D) Pathway analysis of genes associated with altered H3K9me2. (E) Integrative Genome Viewer tracks showing altered H3K9me2 at promoters with loss (top panel) or gain of enrichment (bottom panel). Heatmaps displaying enrichment of H3K9me2 signals across(F) CpG islands and (G) distal enhancers.

5.3.3. Placentae of offspring sired by alcohol-exposed males exhibit sex-specific changes to genes involved in lipid transport and steroid metabolism

Similar to our observations in the GD 14.5 placentae of offspring sired by alcohol-exposed male mice (Chapter 3), we identified sex-specific patterns in the dysregulated genes of GD 16.5 placentae. In male offspring, 259 genes were

significantly altered out of which 159 were downregulated and 100 were upregulated (Figure 5.4 A). On the other hand, in female offspring, out of 224 differentially expressed genes, only 25 were downregulated and 199 were upregulated (Figure 5.4 B). Interestingly, gene ontology (GO) analysis revealed that the most significantly affected pathways in both male and female placentae were lipid transport and metabolism, cholesterol metabolism and steroid metabolism (Figure 5.4 C-D). Additionally, in males, pathways of collagen and extracellular organization were also impacted. Lipid transport was also the top affected pathway in GD 14.5 placentae in both male and female offspring of alcohol-exposed sires (Figure 3.1).

Another theme that emerged from this dataset was the dysregulation of clusters of genes similar to the patterns observed in GD 14.5. Several members of the adhesion protein Ceacam family (Ceacam11-14) on chromosome 7 and of the Lactogen family cluster, Prolactin (Prl3a1, 7b1, 8a6), on chromosome 13 were downregulated in GD 16.5 placenta of alcohol-sired males. Although not on the same genetic locus, members of several gene families were also dysregulated collectively. For example, several Collagen members (Col1a1, 1a2, 5a1, 6a2 and 6a3) and Solute carrier proteins (Slc3a1, 5a1 and 7a9) were upregulated in male and female placentae, respectively. Compared to our GD 14.5 dataset, there was very little overlap in the DEGs between sexes. Interestingly, of the 20 genes that were common, members of the Solute carrier protein (*Slc4a1*, *Slc34a2* and *Slc28a3*), Prolactin (*Prl3a1* and *Prl5a1*) and Granzyme family (*Gzmc* and *Gzme*) formed part of this list (Figure 5.4 E).

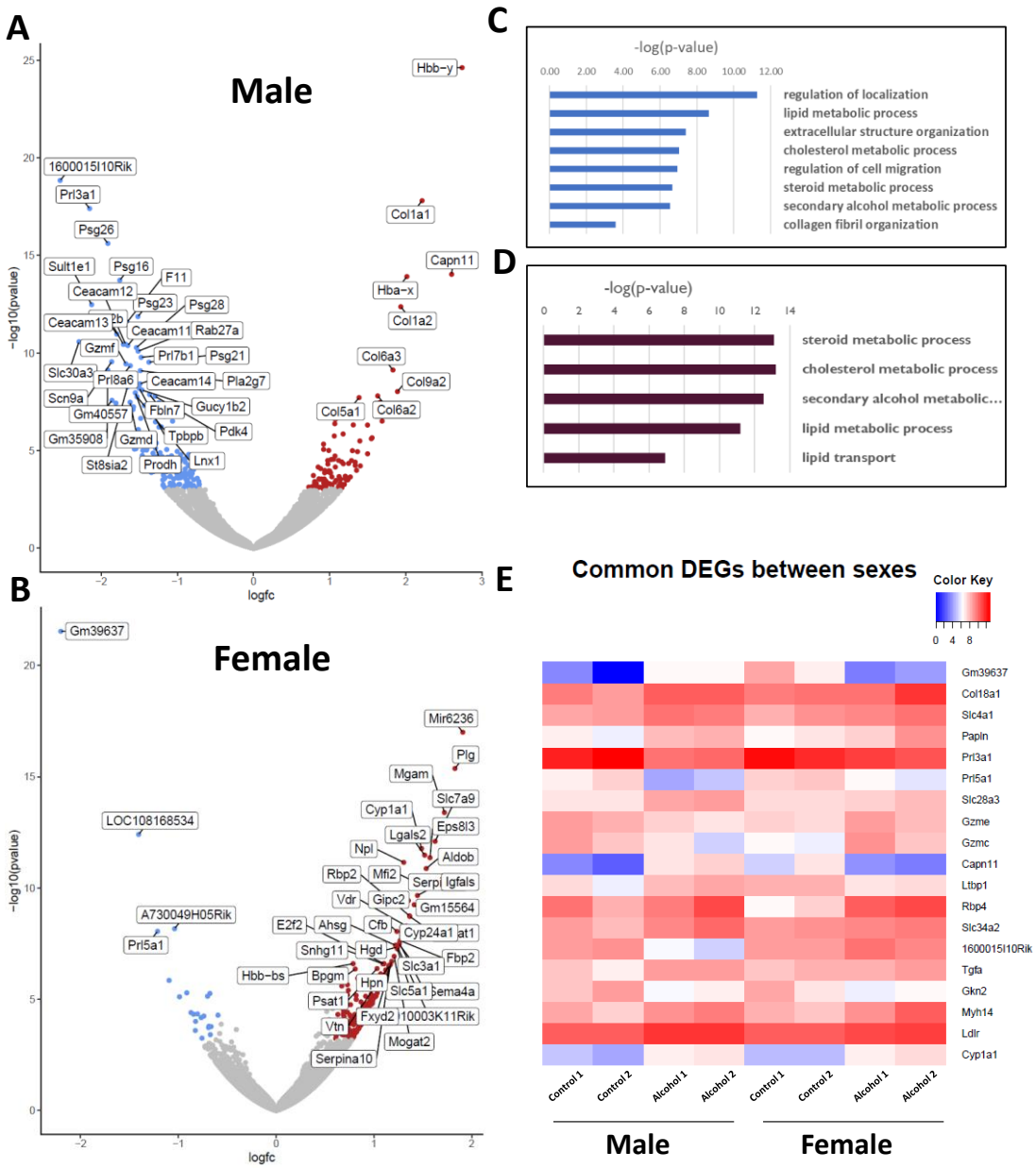

Figure 5.4 Paternal alcohol alters gene expression of common pathways in the GD 16.5 placenta of male and female offspring. Volcano plots highlighting top 40 differentially expressed genes in placenta of **A)** male and **B)** female offspring, **C-D)** the corresponding enriched pathways discovered by GO analysis and **E)** common differentially expressed genes in male and female placenta of offspring sired by alcohol-exposed males

5.3.4. Sperm H3K4me3 abundance correlates with placental CTCF occupancy in male offspring

To assess whether sperm H3K4me3 correlated with other features of chromatin structure, we mapped H3K4me3 profiles of alcohol-exposed and wild-type sperm across known CTCF sites (https://www.encodeproject.org/annotations/ENCSR633QYU/). Interestingly, we found that sperm H3K4me3 was highly enriched within 1kb regions up- and downstream of CTCF sites while distinctly depleted at the CTCF sites themselves. Moreover, there was a higher amount of H3K4me3 enrichment in alcohol-exposed sperm across known CTCF sites (Figure 5.5 A). As sperm from alcohol-exposed males generally had higher H3K4me3 (Figure 5.2), the difference in enrichment across CTCF sites could simply be attributed to this. As we had observed differences in CTCF protein enrichment in male placentae at GD 14.5 (Chapter 3), we analyzed the enrichment of sperm H3K4me3 at the genomic regions where CTCF was altered in the placental dataset. Intriguingly, we observed that alcohol-exposed sperm had higher H3K4me3 in the regions where CTCF was gained in placental chromatin in alcohol-sired offspring and conversely, lower H3K4me3 abundance in regions where CTCF was decreased (Figure 5.5 B-C). This correlation was also evident in the vicinities of genes whose promoters displayed altered H3K4me3 abundance in Figure 5.2 (Figure 5.5 D-E).

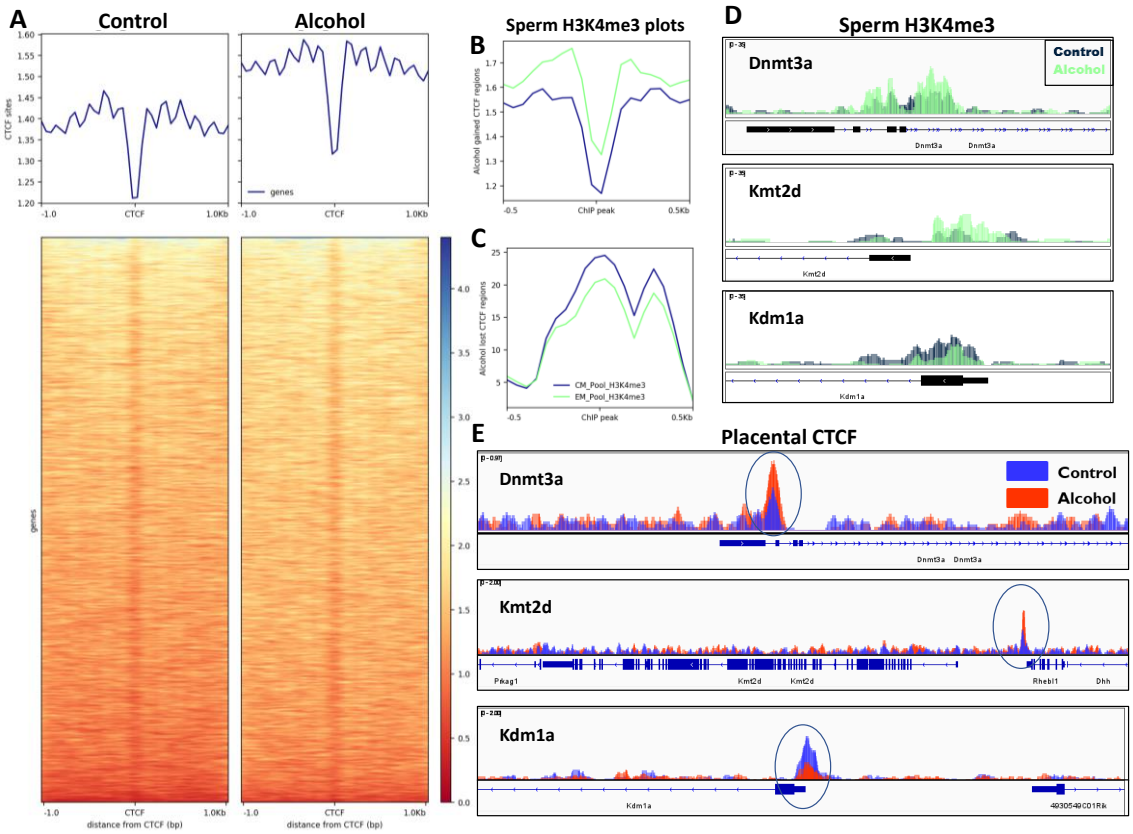

Figure 5.5 Alterations in H3K4me3 in alcohol-exposed sperm correlate with altered CTCF occupancy in the GD 14.5 placenta of male offspring. **A)** Enrichment plot and heatmap of the H3K4me3 from sperm of control and alcohol-exposed mice against known CTCF sites. **B)** Enrichment plot of sperm H3K4me3 across regions that were altered in their CTCF occupancy in the placenta of male offspring of alcohol exposed sires. IGV tracks showing **D)** genes with altered promoter H3K4me3 in alcohol-exposed sperm and **E)** the corresponding CTCF profiles in male placental chromatin in the same region.

5.4. Discussion

Our investigation reveals that alcohol exposure leads to significant changes in the abundance and enrichment of posttranslationally modified histones in sperm chromatin. While several studies from independent groups have confirmed alterations in sperm-retained nucleosomes or histone modifications in response to paternal exposures such as diet and environmental toxins (Lismer et al., 2021; Ben Maamar et al., 2018; Terashima

et al., 2015; Yoshida et al., 2020), this is the first study to analyze the effects of chronic alcohol consumption on sperm retained histones.

The understanding of sperm-retained histones has come a long way from identifying that they are not simply associated with regions depleted of protamines (Gatewood et al., 1987) to where we now know that the sperm epigenome harbors a wide variety of histone marks that associate with very specific genomic features (Brykczynska et al., 2010; Jung et al., 2017; Luense et al., 2016; Ozturk et al., 2021; Yamaguchi et al., 2018). Influencing the histone profile of sperm can have serious deleterious effects on offspring, for e.g. transgene-induced changes to the sperm histone methylation profile in mice impair offspring development and survival (Siklenka et al., 2015). Alterations in human sperm histone profiles have already been linked with poor fertility and blastocyst development in IVF clinics (Denomme et al., 2017). Moreover, certain histone modifications have been shown to escape reprogramming at fertilization (Oikawa et al., 2020) – even transgenerationally across two rounds of epigenetic reprogramming (Hao et al., 2021) signifying a larger role of the paternal epigenome in offspring development than we currently understand.

Our findings describe changes in two different histone modifications in sperm, H3K4me3 and H3K9me2, that largely associate with different regions of chromatin, promoters and distal intergenic regions, respectively. However, pathway analysis suggest that these alterations converge on similar networks of genes, namely those involved in neurodevelopment, cell adhesion and in embryo development (Figure 2D and 3D). Previous work from our lab has identified fetal growth restriction, delayed

parturition and alterations in metabolic functions in the adult offspring (Bedi et al., 2019; Chang et al., 2017, 2019a, 2019b) as consequences of paternal alcohol consumption. While, we did not analyze offspring neurodevelopment in these studies, work from another group has found consistent behavioral defects that correlate with paternal alcohol exposure (Beeler et al., 2019; Rompala et al., 2017a). They also identify changes in sperm small noncoding RNAs and epididymosomes, extracellular vesicles that have been shown to transport a small RNA payload from the surrounding somatic epididymal cells to maturing sperm (Rompala et al., 2018)

Recently, a study of sperm H3K4me3 alterations with low folate diets (Lismer et al., 2021) has found that the altered abundance of H3K4me3 in sperm directly correlates with levels of this modification in the early embryo at the 8-cell stage. While, we have not characterized the early embryo in our studies, we compared the altered sperm H3K4me3 with the altered transcriptomes in GD 16.5 placenta as well as CTCF-bound chromatin in GD 14.5 male placentas from offspring sired from alcohol-exposed males. Unsurprisingly, changes in placental transcription could not be explained by the alteration of H3K4me3 in paternal sperm. The placenta is a highly specialized and differentiated organ with a homogenous population of cells. It would be interesting, however, to characterize the abundance of H3K4me3 in placental chromatin as well as in the early embryo to confirm any correlation or lack thereof to paternal H3K4me3. On the other hand, comparing paternal histone profiles to placental CTCF alterations led us to a surprising finding. Paternal alcohol exposure led to an overall higher H3K4me3 enrichment profile in sperm that correlated highly with regions around known CTCF

sites. Moreover, the sites in the placenta of male offspring that gained CTCF with paternal alcohol exposure also had higher H3K4me3 retention in the sperm that produced them. Also, sites with decreased CTCF abundance had a corresponding loss of H3K4me3 signal in the paternal sperm chromatin as well. Previously, it has been shown that the insulator binding protein CTCF has the unusual ability to position multiple nucleosomes flanking its binding sites (Fu et al., 2008). In our analysis, we observe 5 subpeaks within 1000 bp on either side (up- and downstream) of the CTCF site. These perfectly correlate with a ~200bp nucleosome peak that one would expect in a ChIP of a histone modification. Also, amongst all histone modifications, H3K4me3 has shown to have the highest correlation with CTCF sites (Fu et al., 2008). This suggests that paternal alcohol exposure can potentially influence chromatin structure in highly differentiated tissues separated from the early embryo stage by several rounds of cell divisions. As a lot of these analysis are still correlative, future studies must focus on measuring histone and CTCF enrichment in the early embryos of alcohol-sired offspring.

The intention of using mass spectrometry-based analyses was to cast a wide net to identify alterations in global histone levels that associate with alcohol exposure. Unfortunately, due to the limited amount of starting material per animal, this did not work out. In another preparation, where mice were administered 10% ethanol without sweet'n'low, the results reveal an increase in H3K4me3 (data not shown). However, in that analysis, as well, the proportions of unmodified histones for several histone marks seemed out of range from what we observed in the mature sperm fraction analyzed in Chapter 4. This is still a promising technique for identifying global histone alterations in

sperm, however the strategy going forward needs to involve pools of sperm collected from several mice (>3/treatment at least) to count as a single biological replicate. The large (~45%) increase in global H3K4me3 identified in our study and similar scale of alterations (~50% global reduction) in H3K9me2 in response to low protein or high fat diet (Claycombe-Larson et al., 2020; Yoshida et al., 2020), reveal that alterations in the sperm epigenome in response to environmental exposures are not always subtle and high throughput techniques such as ELISA or mass spectrometry can offer valuable information once optimized for sperm numbers.

Another limitation of this study was the low level of sequencing depth. While the differences we found for broad shifts of histone occupancy as well as at specific promoters is reliable, it is highly likely that we barely scratched the surface in terms of identifying differential regions of enrichment. Compared to our analysis of the sperm chromatin in caput and cauda epididymides (Chapter 4), as well as to a recent study of H3K4me3 in sperm (Lismer et al., 2021) where uniquely mapped reads ranged between 35-65 million reads per sample, this study had roughly 10-15 million reads per sample. Mappability as well as number of peaks identified for most DNA-binding proteins increases proportionally with greater read depth (Landt et al., 2012). This increases the confidence of finding large number of genomic regions of enrichment at very low FDRs (<0.001). To get a more complete picture of genetic networks influenced in sperm, it is even more important to have very high read depth for ChIP-seq experiments owing to the low abundance of histones and relatively inaccessible chromatin. DTT treatment and MNase digestion of sperm chromatin increase the accessibility of nucleosomes several

fold and having several biological replicates helped increase our confidence in the results we obtained. Nevertheless, future experiments will need to take this factor into account.

6. CONCLUSIONS AND FUTURE DIRECTIONS

The studies described in this dissertation sought to analyze the role of the preconception paternal environment in fetal health and development. To do so, we focused on the hitherto understudied aspect of paternal alcohol consumption and its effects on fetal growth. As previously mentioned, (Introduction; Figure 1.1) most research into the detrimental effects of alcohol in reproduction have singularly focused on the role of the mother. Only recently, analyses of public health data, where available, and large-scale retrospective studies of pregnancy outcomes have found paternal alcohol consumption as an important metric for fetal and infant health prospects (McBride and Johnson, 2016; Xia et al., 2018). Several groups have contributed to these efforts using studies in animals, especially in rodents, and report different mechanisms that can explain how the memory of environmental insults can transmit via the paternal germline to the offspring. While there is still no consensus on how this occurs, a growing body of evidence is pointing towards an epigenetic basis of inheritance i.e., mediated by chemical modifications to the DNA itself such as via DNA methylation, by modifications to chromatin via the reorganization of DNA binding proteins such as histones, and even through sperm-inherited non-coding RNAs

In our approach, we use a mouse model where we expose male mice to 10% alcohol for four hours a day during the start of their active cycle. Not only does this approach limit the exposure to a short window, thus avoiding the undesired effects of constant alcohol intake such as dehydration, excessive calorie consumption and liver cirrhosis, it also mimics physiologically relevant binge exposures with blood alcohol

concentration peaking between 100-200 mg/dL within this window. This resembles the alcohol consumption habits of chronic alcoholics as well as younger adults who do not drink as frequently but typically report binge drinking (National Institute of Alcohol Abuse and Alcoholism, 2021). To capture all possible critical exposure windows, we set male sire mice on this schedule for roughly two spermatogenic waves i.e., for 70 days, and then mated these mice to control female mice. The resulting conceptuses were terminated during pregnancy to determine the effects of sire ethanol exposure in fetal growth.

In two separate sets of experiments, we reproducibly observed reductions in fetal growth at different stages of mid-to-late gestation (GD 14.5 and 16.5) accompanied by reductions in placental efficiency. By focusing on the transcriptional regulation of the placenta, an essential conduit of nutrients that determines the growth kinetics of the fetus, we were able to determine large scale pathway alterations induced by paternal alcohol. These effects were consistent between both experiments and centered heavily around changes in genes involved in lipid transport, steroid metabolism, collagen organization and cellular movement. This strongly suggests that paternal alcohol has a programmed mode of action and does not dysregulate offspring development randomly.

Another important finding from the GD 14.5 placental transcriptome analyses was the alterations of large clusters of genes namely, the albumin, apolipoprotein and fibrinogen clusters. This led us to investigate the regulators of large-scale chromatin architecture such as CTCF and members of the Cohesin family of proteins, involved in the formation and insulation of topologically active domains via the extrusion of

chromatin loops. Our analyses revealed significant alterations in the abundance of CTCF across, but not limited to, the genomic regions of interest in the placenta of male offspring. Moreover, annotated gene sets within 10 kb of an altered CTCF site also enriched for networks involved in cellular movement and molecular transport. Although the specific networks of lipid transport and sterol metabolism did not emerge from this analysis, it suggested a convergence of the effects of paternal alcohol on chromatin regulation with effects observed on transcription. Despite the highly studied role of CTCF in chromatin-loop boundary insulation, the effects of its wide-scale depletion or alteration on transcription are not well characterized and they do not always lead to correlative proportional changes in transcript abundance. In this respect, targeted deletion of CTCF at genetic loci has provided some direct evidence of dysregulated expression of involved genes. This formed the basis of our hypothesis implicating the involvement of this architectural protein in the dysregulated clusters of genes in GD 14.5 placenta. Interestingly, clusters of dysregulated genes also emerged in our analysis of GD 16.5 placenta across both sexes. While it is reasonable to expect that the CTCF alterations we identified in GD 14.5 placentae persist into GD 16.5, this needs to be confirmed by repeating those experiments at this timepoint as well. Comparing the transcriptional profiles of genes that were dysregulated (DEGs) in placentae of GD 16.5 offspring, irrespective of sex (Figure 5.4E), to the CTCF ChIP-seq data from GD 14.5 placentae in male offspring, we found several DEGs (*Gzmf, Col18a1, Col6a1/a2* and *Prl5a1*) that contained altered CTCF within 20 kb of their gene bodies. Bolstered by previous studies of localized CTCF alterations, these correlations support our hypothesis

that altered CTCF occupancy precedes and is responsible for the targeted dysregulation of gene networks in the placenta. To our knowledge, this is the first study that links paternal alcohol exposure to the altered prevalence of CTCF in the offspring.

Another important mechanism implicated in sperm-inherited programming of offspring involves the epigenetic inheritance of altered histones. In Chapter 4, we provide evidence revealing that the histone landscape in the sperm cell is more dynamic than previously believed. Through mass spectrometry based global profiling of histones in post-testicular sperm at the proximal caput and distal caudal ends of the epididymis, we show that there are marked changes in the abundance of several histone modifications. Using ChIP-seq experiments for selected histone modifications, H3K27ac and H3K9me2, we identify a highly dynamic profile of these modifications at sites associated with enhancers. Using the same approach, we then characterized histones in mature sperm from alcohol-exposed males. Our analyses revealed substantial increases in global H3K4me3 levels accompanied by altered enrichment at promoters of genes involved in embryo development and neuronal development related pathways. We also identified significant changes in the H3K9me2 profiles of alcohol-exposed sperm at the genomic level. These changes also aligned at genes associated with neuronal development suggesting converging actions of alcohol via different histone marks.

Surprisingly, H3K4me3 appeared to be highly correlated with CTCF sites in the mouse genome (Figure 5.5). Moreover, genetic loci with increased H3K4me3 in response to alcohol appeared to retain higher levels of CTCF in the GD 14.5 affected placentae. Conversely, regions with reduced H3K4me3 also had a corresponding loss of

CTCF signal in the same regions. This exciting finding provides a possible mechanism by which the sperm-inherited histone profile can influence chromatin architecture in the offspring. Studies so far have focused on the immediate impact of an altered sperm H3K4me3 landscape on histone abundance and transcription in the early embryo up to the 8-cell stage. Our studies add another facet to the complex ways in which the histone profile of the male germline influences the developing embryo. It is important to fill the gaps connecting altered histones in sperm to the early embryo leading up to the mid-gestation placenta. Therefore, future studies must focus on measuring both H3K4me3 and CTCF abundance in the genomes of these tissues. Notwithstanding the correlative nature of these analyses, CTCF has previously been shown to position H3K4me3 in the regions flanking its binding sites, thus making this a highly plausible mechanism by which alcohol could impact CTCF abundance in the tissues of the offspring.

This work helps bridge the gap in our understanding of how a memory of the environmental exposure of the male germline can be inherited in the offspring. Using the dynamic sperm histone landscape as a medium, we present evidence linking the effects of paternal alcohol exposure to chromatin alterations persisting in the offspring placenta. These analyses provide a template for assessing the influence of other toxins on fetal health and development in paternal exposure paradigms as well.

REFERENCES

Abel, E.L. (2004). Paternal contribution to fetal alcohol syndrome. Addict. Biol. *9*, 127–133.

Acharya, K.S., Schrott, R., Grenier, C., Huang, Z., Holloway, Z., Hawkey, A., Levin, E.D., and Murphy, S.K. (2020). Epigenetic alterations in cytochrome P450 oxidoreductase (Por) in sperm of rats exposed to tetrahydrocannabinol (THC). Sci. Rep. *10*, 12251.

Adams, P.M., Stein, S.A., Palnitkar, M., Anthony, A., Gerrity, L., and Shanklin, D.R. (1989). Evaluation and characterization of the hypothyroid hyt/hyt mouse. I: Somatic and behavioral studies. Neuroendocrinology *49*, 138–143.

Afgan, E., Baker, D., Batut, B., van den Beek, M., Bouvier, D., Cech, M., Chilton, J., Clements, D., Coraor, N., Grüning, B.A., et al. (2018). The Galaxy platform for accessible, reproducible and collaborative biomedical analyses: 2018 update. Nucleic Acids Res. *46*, W537–W544.

Amanai, M., Brahmajosyula, M., and Perry, A.C.F. (2006). A Restricted Role for Sperm-Borne MicroRNAs in Mammalian Fertilization1. Biol. Reprod. *75*, 877–884.

Anderson, R.A., Willis, B.R., Oswald, C., Reddy, J.M., Beyler, S.A., and Zaneveld, L.J.D. (1980). Hormonal imbalance and alterations in testicular morphology induced by chronic ingestion of ethanol. Biochem. Pharmacol. *29*, 1409–1419.

Anifandis, G., Bounartzi, T., Messini, C.I., Dafopoulos, K., Sotiriou, S., and Messinis, I.E. (2014). The impact of cigarette smoking and alcohol consumption on sperm parameters and sperm DNA fragmentation (SDF) measured by Halosperm(A (R)). Arch. Gynecol. Obstet. *290*, 777–782.

Anway, M.D., Cupp, A.S., Uzumcu, M., and Skinner, M.K. (2005). Epigenetic transgenerational actions of endocrine disruptors and mate fertility. Science (80-.). *308*, 1466–1469.

Ariel, M., Cedar, H., and McCarrey, J. (1994). Developmental changes in methylation of spermatogenesis–specific genes include reprogramming in the epididymis. Nat. Genet. *7*, 59–63.

Arpanahi, A., Brinkworth, M., Iles, D., Krawetz, S.A., Paradowska, A., Platts, A.E., Saida, M., Steger, K., Tedder, P., and Miller, D. (2009). Endonuclease-sensitive regions of human spermatozoal chromatin are highly enriched in promoter and CTCF binding sequences. Genome Res *19*, 1338–1349.

Aszterbaum, M., Feingold, K.R., Menon, G.K., and Williams, M.L. (1993). Glucocorticoids accelerate fetal maturation of the epidermal permeability barrier in the rat. J Clin Invest *91*, 2703–2708.

Bartke, A., Steele, R.E., Musto, N., and Caldwell, B. V. (1973). Fluctuations in plasma testosterone levels in adult male rats and mice. Endocrinology *92*, 1223–1228.

Beamer, W.J., Eicher, E.M., Maltais, L.J., and Southard, J.L. (1981). Inherited primary hypothyroidism in mice. Science (80-.). *212*, 61–63.

Bedi, Y., and Golding, M.C. (2019). Context is King — Questioning the causal role of DNA methylation in environmentally induced changes in gene expression. Curr. Opin. Toxicol. *14*, 46–51.

Bedi, Y., Chang, R.C., Gibbs, R., Clement, T.M., and Golding, M.C. (2019). Alterations in sperm-inherited noncoding RNAs associate with late-term fetal growth restriction induced by preconception paternal alcohol use. Reprod. Toxicol. *87*, 11–20.

Beeler, E., Nobile, Z.L., and Homanics, G.E. (2019). Paternal preconception every-other-day ethanol drinking alters behavior and ethanol consumption in offspring. Brain Sci. *9*.

Bell, A.C., and Felsenfeld, G. (2000). Methylation of a CTCF-dependent boundary controls imprinted expression of the Igf2 gene. Nature *405*, 482–485.

Belleannee, C., Calvo, E., Caballero, J., and Sullivan, R. (2013). Epididymosomes Convey Different Repertoires of MicroRNAs Throughout the Bovine Epididymis. Biol. Reprod. *89*.

Le Blévec, E., Muroňová, J., Ray, P.F., and Arnoult, C. (2020). Paternal epigenetics: Mammalian sperm provide much more than DNA at fertilization. Mol. Cell. Endocrinol. *518*.

Bolger, A.M., Lohse, M., and Usadel, B. (2014). Trimmomatic: a flexible trimmer for Illumina sequence data. Bioinformatics *30*, 2114–2120.

Bromfield, J.J., Schjenken, J.E., Chin, P.Y., Care, A.S., Jasper, M.J., and Robertson, S.A. (2014). Maternal tract factors contribute to paternal seminal fluid impact on metabolic phenotype in offspring. Proc. Natl. Acad. Sci. *111*, 2200–2205.

Brykczynska, U., Hisano, M., Erkek, S., Ramos, L., Oakeley, E.J., Roloff, T.C., Beisel, C., Schübeler, D., Stadler, M.B., and Peters, A.H.F.M. (2010). Repressive and active histone methylation mark distinct promoters in human and mouse spermatozoa. Nat. Struct. Mol. Biol. *17*, 679–687.

Bui, H.T., Wakayama, S., Mizutani, E., Park, K.K., Kim, J.H., Van Thuan, N., and Wakayama, T. (2011). Essential role of paternal chromatin in the regulation of transcriptional activity during mouse preimplantation development. Reproduction *141*, 67–77.

Canteros, G., Retrori, V., Franchi, A., Genaro, A., Cebral, E., Faletti, A., Gimeno, M., Mccanntt, S.M., and Mccann, S.M. (1995). Ethanol inhibits luteinizing hormone-releasing hormone (LHRH) secretion by blocking the response of LHRH neuronal terminals to nitric oxide.

Carnahan, M.N., Veazey, K.J., Muller, D., Tingling, J.D., Miranda, R.C., and Golding, M.C. (2013). Identification of cell-specific patterns of reference gene stability in quantitative reverse-transcriptase polymerase chain reaction studies of embryonic, placental and neural stem models of prenatal ethanol exposure. Alcohol *47*.

Carone, B.R., Fauquier, L., Habib, N., Shea, J.M., Hart, C.E., Li, R.W., Bock, C., Li, C.J., Gu, H.C., Zamore, P.D., et al. (2010). Paternally Induced Transgenerational Environmental Reprogramming of Metabolic Gene Expression in Mammals. Cell *143*, 1084–1096.

Carone, B.R.R., Hung, J.-H.H., Hainer, S.J.J., Chou, M.-T. Te, Carone, D.M.M., Weng, Z., Fazzio, T.G.G., and Rando, O.J.J. (2014). High-Resolution Mapping of Chromatin Packaging in Mouse Embryonic Stem Cells and Sperm. Dev. Cell *30*, 11–22.

Carter, R.C., Jacobson, J.L., Sokol, R.J., Avison, M.J., and Jacobson, S.W. (2013). Fetal Alcohol-Related Growth Restriction from Birth through Young Adulthood and Moderating Effects of Maternal Prepregnancy Weight. Alcohol. Exp. Res. *37*, 452–462.

Castells, S., Mark, E., Abaci, F., and Schwartz, E. (1981). Growth retardation in fetal alcohol syndrome. Unresponsiveness to growth-promoting hormones. Dev Pharmacol Ther *3*, 232–241.

de Castro Barbosa, T., Ingerslev, L.R., Alm, P.S., Versteyhe, S., Massart, J., Rasmussen, M., Donkin, I., Sjögren, R., Mudry, J.M., Vetterli, L., et al. (2016). High-fat diet reprograms the epigenome of rat spermatozoa and transgenerationally affects metabolism of the offspring. Mol Metab *5*, 184–197.

Champroux, A., Torres-Carreira, J., Gharagozloo, P., Drevet, J.R., and Kocer, A. (2016). Mammalian sperm nuclear organization: Resiliencies and vulnerabilities. Basic Clin. Androl. *26*.

Chang, R.C., Skiles, W.M., Chronister, S.S., Wang, H., Sutton, G.I., Bedi, Y.S., Snyder, M., Long, C.R., and Golding, M.C. (2017). DNA methylation-independent growth restriction and altered developmental programming in a mouse model of preconception male alcohol exposure. Epigenetics *12*, 841–853.

Chang, R.C., Wang, H., Bedi, Y., and Golding, M.C. (2019a). Preconception paternal alcohol exposure exerts sex-specific effects on offspring growth and long-term metabolic programming. Epigenetics and Chromatin *12*.

Chang, R.C., Thomas, K.N., Bedi, Y.S., and Golding, M.C. (2019b). Programmed increases in LXRα induced by paternal alcohol use enhance offspring metabolic adaptation to high-fat diet induced obesity. Mol. Metab. *30*, 161–172.

Chen, P., Zhao, J., Wang, Y., Wang, M., Long, H., Liang, D., Huang, L., Wen, Z., Li, W., Li, X., et al. (2013). H3.3 actively marks enhancers and primes gene transcription via opening higher-ordered chromatin. Genes Dev. *27*, 2109–2124.

Chen, Q., Yan, M.H., Cao, Z.H., Li, X., Zhang, Y.Y.F., Shi, J.C., Feng, G.H., Peng, H.Y., Zhang, X.D., Zhang, Y.Y.F., et al. (2016a). Sperm tsRNAs contribute to intergenerational inheritance of an acquired metabolic disorder. Science (80-.). *351*, 397–400.

Chen, Q., Yan, W., and Duan, E.K. (2016b). Epigenetic inheritance of acquired traits through sperm RNAs and sperm RNA modifications. Nat. Rev. Genet. *17*, 733–743.

Cicero, T.J., Adams, M.L., O'Connor, L., Nock, B., Meyer, E.R., and Wozniak, D. (1990). Influence of chronic alcohol administration on representative indices of puberty and sexual maturation in male rats and the development of their progeny. J. Pharmacol. Exp. Ther. *255*.

Ciosk, R., Shirayama, M., Shevchenko, A., Tanaka, T., Toth, A., Shevchenko, A., and Nasmyth, K. (2000). Cohesin's binding to chromosomes depends on a separate complex consisting of Scc2 and Scc4 proteins. Mol. Cell *5*, 243–254.

Claycombe-Larson, K.G., Bundy, A.N., and Roemmich, J.N. (2020). Paternal high-fat diet and exercise regulate sperm miRNA and histone methylation to modify placental inflammation, nutrient transporter mRNA expression and fetal weight in a sex-dependent manner. J. Nutr. Biochem. *81*.

Condorelli, R.A., Calogero, A.E., Vicari, E., and La Vignera, S. (2015). Chronic consumption of alcohol and sperm parameters: our experience and the main evidences. Andrologia *47*, 368–379.

Conine, C.C., Sun, F., Song, L., Rivera-Perez, J.A., and Rando, O.J. (2018). Small RNAs Gained during Epididymal Transit of Sperm Are Essential for Embryonic Development in Mice. Dev. Cell *46*, 470-+.

Consortium, E.P., Moore, J.E., Purcaro, M.J., Pratt, H.E., Epstein, C.B., Shoresh, N., Adrian, J., Kawli, T., Davis, C.A., Dobin, A., et al. (2020). Expanded encyclopaedias of DNA elements in the human and mouse genomes. Nature *583*, 699–710.

Creyghton, M.P., Cheng, A.W., Welstead, G.G., Kooistra, T., Carey, B.W., Steine, E.J., Hanna, J., Lodato, M.A., Frampton, G.M., Sharp, P.A., et al. (2010). Histone H3K27ac separates active from poised enhancers and predicts developmental state. Proc Natl Acad Sci U S A *107*, 21931–21936.

Day, J., Savani, S., Krempley, B.D., Nguyen, M., and Kitlinska, J.B. (2016). Influence of paternal preconception exposures on their offspring: Through epigenetics to phenotype. Am. J. Stem Cells *5*, 11–18.

Day, N.L., Leech, S.L., Richardson, G.A., Cornelius, M.D., Robles, N., and Larkby, C. (2002). Prenatal alcohol exposure predicts continued deficits in offspring size at 14 years of age. Alcohol Clin Exp Res *26*, 1584–1591.

Decato, B.E., Lopez-Tello, J., Sferruzzi-Perri, A.N., Smith, A.D., and Dean, M.D. (2017). DNA Methylation Divergence and Tissue Specialization in the Developing Mouse Placenta. Mol. Biol. Evol. *34*, 1702–1712.

deMello, D.E., Heyman, S., Govindarajan, R., Sosenko, I.R., and Devaskar, U.P. (1994). Delayed ultrastructural lung maturation in the fetal and newborn hypothyroid (Hyt/Hyt) mouse. Pediatr Res *36*, 380–386.

Denomme, M.M., McCallie, B.R., Parks, J.C., Schoolcraft, W.B., and Katz-Jaffe, M.G. (2017). Alterations in the sperm histone-retained epigenome are associated with unexplained male factor infertility and poor blastocyst development in donor oocyte IVF cycles. Hum. Reprod. *32*, 2443–2455.

Dias, B.G., and Ressier, K.J. (2014). Parental olfactory experience influences behavior and neural structure in subsequent generations. Nat. Neurosci. *17*, 89–96.

Dobin, A., Davis, C.A., Schlesinger, F., Drenkow, J., Zaleski, C., Jha, S., Batut, P., Chaisson, M., and Gingeras, T.R. (2013). STAR: ultrafast universal RNA-seq aligner. Bioinformatics *29*, 15–21.

Donkin, I., Versteyhe, S., Ingerslev, L.R., Qian, K., Mechta, M., Nordkap, L., Mortensen, B., Appel, E.V.R., Jorgensen, N., Kristiansen, V.B., et al. (2016). Obesity and Bariatric Surgery Drive Epigenetic Variation of Spermatozoa in Humans. CELL Metab. *23*, 369–378.

Dror, D.K. (2011). Vitamin D status during pregnancy: maternal, fetal, and postnatal outcomes. Curr Opin Obs. Gynecol *23*, 422–426.

Du, Z., Zheng, H., Huang, B., Ma, R., Wu, J., Zhang, X., He, J., Xiang, Y., Wang, Q., Li, Y., et al. (2017). Allelic reprogramming of 3D chromatin architecture during early mammalian development. Nature *547*, 232–235.

Eckhardt, F., Lewin, J., Cortese, R., Rakyan, V.K., Attwood, J., Burger, M., Burton, J., Cox, T. V, Davies, R., Down, T.A., et al. (2006). DNA methylation profiling of human chromosomes 6, 20 and 22. Nat Genet *38*, 1378–1385.

Edwards, J.R., O'Donnell, A.H., Rollins, R.A., Peckham, H.E., Lee, C., Milekic, M.H., Chanrion, B., Fu, Y., Su, T., Hibshoosh, H., et al. (2010). Chromatin and sequence features that define the fine and gross structure of genomic methylation patterns. Genome Res *20*, 972–980.

Emanuele, N. V, LaPaglia, N., Benefield, J., and Emanuele, M.A. (2001). Ethanol-induced hypogonadism is not dependent on activation of the hypothalamic-pituitary-adrenal axis. Endocr. Res. *27*, 465–472.

Erkek, S., Hisano, M., Liang, C.-Y.Y., Gill, M., Murr, R., Dieker, J., Schübeler, D., Vlag, J. van der, Stadler, M.B., Peters, A.H.F.M.F.M., et al. (2013). Molecular determinants of nucleosome retention at CpG-rich sequences in mouse spermatozoa. Nat Struct Mol Biol *20*, 868–875.

Esakky, P., Hansen, D.A., Drury, A.M., Felder, P., Cusumano, A., and Moley, K.H. (2016). Paternal exposure to cigarette smoke condensate leads to reproductive sequelae and developmental abnormalities in the offspring of mice. Reprod. Toxicol. *65*, 283–294.

Espitia Jaimes, C., Fish, R.J., and Neerman-Arbez, M. (2018). Local chromatin interactions contribute to expression of the fibrinogen gene cluster. J. Thromb. Haemost. JTH *16*, 2070–2082.

Fedoriw, A.M., Stein, P., Svoboda, P., Schultz, R.M., and Bartolomei, M.S. (2004). Transgenic RNAi reveals essential function for CTCF in H19 gene imprinting. Science (80-.). *303*, 238–240.

Feil, R., and Fraga, M.F. (2012). Epigenetics and the environment: emerging patterns and implications. Nat. Rev. Genet. *13*, 97–109.

Feng, J., Liu, T., Qin, B., Zhang, Y., and Liu, X.S. (2012). Identifying ChIP-seq enrichment using MACS. Nat. Protoc. *7*, 1728–1740.

Finegersh, A., Rompala, G.R., Martin, D.I.K.K., and Homanics, G.E. (2015). Drinking beyond a lifetime: New and emerging insights into paternal alcohol exposure on subsequent generations. ALCOHOL *49*, 461–470.

Fleming, T.P., Watkins, A.J., Velazquez, M.A., Mathers, J.C., Prentice, A.M., Stephenson, J., Barker, M., Saffery, R., Yajnik, C.S., Eckert, J.J., et al. (2018). Origins of lifetime health around the time of conception: causes and consequences. Lancet *391*, 1842–1852.

Flyamer, I.M., Gassler, J., Imakaev, M., Brandão, H.B., Ulianov, S. V., Abdennur, N., Razin, S. V., Mirny, L.A., and Tachibana-Konwalski, K. (2017). Single-nucleus Hi-C reveals unique chromatin reorganization at oocyte-to-zygote transition. Nature *544*, 110–114.

Friedlander, M.R., Mackowiak, S.D., Li, N., Chen, W., and Rajewsky, N. (2012). miRDeep2 accurately identifies known and hundreds of novel microRNA genes in seven animal clades. Nucleic Acids Res. *40*, 37–52.

Fu, Y., Sinha, M., Peterson, C.L., and Weng, Z. (2008). The insulator binding protein CTCF positions 20 nucleosomes around its binding sites across the human genome. PLoS Genet. *4*, 1000138.

Fuller, G.M., and Zhang, Z. (2001). Transcriptional control mechanism of fibrinogen gene expression. Ann N Y Acad Sci *936*, 469–479.

Fullston, T., Teague, E., Palmer, N.O., DeBlasio, M.J., Mitchell, M., Corbett, M., Print, C.G., Owens, J.A., and Lane, M. (2013). Paternal obesity initiates metabolic disturbances in two generations of mice with incomplete penetrance to the F-2 generation and alters the transcriptional profile of testis and sperm microRNA content. FASEB J. *27*, 4226–4243.

Gao, J., Wei, Y., Huang, Y., Liu, D., Liu, G., Wu, M., Wu, L., Zhang, Q., Zhang, Z., Zhang, R., et al. (2005). The Expression of Intact and Mutant Human apoAI/CIII/AIV/AV Gene Cluster in Transgenic Mice. J. Biol. Chem. *280*, 12559–12566.

Gapp, K., Jawaid, A., Sarkies, P., Bohacek, J., Pelczar, P., Prados, J., Farinelli, L., Miska, E., and Mansuy, I.M. (2014a). Implication of sperm RNAs in transgenerational inheritance of the effects of early trauma in mice. Nat. Neurosci.

Gapp, K., Jawaid, A., Sarkies, P., Bohacek, J., Pelczar, P., Prados, J., Farinelli, L., Miska, E., and Mansuy, I.M. (2014b). Implication of sperm RNAs in transgenerational inheritance of the effects of early trauma in mice. Nat. Neurosci. *17*, 667-+.

Garcia, B.A., Mollah, S., Ueberheide, B.M., Busby, S.A., Muratore, T.L., Shabanowitz, J., and Hunt, D.F. (2007). Chemical derivatization of histones for facilitated analysis by mass spectrometry. Nat. Protoc. *2*, 933–938.

Gardiner-Garden, M., Ballesteros, M., Gordon, M., and Tam, P.P.L. (1998). Histone- and Protamine-DNA Association: Conservation of Different Patterns within the β-Globin Domain in Human Sperm. Mol. Cell. Biol. *18*, 3350–3356.

Gatewood, J.M., Cook, G.R., Balhorn, R., Bradbury, E.M., and Schmid, C.W. (1987). Sequence-specific packaging of DNA in human sperm chromatin. Science (80-.). *236*, 962–964.

Gluckman, P.D., Hanson, M.A., Buklijas, T., Low, F.M., and Beedle, A.S. (2009). Epigenetic mechanisms that underpin metabolic and cardiovascular diseases. Nat. Rev. Endocrinol. *5*, 401–408.

Godfrey, L., Crump, N.T., Thorne, R., Lau, I.J., Repapi, E., Dimou, D., Smith, A.L., Harman, J.R., Telenius, J.M., Oudelaar, A.M., et al. (2019). DOT1L inhibition reveals a distinct subset of enhancers dependent on H3K79 methylation. Nat. Commun. *10*.

Grant, B.F., Chou, S.P., Saha, T.D., Pickering, R.P., Kerridge, B.T., Ruan, W.J., Huang, B.J., Jung, J.S., Zhang, H.T., Fan, A., et al. (2017). Prevalence of 12-Month Alcohol Use, High-Risk Drinking, and DSM-IV Alcohol Use Disorder in the United States, 2001-2002 to 2012-2013 Results From the National Epidemiologic Survey on Alcohol and Related Conditions. JAMA PSYCHIATRY *74*, 911–923.

Gupta, S., Stamatoyannopoulos, J.A., Bailey, T.L., and Noble, W.S. (2007). Quantifying similarity between motifs. Genome Biol. *8*, R24.

Hake, S.B., and Allis, C.D. (2006). Histone H3 variants and their potential role in indexing mammalian genomes: The “H3 barcode hypothesis.” Proc. Natl. Acad. Sci. U. S. A. *103*, 6428–6435.

Hammoud, S.S., Nix, D.A., Zhang, H., Purwar, J., Carrell, D.T., and Cairns, B.R. (2009). Distinctive chromatin in human sperm packages genes for embryo development. Nature *460*, 473–478.

Handoko, L., Xu, H., Li, G., Ngan, C.Y., Chew, E., Schnapp, M., Lee, C.W.H., Ye, C., Ping, J.L.H., Mulawadi, F., et al. (2011). CTCF-mediated functional chromatin interactome in pluripotent cells. Nat Genet *43*, 630–638.

Hao, N., Xin, H., Shi, X., Xin, J., Zhang, H., Guo, S., Wang, Z., and Hao, C. (2021). Paternal reprogramming-escape histone H3K4me3 marks located within promoters of RNA splicing genes. Bioinformatics *37*, 1039–1044.

Van Heertum, K., and Rossi, B. (2017). Alcohol and fertility: how much is too much? Fertil. Res. Pract. *3*, 10.

van der Heijden, G.W., Derijck, A.A.H.A.H.A., Ramos, L., Giele, M., van der Vlag, J., and de Boer, P. (2006). Transmission of modified nucleosomes from the mouse male germline to the zygote and subsequent remodeling of paternal chromatin. Dev. Biol. *298*, 458–469.

Van Der Heijden, G.W., Ramos, L., Baart, E.B., Van Den Berg, I.M., Derijck, A.A.H.A.H.A., Van Der Vlag, J., Martini, E., and De Boer, P. (2008). Sperm-derived histones contribute to zygotic chromatin in humans. BMC Dev. Biol. *8*.

Henikoff, S., and Ahmad, K. (2005). Assembly of variant histones into chromatin. Annu. Rev. Cell Dev. Biol. *21*, 133–153.

Henikoff, S., and Shilatifard, A. (2011). Histone modification: cause or cog? TRENDS Genet. *27*, 389–396.

Higashijima, Y., Matsui, Y., Shimamura, T., Nakaki, R., Nagai, N., Tsutsumi, S., Abe, Y., Link, V.M., Osaka, M., Yoshida, M., et al. (2020). Coordinated demethylation of H3K9 and H3K27 is required for rapid inflammatory responses of endothelial cells. EMBO J. *39*.

Hisano, M., Erkek, S., Dessus-Babus, S., Ramos, L., Stadler, M.B., and Peters, A.H.F.M.F.M. (2013). Genome-wide chromatin analysis in mature mouse and human spermatozoa. Nat Protoc *8*, 2449–2470.

Hochberg, Z., Feil, R., Constancia, M., Fraga, M., Junien, C., Carel, J.C., Boileau, P., Le Bouc, Y., Deal, C.L., Lillycrop, K., et al. (2011). Child Health, Developmental Plasticity, and Epigenetic Programming. Endocr. Rev. *32*, 159–224.

Holland, M.L., Lowe, R., Caton, P.W., Gemma, C., Carbajosa, G., Danson, A.F., Carpenter, A.A.M., Loche, E., Ozanne, S.E., and Rakyan, V.K. (2016). Early-life nutrition modulates the epigenetic state of specific rDNA genetic variants in mice. Science *353*, 495–498.

Hon, G.C., Rajagopal, N., Shen, Y., McCleary, D.F., Yue, F., Dang, M.D., and Ren, B. (2013). Epigenetic memory at embryonic enhancers identified in DNA methylation maps from adult mouse tissues. Nat Genet *45*, 1198–1206.

Hutcheon, K., McLaughlin, E.A., Stanger, S.J., Bernstein, I.R., Dun, M.D., Eamens, A.L., and Nixon, B. (2017). Analysis of the small non-protein-coding RNA profile of mouse spermatozoa reveals specific enrichment of piRNAs within mature spermatozoa. RNA Biol. *14*, 1776–1790.

Ihara, M., Meyer-Ficca, M.L., Leu, N.A., Rao, S., Li, F., Gregory, B.D., Zalenskaya, I.A., Schultz, R.M., and Meyer, R.G. (2014). Paternal Poly (ADP-ribose) Metabolism Modulates Retention of Inheritable Sperm Histones and Early Embryonic Gene Expression. PLoS Genet. *10*.

Iwaki, T., Sandoval-Cooper, M.J., Paiva, M., Kobayashi, T., Ploplis, V.A., and Castellino, F.J. (2002). Fibrinogen stabilizes placental-maternal attachment during embryonic development in the mouse. Am J Pathol *160*, 1021–1034.

Jensen, T.K., Swan, S., Jorgensen, N., Toppari, J., Redmon, B., Punab, M., Drobnis, E.Z., Haugen, T.B., Zilaitiene, B., Sparks, A.E., et al. (2014). Alcohol and male reproductive health: a cross-sectional study of 8344 healthy men from Europe and the USA. Hum. Reprod. *29,* 1801–1809.

Ji, X., Dadon, D.B., Powell, B.E., Fan, Z.P., Borges-Rivera, D., Shachar, S., Weintraub, A.S., Hnisz, D., Pegoraro, G., Lee, T.I., et al. (2016). 3D Chromosome Regulatory Landscape of Human Pluripotent Cells. Cell Stem Cell *18,* 262–275.

Jiménez-Marín, A., Collado-Romero, M., Ramirez-Boo, M., Arce, C., and Garrido, J.J. (2009). Biological pathway analysis by ArrayUnlock and Ingenuity Pathway Analysis. BMC Proc *3 Suppl 4,* S6.

Johnstone, R.W. (2002). Histone-deacetylase inhibitors: Novel drugs for the treatment of cancer. Nat. Rev. Drug Discov. *1,* 287–299.

Joo, K.J., Kwon, Y.W., Myung, S.C., and Kim, T.H. (2012). The Effects of Smoking and Alcohol Intake on Sperm Quality: Light and Transmission Electron Microscopy Findings. J. Int. Med. Res. *40,* 2327–2335.

Jung, Y.H., Sauria, M.E.G., Lyu, X., Cheema, M.S., Ausio, J., Taylor, J., and Corces, V.G. (2017). Chromatin States in Mouse Sperm Correlate with Embryonic and Adult Regulatory Landscapes. Cell Rep *18,* 1366–1382.

Jung, Y.H., Kremsky, I., Gold, H.B., Rowley, M.J., Punyawai, K., Buonanotte, A., Lyu, X., Bixler, B.J., Chan, A.W.S., and Corces, V.G. (2019). Maintenance of CTCF- and Transcription Factor-Mediated Interactions from the Gametes to the Early Mouse Embryo. Mol. Cell *75*, 154-171.e5.

Kagey, M.H., Newman, J.J., Bilodeau, S., Zhan, Y., Orlando, D.A., van Berkum, N.L., Ebmeier, C.C., Goossens, J., Rahl, P.B., Levine, S.S., et al. (2010). Mediator and cohesin connect gene expression and chromatin architecture. Nature *467*, 430–435.

Kalisch-Smith, J.I., Simmons, D.G., Dickinson, H., and Moritz, K.M. (2017). Review: Sexual dimorphism in the formation, function and adaptation of the placenta. Placenta *54*, 10–16.

Kalisch-Smith, J.I., Steane, S.E., Simmons, D.G., Pantaleon, M., Anderson, S.T., Akison, L.K., Wlodek, M.E., and Moritz, K.M. (2019). Periconceptional alcohol exposure causes female-specific perturbations to trophoblast differentiation and placental formation in the rat. Development *146*.

Kaminen-Ahola, N., Ahola, A., Maga, M., Mallitt, K.-A., Fahey, P., Cox, T.C., Whitelaw, E., and Chong, S. (2010). Maternal ethanol consumption alters the epigenotype and the phenotype of offspring in a mouse model. PLoS Genet *6*, e1000811.

Khoury, A., Achinger-Kawecka, J., Bert, S.A., Smith, G.C., French, H.J., Luu, P.-L.L., Peters, T.J., Du, Q., Parry, A.J., Valdes-Mora, F., et al. (2020). Constitutively bound CTCF sites maintain 3D chromatin architecture and long-range epigenetically regulated domains. Nat. Commun. *11*, 54.

Kim, J.G., Jung, H.S., Kim, K.J., Min, S.S., and Yoon, B.J. (2013). Basal blood corticosterone level is correlated with susceptibility to chronic restraint stress in mice. Neurosci. Lett. *555*, 137–142.

Kim, J.H., Jee, B.C., Lee, J.M., Suh, C.S., and Kim, S.H. (2014). Histone acetylation level and histone Acetyltransferase/Deacetylase activity in Ejaculated sperm from Normozoospermic Men. Yonsei Med. J. *55*, 1333–1340.

Klonoff-Cohen, H., Lam-Kruglick, P., and Gonzalez, C. (2003). Effects of maternal and paternal alcohol consumption on the success rates of in vitro fertilization and gamete intrafallopian transfer. Fertil. Steril. *79*, 330–339.

Kota, S.K., and Feil, R. (2010). Epigenetic Transitions in Germ Cell Development and Meiosis. Dev. Cell *19*, 675–686.

Lambrot, R., Xu, C., Saint-Phar, S., Chountalos, G., Cohen, T., Paquet, M., Suderman, M., Hallett, M., and Kimmins, S. (2013). Low paternal dietary folate alters the mouse sperm epigenome and is associated with negative pregnancy outcomes. Nat. Commun. *4*.

Landt, S.G., Marinov, G.K., Kundaje, A., Kheradpour, P., Pauli, F., Batzoglou, S., Bernstein, B.E., Bickel, P., Brown, J.B., Cayting, P., et al. (2012). ChIP-seq guidelines and practices of the ENCODE and modENCODE consortia. Genome Res. *22*, 1813.

Lane, M., Robker, R.L., and Robertson, S.A. (2014). Parenting from before conception. Science (80-.). *345*, 756–760.

Langmead, B., and Salzberg, S.L. (2012). Fast gapped-read alignment with Bowtie 2. Nat. Methods *9*, 357-U54.

Larose, H., Shami, A.N., Abbott, H., Manske, G., Lei, L., and Hammoud, S.S. (2019). Gametogenesis: A journey from inception to conception. In Current Topics in Developmental Biology, (Curr Top Dev Biol), pp. 257–310.

Lesch, B.J., Dokshin, G.A., Young, R.A., McCarrey, J.R., and Page, D.C. (2013). A set of genes critical to deèelopment is epigenetically poised in mouse germ cells from fetal stages through completion of meiosis. Proc. Natl. Acad. Sci. U. S. A. *110*, 16061–16066.

Li, H., and Durbin, R. (2009). Fast and accurate short read alignment with Burrows-Wheeler transform. Bioinformatics *25*, 1754–1760.

Liao, Y., Smyth, G.K., and Shi, W. (2014). featureCounts: an efficient general purpose program for assigning sequence reads to genomic features. BIOINFORMATICS *30*, 923–930.

Lismer, A., Dumeaux, V., Lafleur, C., Lambrot, R., Brind'Amour, J., Lorincz, M.C., and Kimmins, S. (2021). Histone H3 lysine 4 trimethylation in sperm is transmitted to the embryo and associated with diet-induced phenotypes in the offspring. Dev. Cell *56*, 671-686.e6.

Lister, R., Pelizzola, M., Dowen, R.H., Hawkins, R.D., Hon, G., Tonti-Filippini, J., Nery, J.R., Lee, L., Ye, Z., Ngo, Q.-M., et al. (2009). Human DNA methylomes at base resolution show widespread epigenomic differences. Nature *462*, 315–322.

Love, M.I., Huber, W., and Anders, S. (2014). Moderated estimation of fold change and dispersion for RNA-seq data with DESeq2. Genome Biol. 2014 1512 *15*, 1–21.

Lu, X., Simon, M.D., Chodaparambil, J. V., Hansen, J.C., Shokat, K.M., and Luger, K. (2008). The effect of H3K79 dimethylation and H4K20 trimethylation on nucleosome and chromatin structure. Nat. Struct. Mol. Biol. *15*, 1122–1124.

Luense, L.J., Wang, X., Schon, S.B., Weller, A.H., Lin Shiao, E., Bryant, J.M., Bartolomei, M.S., Coutifaris, C., Garcia, B.A., and Berger, S.L. (2016). Comprehensive analysis of histone post-translational modifications in mouse and human male germ cells. Epigenetics Chromatin *9*, 24.

Ma, W., Noble, W.S., and Bailey, T.L. (2014). Motif-based analysis of large nucleotide data sets using MEME-ChIP. Nat. Protoc. *9*, 1428–1450.

Ben Maamar, M., Sadler-Riggleman, I., Beck, D., and Skinner, M.K. (2018). Epigenetic Transgenerational Inheritance of Altered Sperm Histone Retention Sites. Sci. Rep. *8*, 5308.

Ben Maamar, M., Nilsson, E., Sadler-Riggleman, I., Beck, D., McCarrey, J.R., and Skinner, M.K. (2019). Developmental origins of transgenerational sperm DNA methylation epimutations following ancestral DDT exposure. Dev. Biol. *445*, 280–293.

MacLean, B., Tomazela, D.M., Shulman, N., Chambers, M., Finney, G.L., Frewen, B., Kern, R., Tabb, D.L., Liebler, D.C., and MacCoss, M.J. (2010). Skyline: An open source document editor for creating and analyzing targeted proteomics experiments. Bioinformatics *26*, 966–968.

Mann, M.R.W., Chung, Y.G., Nolen, L.D., Verona, R.I., Latham, K.E., and Bartolomei, M.S. (2003). Disruption of imprinted gene methylation and expression in cloned preimplantation stage mouse embryos. Biol Reprod *69*, 902–914.

Manten, G.T.R., Franx, A., Sikkema, J.M., Hameeteman, T.M., Visser, G.H.A., de Groot, P.G., and Voorbij, H.A.M. (2004). Fibrinogen and high molecular weight fibrinogen during and after normal pregnancy. Thromb Res *114*, 19–23.

Marcho, C., Oluwayiose, O.A., and Pilsner, J.R. (2020). The preconception environment and sperm epigenetics. Andrology *8*, 924–942.

Martinez, M., Macera, S., de Assis, G.F., Pinheiro, P.F.F., Almeida, C.C.D., Tirapelli, L.F., Martins, O.A., Mello-Júnior, W., Padovani, C.R., and Martinez, F.E. (2009). Structural evaluation of the effects of chronic ethanol ingestion on the testis of Calomys callosus. Tissue Cell *41*, 199–205.

Matthews, B.J., and Waxman, D.J. (2018). Computational prediction of CTCF/cohesin-based intra-TAD loops that insulate chromatin contacts and gene expression in mouse liver. Elife *7*, e34077.

Mayne, B.T., Bianco-Miotto, T., Buckberry, S., Breen, J., Clifton, V., Shoubridge, C., and Roberts, C.T. (2016). Large Scale Gene Expression Meta-Analysis Reveals Tissue-Specific, Sex-Biased Gene Expression in Humans. Front. Genet. *7*, 183.

McBirney, M., King, S.E., Pappalardo, M., Houser, E., Unkefer, M., Nilsson, E., Sadler-Riggleman, I., Beck, D., Winchester, P., and Skinner, M.K. (2017). Atrazine induced epigenetic transgenerational inheritance of disease, lean phenotype and sperm epimutation pathology biomarkers.

McBride, N., and Johnson, S. (2016). Fathers' Role in Alcohol-Exposed Pregnancies: Systematic Review of Human Studies. Am. J. Prev. Med. *51*, 240–248.

McCarthy, J.C. (1965). Genetic and environmental control of foetal and placental growth in the mouse. Anim. Prod. *7*, 347–361.

McKinnon, B., Li, H., Richard, K., and Mortimer, R. (2005). Synthesis of thyroid hormone binding proteins transthyretin and albumin by human trophoblast. J Clin Endocrinol Metab *90*, 6714–6720.

McLeod, J.F., and Cooke, N.E. (1989). The vitamin D-binding protein, alpha-fetoprotein, albumin multigene family: detection of transcripts in multiple tissues. J Biol Chem *264*, 21760–21769.

Meistrich, M.L., Hughes, T.H., and Bruce, W.R. (1975). Alteration of epididymal sperm transport and maturation in mice by oestrogen and testosterone. Nature *258*, 145–147.

Meyer, C.A., and Liu, X.S. (2014). Identifying and mitigating bias in next-generation sequencing methods for chromatin biology. Nat. Rev. Genet. *15*, 709–721.

Meyer, R.G., Ketchum, C.C., and Meyer-Ficca, M.L. (2017). Heritable sperm chromatin epigenetics: a break to remember. Biol. Reprod. *97*, 784–797.

Mishiro, T., Ishihara, K., Hino, S., Tsutsumi, S., Aburatani, H., Shirahige, K., Kinoshita, Y., and Nakao, M. (2009). Architectural roles of multiple chromatin insulators at the human apolipoprotein gene cluster. EMBO J *28*, 1234–1245.

Moore, E.M., and Riley, E.P. (2015). What Happens When Children with Fetal Alcohol Spectrum Disorders Become Adults? Curr. Dev. Disord. Reports *2*, 219–227.

Morgan, H.L., Paganopoulou, P., Akhtar, S., Urquhart, N., Philomin, R., Dickinson, Y., and Watkins, A.J. (2020). Paternal diet impairs F1 and F2 offspring vascular function through sperm and seminal plasma specific mechanisms in mice. J. Physiol. *598*, 699–715.

Mu, J., Slevin, J.C., Qu, D., McCormick, S., and Adamson, S.L. (2008). In vivo quantification of embryonic and placental growth during gestation in mice using micro-ultrasound. Reprod. Biol. Endocrinol. *6*, 34.

Mukhopadhyay, A., Deplancke, B., Walhout, A.J.M., and Tissenbaum, H.A. (2008). Chromatin immunoprecipitation (ChIP) coupled to detection by quantitative real-time PCR to study transcription factor binding to DNA in Caenorhabditis elegans. Nat Protoc *3*, 698–709.

Murphy, S.K., Itchon-Ramos, N., Visco, Z., Huang, Z., Grenier, C., Schrott, R., Acharya, K., Boudreau, M.-H., Price, T.M., Raburn, D.J., et al. (2018). Cannabinoid exposure and altered DNA methylation in rat and human sperm. Epigenetics.

Muthusami, K.R., and Chinnaswamy, P. (2005). Effect of chronic alcoholism on male fertility hormones and semen quality. Fertil. Steril. *84*, 919–924.

Naimi, T.S., Brewer, R.D., Mokdad, A., Denny, C., Serdula, M.K., and Marks, J.S. (2003). Binge Drinking Among US Adults. JAMA *289*, 70.

National Institute of Alcohol Abuse and Alcoholism (2021). Underage Drinking | National Institute on Alcohol Abuse and Alcoholism (NIAAA).

Ng, S.F., Lin, R.C.Y., Laybutt, D.R., Barres, R., Owens, J.A., and Morris, M.J. (2010). Chronic high-fat diet in fathers programs β 2-cell dysfunction in female rat offspring. Nature *467*, 963–966.

Nixon, B., Stanger, S.J., Mihalas, B.P., Reilly, J.N., Anderson, A.L., Tyagi, S., Holt, J.E., and McLaughlin, E.A. (2015). The MicroRNA Signature of Mouse Spermatozoa Is Substantially Modified During Epididymal Maturation. Biol. Reprod. *93*.

Nora, E.P., Goloborodko, A., Valton, A.-L.L., Gibcus, J.H., Uebersohn, A., Abdennur, N., Dekker, J., Mirny, L.A., and Bruneau, B.G. (2017). Targeted Degradation of CTCF Decouples Local Insulation of Chromosome Domains from Genomic Compartmentalization. Cell *169*, 930-944.e22.

Nugent, B.M., and Bale, T.L. (2015). The omniscient placenta: Metabolic and epigenetic regulation of fetal programming. Front. Neuroendocrinol. *39*, 28–37.

O'Doherty, A.M., and McGettigan, P.A. (2015). Epigenetic processes in the male germline. Reprod. Fertil. Dev. *27*, 725–738.

Oakberg, E.F. (1956). Duration of spermatogenesis in the mouse and timing of stages of the cycle of the seminiferous epithelium. Am. J. Anat. *99*, 507–516.

Oikawa, M., Simeone, A., Hormanseder, E., Teperek, M., Gaggioli, V., O'Doherty, A., Falk, E., Sporniak, M., D'Santos, C., Franklin, V.N.R., et al. (2020). Epigenetic homogeneity in histone methylation underlies sperm programming for embryonic transcription. Nat. Commun. *11*, 1–16.

Osterndorff-Kahanek, E.A., Tiwari, G.R., Lopez, M.F., Becker, H.C., Harris, R.A., and Mayfield, R.D. (2018). Long-term ethanol exposure: Temporal pattern of microRNA expression and associated mRNA gene networks in mouse brain. PLoS One *13*.

Ozturk, N., Dansranjavin, T., Gies, S., Calay, D., Shiplu, S., Creppe, C., Hendrickx, J., and Schagdarsurengin, U. (2021). H4K20me3 marks distal intergenic and repetitive regions in human mature spermatozoa. Development.

Padmanabhan, V., Cardoso, R.C., and Puttabyatappa, M. (2016). Developmental Programming, a Pathway to Disease. Endocrinology *157*, 1328–1340.

Palumbo, J.S., Zogg, M., Talmage, K.E., Degen, J.L., Weiler, H., and Isermann, B.H. (2004). Role of fibrinogen- and platelet-mediated hemostasis in mouse embryogenesis and reproduction. J Thromb Haemost *2*, 1368–1379.

Peng, H.Y., Shi, J.C., Zhang, Y., Zhang, H., Liao, S.Y., Li, W., Lei, L., Han, C.S., Ning, L.N., Cao, Y.J., et al. (2012). A novel class of tRNA-derived small RNAs extremely enriched in mature mouse sperm. CELL Res. *22*, 1609–1612.

Pradeepa, M.M., Grimes, G.R., Kumar, Y., Olley, G., Taylor, G.C.A.A., Schneider, R., and Bickmore, W.A. (2016). Histone H3 globular domain acetylation identifies a new class of enhancers. Nat. Genet. *48*, 681–686.

Price, E.M., Cotton, A.M., Peñaherrera, M.S., McFadden, D.E., Kobor, M.S., and Robinson, W. (2012). Different measures of “genome-wide” DNA methylation exhibit unique properties in placental and somatic tissues. Epigenetics *7*, 652–663.

Qiao, Y., Wang, Z., Tan, F., Chen, J., Lin, J., Yang, J., Li, H., Wang, X., Sali, A., Zhang, L., et al. (2020). Enhancer Reprogramming within Pre-existing Topologically Associated Domains Promotes TGF-β-Induced EMT and Cancer Metastasis. Mol. Ther. *28*, 2083–2095.

Qu, K., Zaba, L.C., Giresi, P.G., Li, R., Longmire, M., Kim, Y.H., Greenleaf, W.J., and Chang, H.Y. (2015). Individuality and variation of personal regulomes in primary human T cells. Cell Syst. *1*, 51–61.

Quinlan, A.R., and Hall, I.M. (2010). BEDTools: a flexible suite of utilities for comparing genomic features. Bioinformatics *26*, 841–842.

Rada-Iglesias, A., Bajpai, R., Swigut, T., Brugmann, S.A., Flynn, R.A., and Wysocka, J. (2011). A unique chromatin signature uncovers early developmental enhancers in humans. Nature *470*, 279–283.

Radford, E.J., Isganaitis, E., Jimenez-Chillaron, J., Schroeder, J., Molla, M., Andrews, S., Didier, N., Charalambous, M., McEwen, K., Marazzi, G., et al. (2012). An Unbiased Assessment of the Role of Imprinted Genes in an Intergenerational Model of Developmental Programming. PLOS Genet. *8*, 41–53.

Radford, E.J., Ito, M., Shi, H., Corish, J.A., Yamazawa, K., Isganaitis, E., Seisenberger, S., Hore, T.A., Reik, W., Erkek, S., et al. (2014). In utero undernourishment perturbs the adult sperm methylome and intergenerational metabolism. Science (80-.). *345*, 785-+.

Rahimipour, M., Talebi, A.R., Anvari, M., Sarcheshmeh, A.A., and Omidi, M. (2013). Effects of different doses of ethanol on sperm parameters, chromatin structure and apoptosis in adult mice. Eur. J. Obstet. Gynecol. Reprod. Biol. *170*, 423–428.

Rando, O.J. (2016). Intergenerational transfer of epigenetic information in sperm. Cold Spring Harb. Perspect. Med. *6*, 1–14.

Rando, O.J., and Simmons, R.A. (2015). I'm Eating for Two: Parental Dietary Effects on Offspring Metabolism. Cell *161*, 93–105.

Rao, S.S.P., Huntley, M.H., Durand, N.C., Stamenova, E.K., Bochkov, I.D., Robinson, J.T., Sanborn, A.L., Machol, I., Omer, A.D., Lander, E.S., et al. (2014). A 3D map of the human genome at kilobase resolution reveals principles of chromatin looping. Cell *159*, 1665–1680.

Ratajczak, C.K., and Muglia, L.J. (2008). Insights into parturition biology from genetically altered mice. Pediatr Res *64*, 581–589.

Reilly, J.N., McLaughlin, E.A., Stanger, S.J., Anderson, A.L., Hutcheon, K., Church, K., Mihalas, B.P., Tyagi, S., Holt, J.E., Eamens, A.L., et al. (2016). Characterisation of mouse epididymosomes reveals a complex profile of microRNAs and a potential mechanism for modification of the sperm epigenome. Sci. Rep. *6*.

Reiter, F., Wienerroither, S., and Stark, A. (2017). Combinatorial function of transcription factors and cofactors. Curr Opin Genet Dev *43*, 73–81.

Ren, G., Jin, W., Cui, K., Rodrigez, J., Hu, G., Zhang, Z., Larson, D.R., and Zhao, K. (2017). CTCF-Mediated Enhancer-Promoter Interaction Is a Critical Regulator of Cell-to-Cell Variation of Gene Expression. Mol Cell *67*, 1049-1058.e6.

Rinn, J.L., Rozowsky, J.S., Laurenzi, I.J., Petersen, P.H., Zou, K., Zhong, W., Gerstein, M., and Snyder, M. (2004). Major molecular differences between mammalian sexes are involved in drug metabolism and renal function. Dev. Cell *6*, 791–800.

Robaire, B., and Hinton, B.T. (2015). The Epididymis. In Knobil and Neill's Physiology of Reproduction: Two-Volume Set, (Academic Press), pp. 691–771.

Rodgers, A.B., Morgan, C.P., Bronson, S.L., Revello, S., and Bale, T.L. (2013). Paternal Stress Exposure Alters Sperm MicroRNA Content and Reprograms Offspring HPA Stress Axis Regulation. J. Neurosci. *33*, 9003-+.

Rodgers, A.B., Morgan, C.P., Leu, N.A., and Bale, T.L. (2015). Transgenerational epigenetic programming via sperm microRNA recapitulates effects of paternal stress. Proc Natl Acad Sci U S A *112*, 13699–13704.

Rompala, G.R., Finegersh, A., Slater, M., and Homanics, G.E. (2017a). Paternal preconception alcohol exposure imparts intergenerational alcohol-related behaviors to male offspring on a pure C57BL/6J background. Alcohol *60*, 169–177.

Rompala, G.R., Finegersh, A., Slater, M., and Homanics, G.E. (2017b). Paternal preconception alcohol exposure imparts intergenerational alcohol-related behaviors to male offspring on a pure C57BL/6J background. ALCOHOL *60*, 169–177.

Rompala, G.R., Mounier, A., Wolfe, C.M., Lin, Q., Lefterov, I., and Homanics, G.E. (2018). Heavy chronic intermittent ethanol exposure alters small noncoding RNAs in mouse sperm and epididymosomes. Front. Genet. *9*.

Rompala, G.R., Homanics, G.E., GR, R., and GE, H. (2019). Intergenerational effects of alcohol: a review of paternal preconception ethanol exposure studies and epigenetic mechanisms in the male germline. Alcohol Clin Exp Res *43*, 1032–1045.

Rooney, S.A. (1989). Fatty acid biosynthesis in developing fetal lung. Am J Physiol *257*, L195-201.

Roozen, S., Peters, G.J.Y., Kok, G., Townend, D., Nijhuis, J., and Curfs, L. (2016). Worldwide Prevalence of Fetal Alcohol Spectrum Disorders: A Systematic Literature Review Including Meta-Analysis. Alcohol. Clin. Exp. Res. *40*, 18–32.

Rosenfeld, C.S. (2015). Sex-Specific Placental Responses in Fetal Development. Endocrinology *156*, 3422–3434.

Rossi, B. V, Berry, K.F., Hornstein, M.D., Cramer, D.W., Ehrlich, S., and Missmer, S.A. (2011). Effect of Alcohol Consumption on In Vitro Fertilization. Obstet. Gynecol. *117*, 136–142.

Rousseaux, S., Caron, C., Govin, J., Lestrat, C., Faure, A.K., and Khochbin, S. (2005). Establishment of male-specific epigenetic information. Gene *345*, 139–153.

Royo, H., Stadler, M.B., and Peters, A.H.F.M. (2016). Alternative Computational Analysis Shows No Evidence for Nucleosome Enrichment at Repetitive Sequences in Mammalian Spermatozoa. Dev. Cell *37*, 98–104.

Ruggieri, A., Barbati, C., and Malorni, W. (2010). Cellular and molecular mechanisms involved in hepatocellular carcinoma gender disparity. Int. J. Cancer *127*, 499–504.

Saad, M.A., Kuo, S.Z., Rahimy, E., Zou, A.E., Korrapati, A., Rahimy, M., Kim, E., Zheng, H., Yu, M.A., Wang-Rodriguez, J., et al. (2015). Alcohol-dysregulated miR-30a and miR-934 in head and neck squamous cell carcinoma. Mol. Cancer *14*.

Saadoon, A., Ambalavanan, N., Zinn, K., Ashraf, A.P., MacEwen, M., Nicola, T., Fanucchi, M. V, and Harris, W.T. (2017). Effect of Prenatal versus Postnatal Vitamin D Deficiency on Pulmonary Structure and Function in Mice. Am J Respir Cell Mol Biol *56*, 383–392.

Salonen, I., Pakarinen, P., and Huhtaniemi, I. (1992). Effect of chronic ethanol diet on expression of gonadotropin genes in the male rat. J. Pharmacol. Exp. Ther. *260*, 463–467.

Samans, B., Yang, Y., Krebs, S., Sarode, G.V., Blum, H., Reichenbach, M., Wolf, E., Steger, K., Dansranjavin, T., and Schagdarsurengin, U. (2014). Uniformity of nucleosome preservation pattern in mammalian sperm and Its connection to repetitive DNA elements. Dev. Cell *30*, 23–35.

Sánchez-Martín, F.J., Lindquist, D.M., Landero-Figueroa, J., Zhang, X., Chen, J., Cecil, K.M., Medvedovic, M., and Puga, A. (2015). Sex- and tissue-specific methylome changes in brains of mice perinatally exposed to lead. Neurotoxicology *46*, 92–100.

Sanchez, M.C., Fontana, V.A., Galotto, C., Cambiasso, M.Y., Sobarzo, C.M.A.A., Calvo, L., Calvo, J.C., Cebral, E., Sánchez, M.C., Fontana, V.A., et al. (2018). Murine sperm capacitation, oocyte penetration and decondensation following moderate alcohol intake. Reproduction *155*, 529–541.

Schmittgen, T.D., and Livak, K.J. (2008). Analyzing real-time PCR data by the comparative C(T) method. Nat Protoc *3*, 1101–1108.

Schroeder, D.I., Blair, J.D., Lott, P., Yu, H.O.K., Hong, D., Crary, F., Ashwood, P., Walker, C., Korf, I., Robinson, W.P., et al. (2013). The human placenta methylome. Proc Natl Acad Sci U S A *110*, 6037–6042.

Sharma, U. (2019). Paternal Contributions to Offspring Health: Role of Sperm Small RNAs in Intergenerational Transmission of Epigenetic Information. Front. Cell Dev. Biol. *7*.

Sharma, U., Conine, C.C., Shea, J.M., Boskovic, A., Derr, A.G., Bing, X.Y., Belleannee, C., Kucukural, A., Serra, R.W., Sun, F., et al. (2016). Biogenesis and function of tRNA fragments during sperm maturation and fertilization in mammals. Science (80-.).

Sharma, U., Sun, F., Conine, C.C., Reichholf, B., Kukreja, S., Herzog, V.A., Ameres, S.L., and Rando, O.J. (2018). Small RNAs Are Trafficked from the Epididymis to Developing Mammalian Sperm. Dev. Cell *46*, 481-494.e6.

Shea, J.M., Serra, R.W., Carone, B.R., Shulha, H.P., Kucukural, A., Ziller, M.J., Vallaster, M.P., Gu, H.C., Tapper, A.R., Gardner, P.D., et al. (2015). Genetic and Epigenetic Variation, but Not Diet, Shape the Sperm Methylome. Dev. Cell *35*, 750–758.

Shen, Y., Yue, F., McCleary, D.F., Ye, Z., Edsall, L., Kuan, S., Wagner, U., Dixon, J., Lee, L., Lobanenkov, V. V, et al. (2012). A map of the cis-regulatory sequences in the mouse genome. Nature *488*, 116–120.

Shogren-Knaak, M., Ishii, H., Sun, J.M., Pazin, M.J., Davie, J.R., and Peterson, C.L. (2006). Histone H4-K16 acetylation controls chromatin structure and protein interactions. Science (80-.). *311*, 844–847.

Short, A.K., Fennell, K.A., Perreau, V.M., Fox, A., O'Bryan, M.K., Kim, J.H., Bredy, T.W., Pang, T.Y., and Hannan, A.J. (2016). Elevated paternal glucocorticoid exposure alters the small noncoding RNA profile in sperm and modifies anxiety and depressive phenotypes in the offspring. Transl. Psychiatry *6*.

Siddeek, B., Mauduit, C., Simeoni, U., and Benahmed, M. (2018). Sperm epigenome as a marker of environmental exposure and lifestyle, at the origin of diseases inheritance. Mutat. Res. Mutat. Res. *778*, 38–44.

Siklenka, K., Erkek, S., Godmann, M., Lambrot, R., McGraw, S., Lafleur, C., Cohen, T., Xia, J., Suderman, M., Hallett, M., et al. (2015). Disruption of histone methylation in developing sperm impairs offspring health transgenerationally. Science (80-.). *350*, aab2006.

Sillaste, G., Kaplinski, L., Meier, R., Jaakma, Ü., Eriste, E., and Salumets, A. (2017). A novel hypothesis for histone-to-protamine transition in Bos taurus spermatozoa. Reproduction *153*, 241–251.

Skinner, M.K., Nilsson, E., Sadler-Riggleman, I., Beck, D., Ben Maamar, M., and McCarrey, J.R. (2019). Transgenerational sperm DNA methylation epimutation developmental origins following ancestral vinclozolin exposure. Epigenetics *14*, 721–739.

Stadler, M.B., Murr, R., Burger, L., Ivanek, R., Lienert, F., Schöler, A., van Nimwegen, E., Wirbelauer, C., Oakeley, E.J., Gaidatzis, D., et al. (2011). DNA-binding factors shape the mouse methylome at distal regulatory regions. Nature *480*, 490–495.

Stanford, K.I., Rasmussen, M., Baer, L.A., Lehnig, A.C., Rowland, L.A., White, J.D., So, K., De Sousa-Coelho, A.L., Hirshman, M.F., Patti, M.E., et al. (2018). Paternal exercise improves glucose metabolism in adult offspring. Diabetes *67*, 2530–2540.

Sun, W., Dong, H., Becker, A.S., Dapito, D.H., Modica, S., Grandl, G., Opitz, L., Efthymiou, V., Straub, L.G., Sarker, G., et al. (2018). Cold-induced epigenetic programming of the sperm enhances brown adipose tissue activity in the offspring. Nat. Med. *24*, 1372–1383.

Susiarjo, M., Sasson, I., Mesaros, C., and Bartolomei, M.S. (2013). Bisphenol a exposure disrupts genomic imprinting in the mouse. PLoS Genet *9*, e1003401.

Talebi, A.R., Sarcheshmeh, A.A., Khalili, M.A., and Tabibnejad, N. (2011). Effects of ethanol consumption on chromatin condensation and DNA integrity of epididymal spermatozoa in rat. Alcohol *45*, 403–409.

Taylor, G.C.A.A., Eskeland, R., Hekimoglu-Balkan, B., Pradeepa, M.M., and Bickmore, W.A. (2013). H4K16 acetylation marks active genes and enhancers of embryonic stem cells, but does not alter chromatin compaction. Genome Res. *23*, 2053–2065.

Terashima, M., Barbour, S., Ren, J.K., Yu, W.S., Han, Y.X., and Muegge, K. (2015). Effect of high fat diet on paternal sperm histone distribution and male offspring liver gene expression. EPIGENETICS *10*, 861–871.

Thorvaldsdóttir, H., Robinson, J.T., and Mesirov, J.P. (2013). Integrative Genomics Viewer (IGV): high-performance genomics data visualization and exploration. Brief. Bioinform. *14*, 178–192.

Trapnell, C., Roberts, A., Goff, L., Pertea, G., Kim, D., Kelley, D.R., Pimentel, H., Salzberg, S.L., Rinn, J.L., and Pachter, L. (2012). Differential gene and transcript expression analysis of RNA-seq experiments with TopHat and Cufflinks. Nat. Protoc. *7*, 562–578.

Valimaki, M., Tuominen, J.A., Huhtaniemi, I., and Ylikahri, R. (1990). The Pulsatile Secretion of Gonadotropins and Growth Hormone, and the Biological Activity of Luteinizing Hormone in Men Acutely Intoxicated with Ethanol. Alcohol. Clin. Exp. Res. *14*, 928–931.

Vassoler, F.M., White, S.L., Schmidt, H.D., Sadri-Vakili, G., and Pierce, R.C. (2013). Epigenetic inheritance of a cocaine-resistance phenotype. Nat Neurosci *16*, 42–47.

Veazey, K.J., Parnell, S.E., Miranda, R.C., and Golding, M.C. (2015). Dose-dependent alcohol-induced alterations in chromatin structure persist beyond the window of exposure and correlate with fetal alcohol syndrome birth defects. Epigenetics and Chromatin *8*.

VonHandorf, A., Sánchez-Martín, F.J., Biesiada, J., Zhang, H., Zhang, X., Medvedovic, M., and Puga, A. (2018). Chromium disrupts chromatin organization and CTCF access to its cognate sites in promoters of differentially expressed genes. Epigenetics *13*, 363–375.

Wang, H., Maurano, M.T., Qu, H., Varley, K.E., Gertz, J., Pauli, F., Lee, K., Canfield, T., Weaver, M., Sandstrom, R., et al. (2012). Widespread plasticity in CTCF occupancy linked to DNA methylation. Genome Res. *22*, 1680–1688.

Waxman, D.J., and Holloway, M.G. (2009). Sex differences in the expression of hepatic drug metabolizing enzymes. Mol. Pharmacol. *76*, 215–228.

Wei, Y., Yang, C.-R., Wei, Y.-P., Zhao, Z.-A., Hou, Y., Schatten, H., and Sun, Q.-Y. (2014). Paternally induced transgenerational inheritance of susceptibility to diabetes in mammals. PNAS *111*, 1873–1878.

Van De Werken, C., Van Der Heijden, G.W., Eleveld, C., Teeuwssen, M., Albert, M., Baarends, W.M., Laven, J.S.E., Peters, A.H.F.M., and Baart, E.B. (2014). Paternal heterochromatin formation in human embryos is H3K9/HP1 directed and primed by sperm-derived histone modifications. Nat. Commun. *5*.

Whalen, S., Truty, R.M., and Pollard, K.S. (2016). Enhancer-promoter interactions are encoded by complex genomic signatures on looping chromatin. Nat Genet *48*, 488–496.

White, A.M., Kraus, C.L., and Swartzwelder, H.S. (2006). Many college freshmen drink at levels far beyond the binge threshold. Alcohol. Exp. Res. *30*, 1006–1010.

Whyte, W.A., Bilodeau, S., Orlando, D.A., Hoke, H.A., Frampton, G.M., Foster, C.T., Cowley, S.M., and Young, R.A. (2012). Enhancer decommissioning by LSD1 during embryonic stem cell differentiation. Nature *482*, 221–225.

Wilson, M.E., and Ford, S.P. (2001). Comparative aspects of placental efficiency. In CONTROL OF PIG REPRODUCTION VI, R.D. Geisert, H. Niemann, and C. Doberska, eds. pp. 223–232.

Wu, L., Lu, Y., Jiao, Y., Liu, B., Li, S., Li, Y., Xing, F., Chen, D., Liu, X., Zhao, J., et al. (2016). Paternal Psychological Stress Reprograms Hepatic Gluconeogenesis in Offspring. Cell Metab. *23*, 735–743.

Xia, R., Jin, L., Li, D., Liang, H., Yang, F., Chen, J., Yuan, W., and Miao, M. (2018). Association Between Paternal Alcohol Consumption Before Conception and Anogenital Distance of Offspring. Alcohol. Clin. Exp. Res. *42*, 735–742.

Xu, C., and Corces, V.G. (2018). Nascent DNA methylome mapping reveals inheritance of hemimethylation at CTCF/cohesin sites. Science *359*, 1166–1170.

Yamaguchi, K., Hada, M., Fukuda, Y., Inoue, E., Makino, Y., Katou, Y., Shirahige, K., and Okada, Y. (2018). Re-evaluating the Localization of Sperm-Retained Histones Revealed the Modification-Dependent Accumulation in Specific Genome Regions. Cell Rep. *23*, 3920–3932.

Yang, Q.Y., Lin, J.M., Liu, M., Li, R.H., Tian, B., Zhang, X., Xu, B.Y., Liu, M.F., Zhang, X., Li, Y.P., et al. (2016). Highly sensitive sequencing reveals dynamic modifications and activities of small RNAs in mouse oocytes and early embryos. Sci. Adv. *2*.

Yoshida, K., Muratani, M., Araki, H., Miura, F., Suzuki, T., Dohmae, N., Katou, Y., Shirahige, K., Ito, T., and Ishii, S. (2018). Mapping of histone-binding sites in histone replacement-completed spermatozoa. Nat. Commun. *9*, 1–11.

Yoshida, K., Maekawa, T., Ly, N.H., Fujita, S. ichiro, Muratani, M., Ando, M., Katou, Y., Araki, H., Miura, F., Shirahige, K., et al. (2020). ATF7-Dependent Epigenetic Changes Are Required for the Intergenerational Effect of a Paternal Low-Protein Diet. Mol. Cell *78*, 445-458.e6.

Young Lee, H., Imran Naseer, M., Yoel Lee, S., and Ok Kim, M. (2010). Time-dependent effect of ethanol on GnRH and GnRH receptor mRNA expression in hypothalamus and testis of adult and pubertal rats. Neurosci. Lett. *471*, 25–29.

Zalenskaya, I.A., Bradbury, E.M., and Zalensky, A.O. (2000). Chromatin structure of telomere domain in human sperm. Biochem. Biophys. Res. Commun. *279*, 213–218.

Zeybel, M., Hardy, T., Wong, Y.K., Mathers, J.C., Fox, C.R., Gackowska, A., Oakley, F., Burt, A.D., Wilson, C.L., Anstee, Q.M., et al. (2012). Multigenerational epigenetic adaptation of the hepatic wound-healing response. Nat. Med. *18*, 1369-+.

Zhang, S., Wang, L., Yang, T., Chen, L., Zhao, L., Wang, T., Chen, L., Ye, Z., Zheng, Z., and Qin, J. (2019). Parental alcohol consumption and the risk of congenital heart diseases in offspring: An updated systematic review and meta-analysis. Eur. J. Prev. Cardiol. 204748731987453.

Zheng, H., Huang, B., Zhang, B., Xiang, Y., Du, Z., Xu, Q., Li, Y., Wang, Q., Ma, J., Peng, X., et al. (2016). Resetting Epigenetic Memory by Reprogramming of Histone Modifications in Mammals. Mol. Cell *63*, 1066–1079.

Zheng, Y., Thomas, P.M., and Kelleher, N.L. (2013). Measurement of acetylation turnover at distinct lysines in human histones identifies long-lived acetylation sites. Nat. Commun. *4*.

Ziller, M.J., Hansen, K.D., Meissner, A., and Aryee, M.J. (2015). Coverage recommendations for methylation analysis by whole-genome bisulfite sequencing. Nat Methods *12*, 230–232, 1 p following 232.

APPENDIX A

TABLES

Table 1 Primers for RT-qPCR

Primer name	Fwd/Rev	Sequence
ApoA1	Fwd	CTTCAGGATGAAAGCTGTGGT
	Rev	AGATTCAGGTTCAGCTGTTGG
Apoa2	Fwd	AGAGTAGACGGGAAGGACTG
	Rev	TCAAAGTATGCCTTGGCCTG
ApoA4	Fwd	GTACCCTCTTCCAGGACAAAC
	Rev	CCAGCTCCTTCTTGATCTCTTC
ApoA5	Fwd	GACGACCTGTGGGAAGATATTG
	Rev	CTCCACCCTCTGCCTAATAGA
ApoB	Fwd	GATCAACTGTAAGGTAGAGCTGGA
	Rev	GCTTGAGTTCGTACCTGGAC
ApoC2	Fwd	TCAGATGCAGGAGGCAAAG
	Rev	TAGTGGCAGGAAGGGACTAT
ApoC3	Fwd	ATGGAACAAGCCTCCAAGAC
	Rev	GCCGGTGAACTTGTCAGTAA
ApoE	Fwd	CACAAGAACTGACGGCACTG
	Rev	CCCGTATCTCCTCTGTGCTC
ApoM	Fwd	CTCTCTCTCTATGGCCTTCTCT
	Rev	GCTCCCGCAATAAAGTACCA
Alb	Fwd	GCAGACTTGCTGCGATAAAC
	Rev	CACTTCCTGGTCCTCAACAA
Gc	Fwd	CACCTACGTGGAACCAACAA
	Rev	CAGAGGCGCTTGTCCATAAT
Afm	Fwd	CATGCTGGATTACAGGGATAGG
	Rev	CAGTCCCTCCATGTCACATAAC
Afp	Fwd	AGGAGTGCTTCCAGACAAAG
	Rev	GGAGGTTTCGGGATCCAAAT
Fgb	Fwd	AAGCTGCCGATGATGACTAC
	Rev	GGGTCTCCGTTCTACTTTCTTC
Fgg	Fwd	GAAGGACAGCAGCATCACAT
	Rev	GAGGTCCTGAAAGTCCATTGTC

Table 1 Continued. Primers for RT-qPCR

Primer name	Fwd/Rev	Sequence
Fga	Fwd	CCAACGAGAGACTGTGATGATG
	Rev	CTTGCCAGGTCCGGTTAAA
Sdha	Fwd	GCTCCTGCCTCTGTGGTTGA
	Rev	AGCAACACCGATGAGCCTG
Mrpl1	Fwd	AACTTCCTCAGCACCAAAATAGC
	Rev	GACCACAAACGGACCCAGATT
Hprt	Fwd	CTGGTGAAAAGGACCTCTCGAA
	Rev	CTGAAGTACTCATTATAGTCAAGGGCAT
Zfy	Fwd	AAGATAAGCTTACATAATCACATGGA
	Rev	CCTATGAAATCCTTTGCTGCACATGT
Xist	Fwd	TTGCGGGATTCGCCTTGAT
	Rev	TGAGCAGCCCTTAAAGCCAC

Table 2 Primers for ChIP-qPCR

Primer name	Fwd/Rev	Sequence
Fga promoter	Fwd	CTCTGCTCCACAGAAGTGATAG
	Rev	TGAGCAAGAGTTTCTGGGATAC
Fgb promoter	Fwd	AGACAGGGCTCTTTACAGAATG
	Rev	GTTCACTTGTTGGCTGAACTG
Fgg promoter	Fwd	GGTGGTGTACTGGAAGTAGTTG
	Rev	AGGTTTAAGCTCCTCCCTTTG
CNC12	Fwd	GGGTGACTGTGATTACAACAGA
	Rev	TGTAGGTGTGCAACCTTGAG
Fgg CI1	Fwd	TCGTGAGGCTCAGCAGAAA
	Rev	CATTCCTCCTCCCAAGTTCATC
Fgg CE1	Fwd	CATGGCATCGCAGGTATAGT
	Rev	CTGACTGCAGAAAGAGGAGAG
Fgg CE2	Fwd	GGAACCTGTCTTCCAGTCATC
	Rev	CCTCCTTTCATGTCTAAGGTCTG
Fgb CE1	Fwd	AGTGATGCTTGGGTACTTGG
	Rev	CCAGATTCCCACCACTTTCA
Fgb CE2 region1	Fwd	GTGAACTGACCCTCATGGATATG
	Rev	ACCTCTGATCCTCAGCTCTATC
Fgb CE2 region2	Fwd	ACTGGTTCTACAGTGGTCCT
	Rev	GTGGATCTGATTCTCCGCTTAC
Fgb CE3	Fwd	AGATGCTTAACCCAAGTTCCC
	Rev	CAGATGGTGACGACCAAGAAG
Fgb CE4	Fwd	CTCCTGAGTGCTGGGATTAAA
	Rev	CACATGGGAGAGAAAGACACA
Alb E1	Fwd	CACTGCCTGGCTACAATCTAT
	Rev	TGCTCACAGTCTGTATGTTCTC
Afp promoter	Fwd	CCACTCTGAAGTGGTCTTTGTC
	Rev	CCTGTTTAAGGGATGCCTGTT
Afm promoter	Fwd	GGAGGATTATTCTTACCCTGTGG
	Rev	GTCCTGGTGCAAATTTCTAGGT
Gc promoter	Fwd	TCCCAGACTCTCCTCCATATTC
	Rev	CCAGAAGCAAGGGACAATCA
Afp E1	Fwd	CATGTGGCAGATAACGGAGA
	Rev	GAACGGTACACAGGGACATAG
Afp E2 region1	Fwd	GTCACATTGTACCTGGGAAGAT

Table 2 Continued. Primers for ChIP-qPCR

Primer name	Fwd/Rev	Sequence
	Rev	CTCAAAGCGCAGTCCTAAGT
Afp E2 region2	Fwd	GCTGTCTCTGATTCTGCTCTATC
	Rev	TTGGCTTATCGCTTCCTATCTC
Afp E2 region3	Fwd	AGGTGGCTCACAGCATACTA
	Rev	CTGACAACGTCTAACGCTCTTT
Afp E3	Fwd	CACTCCACTGACATTGCTGTAG
	Rev	GAGCTGCCTGTCGAACTTAAA
ApoA1 promoter	Fwd	ACAGAGCTGATCCTTGAACTC
	Rev	AGCTCTTCTTCCCTGGTCTA
ApoC3 promoter	Fwd	TGTCTCACCGACCTCATCTA
	Rev	GAGGAGTTGAGAAATCCCTCTG
ApoA4 promoter	Fwd	TGGTACCATCTCTGTAGCTGA
	Rev	GTGCCAGTCTGAGAGAACAA
ApoA5 promoter	Fwd	CTGGCCAGTCATTCAGTAAGT
	Rev	CCTCGAGCCTTTACTAAGTGTG
ApoC3 E	Fwd	CCCTGCTCCTATCTCAGGATTA
	Rev	GTGAGAGAAGGACAAAGGTCAC
ApoA1 CE1	Fwd	GGGAGAGGCGCATATAAGAAAG
	Rev	GCCCATCACTGGTTCCAAA
ApoA1 CE2	Fwd	GTGCTGAGACAGAAGTTGTGA
	Rev	CTCCAAAGTGACTCCTGGATTG
ApoA1 CE3	Fwd	AGTGAAGGAGCCCACAATTC
	Rev	TCCCGAGGTGTATGTCTTCT
ApoA1 CE4	Fwd	CAGAGAGACCAGTGAGAAGATG
	Rev	GTTACCCAACAGCCAGATGA
ApoA1 CI1	Fwd	GCATGGGATTGTCAGAGTGAT
	Rev	ATGGGTGCTGGAAGAGAGA
ApoC3 CE1	Fwd	AGAAATGGAAGCCGCTACAC
	Rev	TAAACAGGCGGAAAGGAAGG
ApoC3 CI1	Fwd	ATCAGAACCTCAGTGCCTTC
	Rev	GCTGCATTGTAGCTGACCTTA
ApoA4 CE1	Fwd	ACAGCTACCAATCAGCCTTAC
	Rev	AAGAGCAGACCACCTTATGC
ApoA4 CE2	Fwd	ACATGCAAGGACATCAGACC
	Rev	CCCACCATGTGACTTGAGAA

Table 2 Continued. Primers for ChIP-qPCR

Primer name	Fwd/Rev	Sequence
ApoA4 CI1	Fwd	ACAGAAGGATCACGGAAGGA
	Rev	GCCATCAAGTATCTGGTGAAGG
ApoA4 CI2	Fwd	GTTTCTGCTGCTCGGTATCT
	Rev	CCGTCCTGGCTTCAATACAA
ApoA4 CE3	Fwd	GTGGGACAACGGGAAAGTAA
	Rev	CCTCTGATGTCCAGTTCAGTTC
ApoA4 CE4	Fwd	GTTTCCACTGACCCTGACAA
	Rev	GGATATGAAGAAGCAGCAGGAG
ApoA5 CI1	Fwd	GCAAACGAGGGAGCTAGATT
	Rev	GATGACTTCCTCAGACAACAGG
ApoA5 CI2	Fwd	GCTATGGTAAGTCCCACCATTC
	Rev	GCCGATGTAACATGATCCTACC
ApoA5 CI3	Fwd	GACCACTGTCTGCCTTGTTT
	Rev	TTATGCAGCCTATGGCACTG
Alb promoter	Fwd	CCAAGGCCCACACTGAAATG
	Rev	CCCATGCACAAGACTTTGTC
Gapdh	Fwd	TCCTATCCTGGGAACCATCACC
	Rev	TCTTTGGACCCGCCTCATTT

Table 3 Differentially methylated CpGs in placenta of offspring from alcohol-exposed sires

Gene Symbol	Accession	Chrom-osome	Position	Distance To Nearest Gene	% Change Methylation	Genomic Feature	Repetitive Element	q-value	Enrichment of H3K27Ac
Cr2	NM_007758	chr1	195241723	-65009	9.5	Intergenic	-	0.0227	Yes
Lrig3	NM_177152	chr10	125824785	-141434	16.54	Intergenic	LINE	0.0479	Yes
Sfi1	NM_030207	chr11	3193188	276	24.55	Promoter	-	0.0005	Yes
Sfi1	NM_030207	chr11	3193297	167	-37.89	Promoter	-	0.0010	Yes
Sfi1	NM_030207	chr11	3193699	-237	25.41	Promoter	-	0.0086	-
Vwc2	NM_177033	chr11	10443724	-670292	18.99	Intergenic	Viral LTR (RLTR6)	0.0113	-
1700030-C10Rik	NR_015521	chr12	20230693	585087	28.57	Intergenic	Viral LTR (MMERGLN)	0.0069	-
Jarid2	NM_025772	chr13	44869619	132478	15.31	Gene Body	-	0.0370	Yes
Mtrr	NM_001308475	chr13	68449775	132330	16.26	Intergenic	Viral LTR	0.0039	-
Gm5458	NM_001024706	chr14	19416344	186244	20.54	Intergenic	GSAT	0.0028	Yes
Gm5458	NM_001024706	chr14	19418213	184375	17.3	Intergenic	GSAT	0.0146	Yes
Mir7210	NR_106069	chr14	24100484	11609	27.57	Intergenic	Viral LTR (IAPLTR2a)	0.0146	-
Rn45s	NR_046233	chr17	39844089	1094	21.51	Intergenic	RNA repeat	0.0020	-
Rn45s	NR_046233	chr17	39844504	1509	5.86	Intergenic	RNA repeat	0.0388	-
Rn45s	NR_046233	chr17	39844510	1515	6.38	Intergenic	RNA repeat	0.0479	-
Rn45s	NR_046233	chr17	39844516	1521	7.59	Intergenic	RNA repeat	0.0449	-
Rn45s	NR_046233	chr17	39847676	4681	-19	Intergenic	RNA repeat	0.0056	-
Gm20752	NR_040750	chr3	158875281	-201083	-28.19	Intergenic	Viral LTR (MERVL 2A)	0.0211	-
Mycs	NM_010850	chrX	5370036	99230	-28.87	Intergenic	Viral LTR (MuRRS)	0.0103	-

Table 4 Differentially methylated CpG tiles in placentas of offspring sired from alcohol-exposed sires

Chromo-some	Tile Position	Distance To Nearest Gene (bp)	Gene Symbol	Accession	% Change Methyl-ation	Genomic Feature	Repetitive Element	q-value	Enrichment of H3K27Ac
chr10	51229001-51230000	-250612	Lilr4b	NM_008147	-10.29	Intergenic	LINE	0.0361	-
chr10	58224001-58225000	7676	Dux	NM_001081954	5.51	Intergenic	LINE	0.0458	-
chr10	125824001-125825000	-141219	Lrig3	NM_177152	16.54	Intergenic	LINE	0.0246	Yes
chr11	10443001-10444000	-670016	Vwc2	NM_177033	6.19	Intergenic	Viral LTR (RLTR6)	0.0361	-
chr12	22475001-22476000	-318356	Gm4425	NR_136920	6.69	Intergenic	Viral LTR (RLTR6)	0.0246	-
chr12	95585001-95586000	-106226	Flrt2	NM_201518	11.5	Intergenic	LINE	0.0401	-
chr13	44869001-44870000	132097	Jarid2	NM_025772	11.46	Gene Body		0.0000	Yes
chr13	68449001-68450000	132105	Mtrr	NM_001308475	7.92	Intergenic	Viral LTR (RLTR6)	0.0040	-
chr14	24100001-24101000	11126	Mir7210	NR_106069	14.41	Intergenic	Viral LTR (IAP)	0.0401	-
chr19	14021001-14022000	101981	Olfr1505	NM_001011850	14.11	Intergenic	Viral LTR (IAP)	0.0458	-
chr1	30859001-30860000	3257	Phf3	NM_001081080	15.67	Gene Body	LINE	0.0059	Yes
chr1	95696001-95697000	19519	4930598F16Rik	NR_040479	6.68	Intergenic	Viral LTR (IAP)	0.0458	Yes
chr2	30256001-30257000	-9203	Lcrr8	NM_001252568	8.41	Gene Body		0.0458	-

Table 4 Continued. Differentially methylated CpG tiles in placentas of offspring sired from alcohol-exposed sires

Chromo-some	Tile Position	Distance To Nearest Gene (bp)	Gene Symbol	Accession	% Change Methyl-ation	Genomic Feature	Repetitive Element	q-value	Enrichment of H3K27Ac
chr2	98663001-98664000	1195346	Lrrc4c	NM_001289744	9	Intergenic	LINE	0.0246	-
chr2	170027001-170028000	42672	A630075F10Rik	NR_033634	25.63	Intergenic	SINE	0.0401	Yes
chr2	181917001-181918000	52643	Polr3k	NM_025901	11.2	Intergenic	SINE	0.0374	-
chr3	158875001-158876000	-200364	Gm20752	NR_040750	-22.07	Intergenic	Viral LTR (RLTR21)	0.0021	Yes
chr5	66026001-66027000	-21717	9130230L23Rik	NR_027961	10.97	Gene Body		0.0361	Yes
chr5	94194001-94195000	111797	A430089I19Rik	NM_177913	16.23	Intergenic	LINE	0.0401	-
chr5	142872001-142873000	22239	Fbxl18	NM_001033312	17.87	Gene Body		0.0164	Yes
chr6	3201001-3202000	-86519	Gm8579	NR_036696	5.72	Intergenic	Viral LTR (IAP)	0.0246	-
chr8	55395001-55396000	440275	Gpm6a	NM_001253756	-18.44	Intergenic	RLTR10	0.0153	-
chr9	3030001-3031000	7744	Mir101c	NR_039546	6.04	Intergenic	GSAT	0.0361	Yes
chr9	3034001-3035000	3744	Mir101c	NR_039546	8.58	Intergenic	GSAT	0.0246	Yes
chr9	73300001-73301000	186534	Rsl24d1	NM_198609	-11.06	Intergenic	Viral LTR (IAPEz)	0.0246	Yes
chrX	143483001-143484000	-34591	Pak3	NM_001195048	-6.24	Intergenic	LINE	0.0401	-

Table 5 Mass Spectrometry analysis of Histone extracts from Caput and Caudal spermatozoa

Peptide	% of Peptide Pool		Standard Deviation	
	Caput	Mature	Caput	Mature
H1.4: K25UN	0.0000	0.0000	0.0000	0.0000
H1.4: K25AC	0.0000	0.0000	0.0000	0.0000
H1.4: K25ME1	0.0000	0.0000	0.0000	0.0000
H1.4: K25ME2	0.0000	0.0000	0.0000	0.0000
H1.4: K25ME3	0.0000	0.0000	0.0000	0.0000
H2A: K5UN	96.3176	96.9260	0.0556	0.1187
H2A: K5AC	3.6824	3.0740	0.0556	0.1187
H2A: K9UN	99.6132	99.5666	0.0327	0.0237
H2A: K9AC	0.3868	0.4334	0.0327	0.0237
H2A: K36UN	99.9844	99.9930	0.0073	0.0007
H2A: K36AC	0.0156	0.0070	0.0073	0.0007
H2A1: K13UN	99.9765	99.9640	0.0059	0.0111
H2A1: K13AC	0.0235	0.0360	0.0059	0.0111
H2A1: K15UN	99.9811	99.9744	0.0144	0.0073
H2A1: K15AC	0.0189	0.0256	0.0144	0.0073
H2A1: K15UB	0.0000	0.0000	0.0000	0.0000
H2A3: K13UN	99.9962	99.9941	0.0008	0.0015
H2A3: K13AC	0.0038	0.0059	0.0008	0.0015
H2A3: K15UN	99.8629	99.9150	0.0264	0.0011
H2A3: K15AC	0.1371	0.0850	0.0264	0.0011
H2A3: K15UB	0.0000	0.0000	0.0000	0.0000
H3R2UN: K4UN	85.9994	93.9101	0.8697	0.2383
H3R2UN: K4ME1	13.1328	5.8878	0.8027	0.2447
H3R2UN: K4ME2	0.5731	0.1035	0.0221	0.0073
H3R2UN: K4ME3	0.1966	0.0650	0.0043	0.0106
H3R2UN: K4AC	0.0981	0.0337	0.0505	0.0077
H3R2UN: Q5UN	99.5822	99.3587	0.1437	0.0357
H3R2UN: Q5ME1	0.4178	0.6413	0.1437	0.0357
H3: K9UN	25.5826	35.4977	0.5032	1.4811

Table 5 Continued. Mass Spectrometry analysis of Histone extracts from Caput and Caudal spermatozoa

Peptide	% of Peptide Pool		Standard Deviation	
	Caput	Mature	Caput	Mature
H3: K9AC	1.9238	1.0746	0.1008	0.0440
H3: K9ME1	17.0374	20.4420	0.3657	1.1311
H3: K9ME2	50.6398	37.1746	0.6736	2.3022
H3: K9ME3	4.8164	5.8111	0.2312	0.2292
H3: K14UN	65.1194	77.9169	1.2187	0.1887
H3: K14AC	34.8806	22.0831	1.2187	0.1887
H3: K18UN	92.4074	95.2197	0.1886	0.1260
H3: K18AC	5.9059	3.3090	0.1480	0.1034
H3: K18ME1	1.6867	1.4713	0.0523	0.0235
H3: Q19UN	99.2130	99.1489	0.0315	0.0520
H3: Q19ME1	0.7870	0.8511	0.0315	0.0520
H3: K23UN	76.1485	85.6374	0.2478	0.4696
H3: K23AC	23.7872	14.3045	0.2481	0.4714
H3: K23ME1	0.0644	0.0582	0.0004	0.0020
H3: R42UN	99.8860	99.9609	0.0111	0.0064
H3: R42ME2	0.1140	0.0391	0.0111	0.0064
H3: R49UN	99.1648	99.6527	0.0471	0.0155
H3: R49ME2	0.8352	0.3473	0.0471	0.0155
H3: Q55UN	99.0697	99.1452	0.0675	0.1368
H3: Q55ME1	0.9303	0.8548	0.0675	0.1368
H3: K56UN	99.9021	99.9567	0.0099	0.0084
H3: K56AC	0.0461	0.0094	0.0108	0.0034
H3: K56ME1	0.0518	0.0339	0.0045	0.0114
H3: K64UN	99.9502	99.9964	0.0101	0.0020
H3: K64AC	0.0498	0.0036	0.0101	0.0020
H3: K79UN	64.8058	74.6111	0.6891	0.6047
H3: K79AC	2.4566	0.2751	0.5427	0.0369
H3: K79ME1	22.4755	22.2183	1.1154	0.5423
H3: K79ME2	9.7182	2.7964	0.5706	0.1408
H3: K79ME3	0.5439	0.0991	0.0949	0.0206
H3: K122UN	99.9177	99.9944	0.0186	0.0021
H3: K122AC	0.0823	0.0056	0.0186	0.0021
H3.1: K27UN	4.5545	7.1125	0.1255	0.1315

Table 5 Continued. Mass Spectrometry analysis of Histone extracts from Caput and Caudal spermatozoa

Peptide	% of Peptide Pool		Standard Deviation	
	Caput	Mature	Caput	Mature
H3.1: K27AC	0.4007	0.3658	0.0159	0.0297
H3.1: K27ME1	17.9117	23.2793	0.1229	0.3257
H3.1: K27ME2	60.3402	52.3566	0.4733	0.9144
H3.1: K27ME3	16.7929	16.8859	0.2818	0.4748
H3.1: K36UN	34.4332	46.5101	0.3291	0.9926
H3.1: K36AC	0.3476	0.1773	0.0327	0.0100
H3.1: K36ME1	32.9712	29.6224	0.6968	0.6240
H3.1: K36ME2	25.3115	17.0510	0.5236	0.3672
H3.1: K36ME3	6.9366	6.6393	0.1517	0.0948
H3.3: K27UN	15.6087	21.5735	0.0898	0.3994
H3.3: K27AC	5.7669	1.2728	0.0839	0.0772
H3.3: K27ME1	37.0931	40.9767	0.5177	0.7139
H3.3: K27ME2	32.5514	27.4683	0.5155	0.6025
H3.3: K27ME3	8.9799	8.7087	0.0921	0.1245
H3.3: K27M	0.0000	0.0000	0.0000	0.0000
H3.3: K36UN	12.3472	20.3914	0.0631	0.5412
H3.3: K36AC	3.3652	0.5646	0.0781	0.0611
H3.3: K36ME1	20.5358	20.9744	0.3176	0.5865
H3.3: K36ME2	43.7126	42.3354	0.3356	0.7476
H3.3: K36ME3	20.0392	15.7343	0.0191	0.5061
H4: K5UN	96.7950	96.9913	0.0972	0.0712
H4: K5AC	3.2050	3.0087	0.0972	0.0712
H4: K8UN	96.5168	95.5257	0.1445	0.1110
H4: K8AC	3.4832	4.4743	0.1445	0.1110
H4: K12UN	98.3628	97.6182	0.0839	0.0151
H4: K12AC	1.6372	2.3818	0.0839	0.0151
H4: K16UN	80.4056	66.7116	0.5865	1.2699
H4: K16AC	19.5944	33.2884	0.5865	1.2699
H4: K20UN	0.1227	1.5444	0.0483	0.1471
H4: K20ME1	0.1960	1.0499	0.0055	0.0546
H4: K20ME2	86.9996	68.0631	0.0691	0.4516
H4: K20ME3	12.4903	29.2798	0.0567	0.3583
H4: K20AC	0.1914	0.0627	0.0333	0.0082